ALCATEL ALENIA SPACE
An Alcatel/Finmeccanica company

REFERENCE : H-P-3-ASP-AN-323

DATE : 12/2/2007

ISSUE : 3    Page : 1/126

TOTAL PAGES : 126

## HERSCHEL / PLANCK

# Planck PLM RF Performance Analysis

| Rédigé par/*Written by* | Responsabilité-Service-Société *Responsibility-Office -Company* | Date | Signature |
|---|---|---|---|
| M. Nadarassin | Planck RF analysis | 12/02/07 | PO Dubruel |
| D. Dubruel | Planck RF analysis | 12/02/07 | Dubruel |
| **Vérifié par/*Verified by*** | | | |
| JB. Riti | Planck PLM system engineer. | 13.02.07 | |
| **Approbation/*Approved*** | | | |
| T. Banos | Planck spacecraft manager | 14/02/07 | |
| T. Grassin | Product Assurance | 14.2.07 | |
| JM. Reix | Project Manager Deputy | 14/02/07 | |
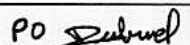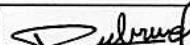
**Entité Emettrice** : Alcatel Alenia Space - France
(détentrice de l'original) :

**ALCATEL ALENIA SPACE**
An Alcatel/Finmeccanica company

REFERENCE : H-P-3-ASP-AN-323

DATE : 12/2/2007

ISSUE : 3

Page : 2/126

| HERSCHEL/PLANCK | DISTRIBUTION RECORD | | |
|---|---|---|---|
| DOCUMENT NUMBER : H-P-3-ASP-AN-323 | Issue : 3 Date: 12/02/2007 | | |
| EXTERNAL DISTRIBUTION | | INTERNAL DISTRIBUTION | |
| ESA | X | HP team | X |
| | | CIt Documentation | Orig. |

## ENREGISTREMENT DES EVOLUTIONS / CHANGE RECORDS

| ISSUE | DATE | § : DESCRIPTION DES EVOLUTIONS<br>§ : CHANGE RECORD | REDACTEUR<br>AUTHOR |
|-------|------|-----------------------------------------------------|---------------------|
| 1 | | Initial release | D. Dubruel |
| 2 | 09-04-2004 | Document update with CDR data configuration | D. Dubruel |
| 3 | 12/02/2007 | Document update with QR data | D. Dubruel |

# TABLE OF CONTENTS

1. INTRODUCTION

## 2. INTRODUCTION

### 2.1 Purpose of this note

This note updates the CDR analysis.

### 2.2 Applicable documents.

[AD 1] System requirements specification – SCI – PR-RS-05991- issue 3/ 0- 27 july 2004

[AD 2] H-P-3-ASPI-SP-0274 -issue 1 - rev 0 -Planck Telescope optical and RF system specification.

### 2.3 Reference documents

[RD 1] Planck RF expertise  Phase B - WP4 - RF calculation report : Incident RF power exchange between detector and structural elements - October, 2002 - S-1117-07

[RD 2] H-P-1-ASP-RP 1248    01/02/2007  ISSUE 1.

[RD 3] NIL

[RD 4] Planck RF expertise model verification & computations WP 2 & WP3 - November , 2003 -TICRA - s-1188-03

[RD 5] Update of the inputs for the RF numerical model - H-P-3-ASP-TN-0564 - issue 1 - rev 0 - 16/09/2003

[ RD 6 ] H-P-3-ASPI-TN-0517 -issue 1 - rev 0 - Planck LFI detector data processing.

[ RD 7 ] H-P-3-ASPI-TN-0559 -issue 1 - rev 2 - HFI detector data processing.

[RD 8] Planck RF expertise - Manual for computations of far out side lobe patterns - November, 2003 - s1188-04

[RD 9] Reflector quilting analysis – H-P-3-ASP-TN-1015 – issue 1 – 10/01/2007.

[RD 10] Planck RFQM evaluation report H-P-3-ASP-TR-1144   -  issue 1  - 10/02/2007

[RD 11] NIL.

[RD 12] NIL

[RD 13 NIL

[RD 14] Analysis of the diffusion by primary reflector using the MAP method - H-P-3-ASP-TN-0528 - issue 1 - rev 0 - 11/06/2003.

[RD 15] Dust contamination analysis  - H-P-3-TN-0468 - issue 1 - rev 0 - 27 /05 /2003

[RD 16] H-P-3-ASP-TN-0821  Revisited dust analysis answer to CDR RID POEI-03 – issue 1 – 22/07/2004

[RD 17] NIL

[RD 18] NIL

[RD 19] NIL

[RD 20]  Planck Optical Analysis, Inputs for WFE and Gain Budgets, H-P-3-ASPI-AN-0742 issue 1 Rev 0 20/04/2004

[RD 21]  Planck Reflector Global Shape data SCI-PT/041726 issue 1 07/04/2006

[RD 22] Planck Reflector Interface Position data SCI-PT/042052 issue 2 02/05/2006]

[RD 23] Planck Payload Optical Performance Analysis, H-P-3-ASPI-TN-0331, issue 2 Apr. 2004.

[RD 24] Planck alignment plan H-P-3-ASPI-PL-0078 issue 3 rev 0 04/2004

[RD 25] Planck Telescope alignment in operational environment-computation results H-P-3-ASP-TN-1117 11/05/2006

[RD 26] Planck Telescope FM alignment determination logic ASP-04-OS /1/1/99

[RD 27] Planck Payload FM Optical WFE Budget H-P-3-ASP-BD-1151 11/2006

# 3. SELF SPACECRAFT EMISSION ANALYSIS.

## 3.1 Scope

This section presents the analysis of the self spacecraft emission level.

The analysis starts with the understanding of the requirement. Then the sensitivity analysis method is explained and applied. This sensitivity analysis allows to identify the most critical surface element wrt to the performance.

The last phase is the performance budget based upon the results of the thermal analysis.

The main update wrt the CDR analysis are the following :
-Fourier transform of the updated temporal thermal

## 3.2  Self spacecraft emission requirement

The self spacecraft emission requirement is defined in the System Requirement Specification (requirement ref SPER 065 P).

*********************************************************

The ASD ( in Watts / √Hz ) of each frequency component between 0.01 Hz and 100 Hz shall be such that :

| Frequency [ GHz ] | ASD [ Watt / √Hz ] |
|---|---|
| 30 | < 3.4 E-18 X |
| 100 ( LFI ) | < 1.1 E-17 X |
| 100 ( HFI ) | < 2.1 E-18 X |
| 353 | < 1.8 E-18 X |
| 857 | < 2.2 E-17 X |

**Note :**

X is equal to one for any frequency component $f_o$ of the fluctuation source synchronous with the Planck S/C spinning rate ( i.e. multiple of f.spin = 1 / 60 Hz ).

Otherwise , X = ( B * t.obs * Delta.f ) , where   Delta.f = fo – k * f.spin and k is chosen to minimise Delta.f .
t.obs = 3600 * FWHM / 2.5 arcmin   , and FWHM is the angular resolution of the antenna radiation pattern in arc minutes .
*********************************************************

The above requirement is derived in order to obtain  for any component $f_o$ of the fluctuating source, the maximum allowed level of ASD.

Delta_f is the difference between the fluctuating component $f_o$ and the nearest multiple of the spin frequency. Then  (Delta_f)$_{max}$ is equal to f_spin/2.

If $f_o$ = k*f_spin then X=1.
If $f_o$ different from f_spin  X is a linear function varying with $f_o$. X is a periodic function. The period is f_spin.

For $f_o$ varying from k*f_spin to k*(f_spin+f_spin/2), X is linearly increasing  from 1 up to PI*t_obs*f_spin/2.

For $f_o$ varying from k*(f_spin+f_spin/2) to (k+1)*f_spin, X is linearly decreasing  from PI*t_obs*f_spin/2  down to 1.

The following table details for each frequency the ASD allowed deviation. The Second column is obtained from the computation of the telescope main lobe. The fourth column is the requirement to be multiplied by X function of $f_o$.

In this table (Table 3.2-1) the most stringent requirement is only applicable to spin-synchronous fluctuating sources. The most relaxed requirement is applicable to sources fluctuating at $f=k*3/2*f\_spin$.

| Central frequency (GHz) | FWHM (arcmin) | PI*t_obs(s) | Qantity (to multiplied by X) | X_max | ASD_min (W/Hz^-05) = ASD * 1 | ASD_min (dBW/Hz^-0.5) | ASD_max (W/Hz^-0.5) | ASD_max (dBW/Hz^-0.5) |
|---|---|---|---|---|---|---|---|---|
| 30 | 33 | 149288.48 | 3.40E-18 | 1244.07 | 3.40E-18 | -174.69 | 4.23E-15 | -143.74 |
| 100 (LFI) | 10 | 45238.93 | 1.10E-17 | 376.99 | 1.10E-17 | -169.59 | 4.15E-15 | -143.82 |
| 100 (HFI) | 10 | 45238.93 | 2.10E-18 | 376.99 | 2.10E-18 | -176.78 | 7.92E-16 | -151.01 |
| 353 | 5.0 | 22619.47 | 1.80E-18 | 188.50 | 1.80E-18 | -177.45 | 3.39E-16 | -154.69 |
| 857 | 5.0 | 22619.47 | 2.20E-17 | 188.50 | 2.20E-17 | -166.58 | 4.15E-15 | -143.82 |

Table 3.2-1 :  Minimum and Maximum amplitude deviations of the ASD.

The Figure 3.2-1 presents all the five curves on the same plot. The maxima of the LFI 30 LFI 100 and HFI 857 are almost the same. The three corresponding curves appear merged. The most stringent requirement is the one for the HFI 353 GHz channel.

The  Figure 3.2-2 and  Figure 3.2-6  present the requirements curves one by one for each specified frequency.

The curves are plotted for the first few multiples of the spin frequency. Due to the wide dynamic variation, the ordinate is plotted as $10*log10(ASD)$. Hence the linear behaviour of the requirement is plotted as a logarithmic curve instead of a linear curve.

ALCATEL ALENIA SPACE
An Alcatel/Finmeccanica company

REFERENCE : H-P-3-ASP-AN-323

DATE : 12/2/2007

ISSUE : 3

Page : 11/126

Requirement for 30,100(LFI),100(HFI),353,857 GHz
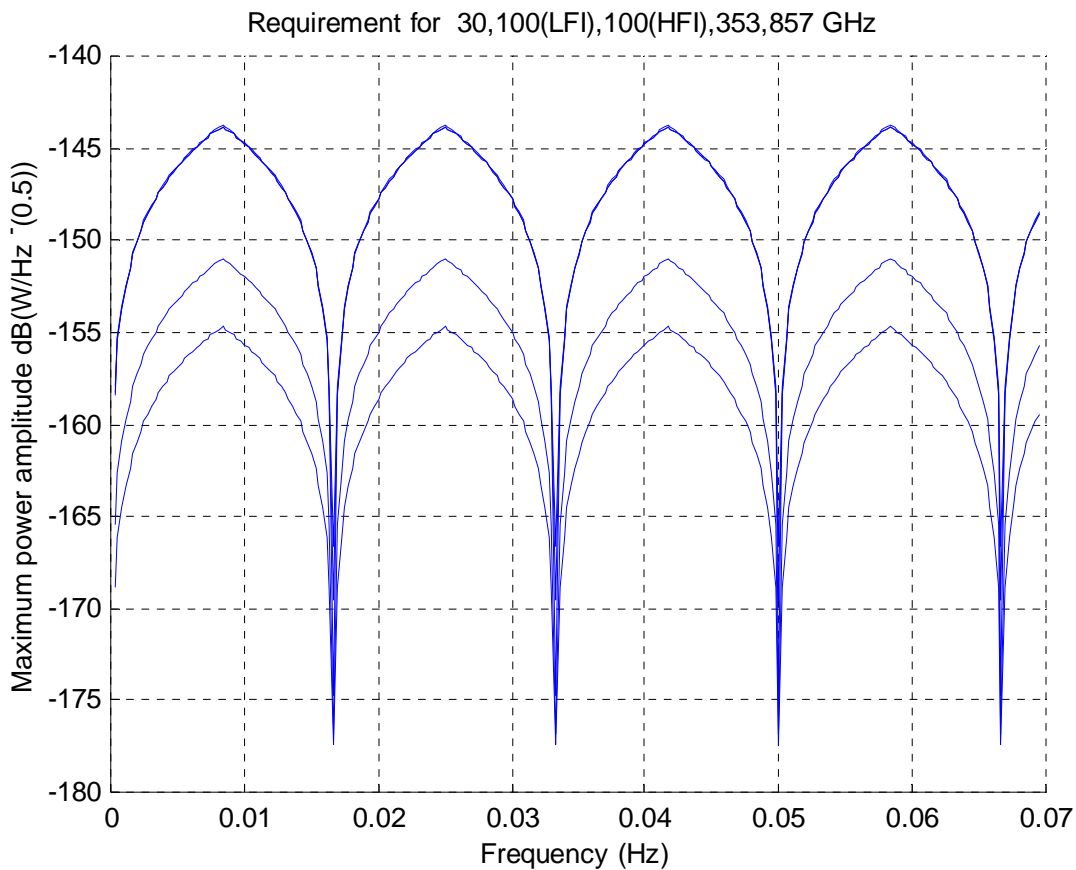


Figure 3.2-1 : All 5 curves from top : LFI 30,HFI 100,HFI 857 (merged), HFI 100 then HFI 353

ALCATEL ALENIA SPACE
An Alcatel/Finmeccanica company

REFERENCE : H-P-3-ASP-AN-323

DATE : 12/2/2007

ISSUE : 3

Page : 12/126
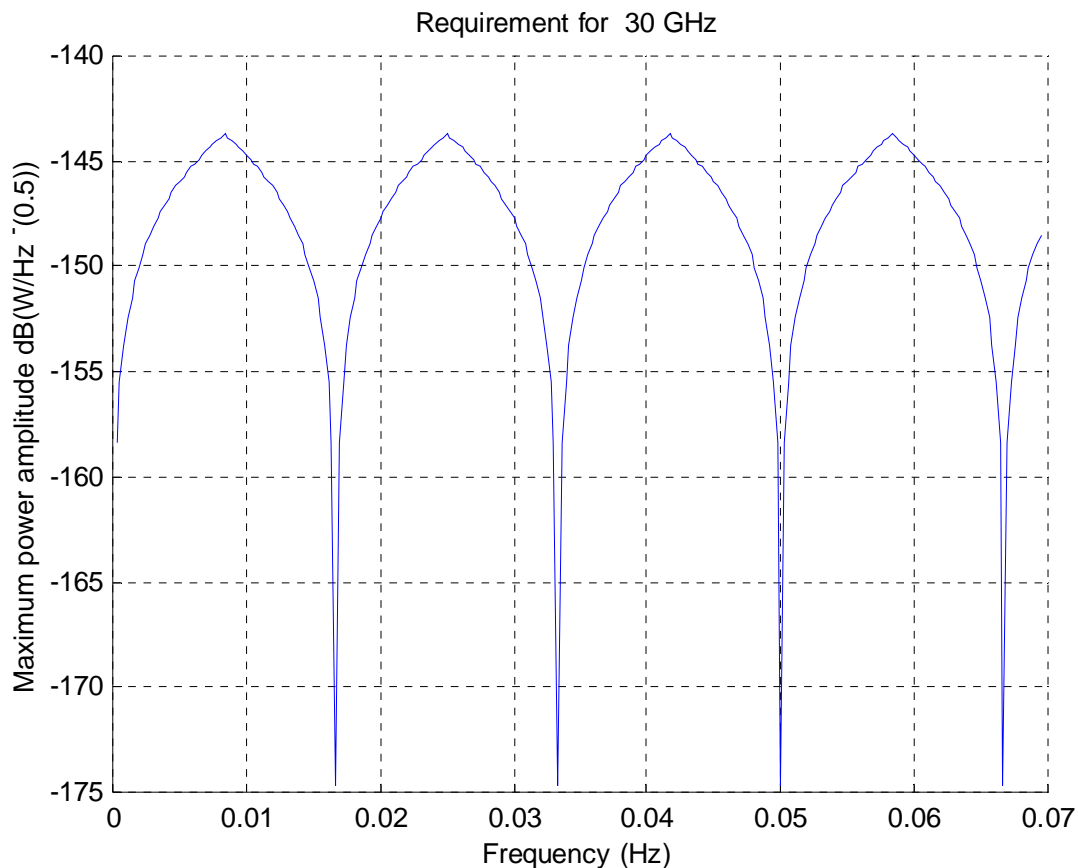
Figure 3.2-2 : 30 GHz requirement curve.

Requirement for 100(LFI) GHz
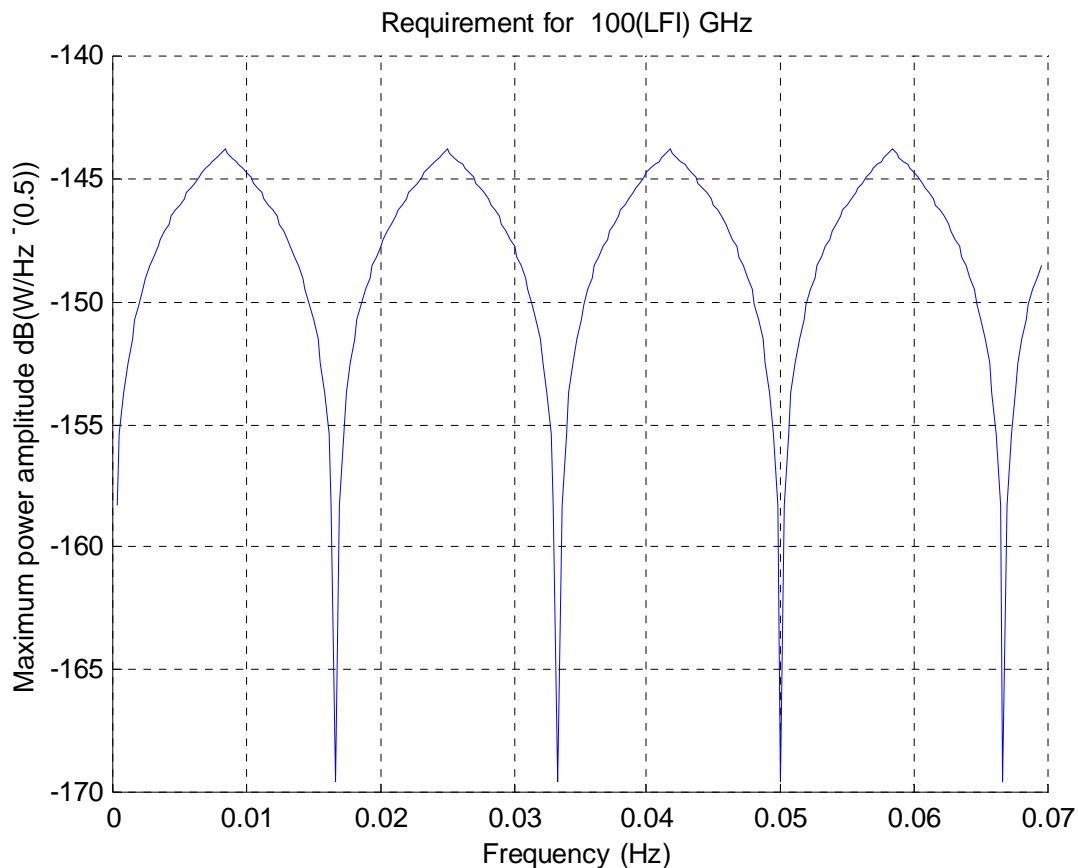


Figure 3.2-3 : 100 GHz LFI requirement curve.

Requirement for 100(HFI) GHz
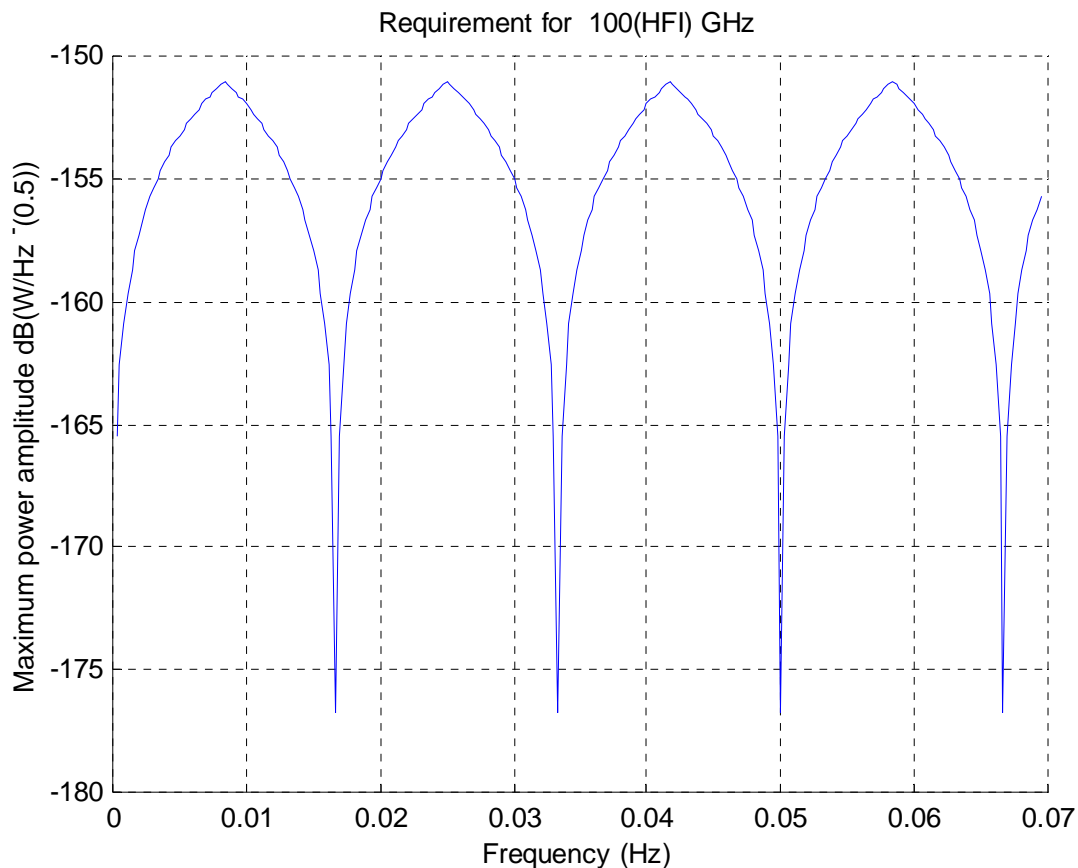


Figure 3.2-4 :  100 GHz  HFI requirement curve.

ALCATEL ALENIA SPACE
An Alcatel/Finmeccanica company

REFERENCE : H-P-3-ASP-AN-323
DATE : 12/2/2007
ISSUE : 3
Page : 15/126

Requirement for 353 GHz
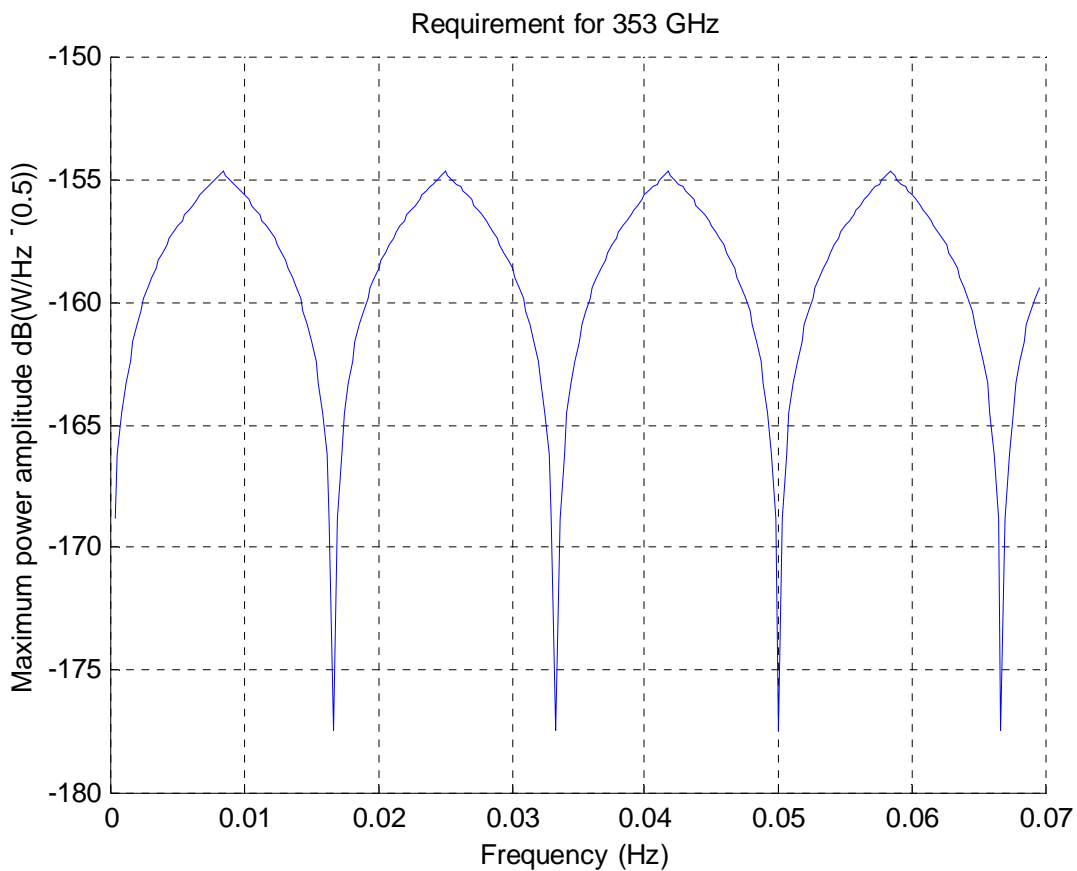


Figure 3.2-5 :  353 GHz  HFI requirement curve.
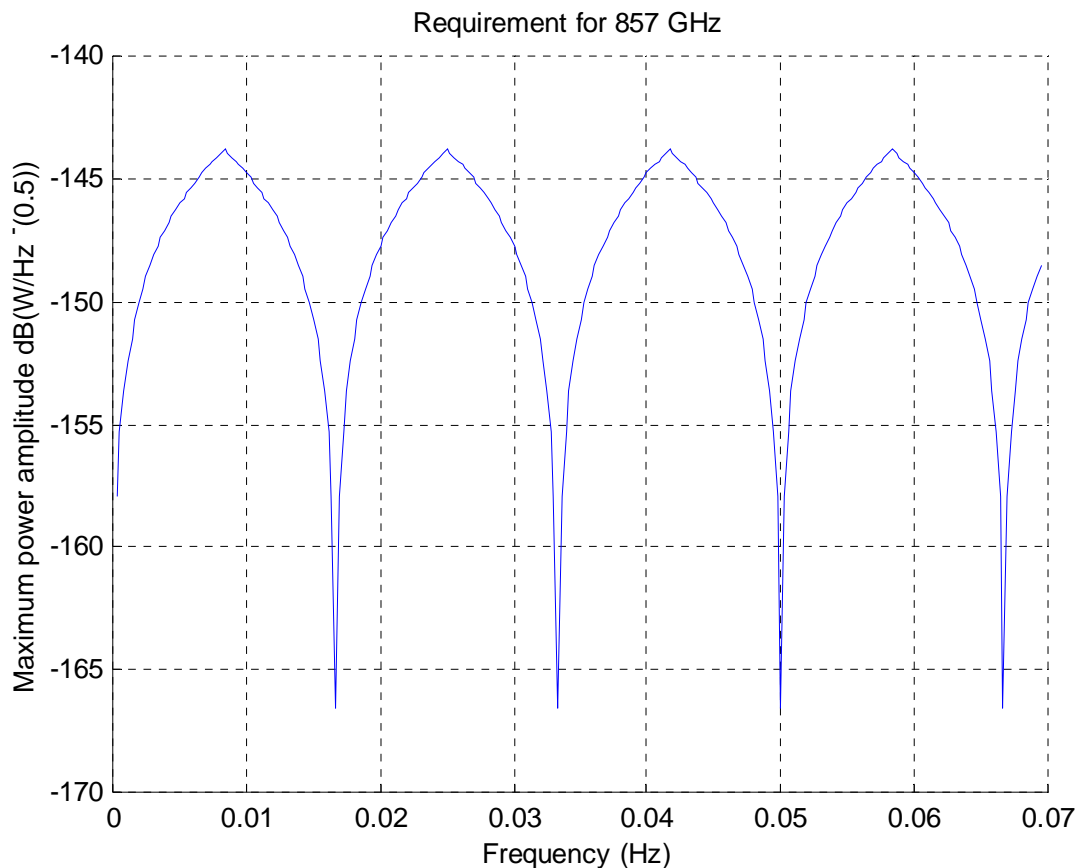
Figure 3.2-6 :  857 GHz  HFI requirement curve.

## 3.3 Conversion of the temperature fluctuation law into power fluctuation law.

The SPER 065 P requirement is expressed in terms of power fluctuation. The input for the analysis is provided as temperature deviation. Hence it is necessary to convert the temperature fluctuation law into a power fluctuation law. The conversion is detailed here below.

The received power by a detector is :

$$P = \frac{A_r}{2} \int_{f_1}^{f_2} \iint_{4\pi} B(\theta, \varphi, f, T) f_n(\theta, \varphi) d\Omega df \quad [1]$$

$$B(\theta, \varphi, f, T) = \frac{(\frac{2.h}{c^2}).f^3}{\exp(\frac{h.f}{k.T}) - 1} \quad [2] \text{ is the spectral brightness of a black body (Planck's law)}$$

T : black body temperature
$f_n$ : normalised power radiation pattern of the detector
$f_1, f_2$ : bandwidth limit
$A_r$ : effective area of horn

The power fluctuations are :

$$\Delta P = \frac{\partial P}{\partial T} * \Delta T \quad [3]$$

then

$$\frac{\partial P}{\partial T} = \frac{A_r}{2} \int_{f_1}^{f_2} \iint_{4\pi} f_n(\theta, \varphi) \frac{\partial B(\theta, \varphi, f, T)}{\partial T} d\Omega df \quad [4]$$

$$\frac{\partial}{\partial T}(B(\theta, \varphi, f, T)) = (\frac{2.h^2.f^4}{k.c^2.T^2}).\frac{\exp(\frac{h.f}{k.T})}{\left(\exp(\frac{h.f}{k.T}) - 1\right)^2} \quad [5]$$

$$\Delta P = \frac{A_r}{2} \Delta T \iint_{4\pi} f_n(\theta, \varphi)(\int_{f_1}^{f_2} \frac{\partial B(\theta, \varphi, f, T)}{\partial T} df).d\Omega \quad [6]$$

Let consider :

$$I(T(\theta, \varphi)) = \int_{f_1}^{f_2} \frac{\partial B(\theta, \varphi, f, T)}{\partial T} df \quad [7]$$

The fluctuating surface considered as a black body is seen by the horn inside a solid angle $\Omega_S$, then $I(\theta, \varphi) = 0$ outside $\Omega_S$ :

$$\Delta P = \Delta T . \frac{A_r}{2} \iint_{4p} f_n(q,j).I(T(q,j)).d\Omega = \Delta T . \frac{A_r}{2} I. \iint_{\Omega_S} f_n(q,j).d\Omega \qquad [8]$$

The effective area is defined by :

$$A_r = \frac{l^2}{\iint_{4p} f_n(q,j).d\Omega} \qquad [9]$$

Then

$$\Delta P = \frac{\Delta T}{2} . l^2 .I. \frac{\iint_{\Omega_S} f_n(q,j).d\Omega}{\iint_{4p} f_n(q,j).d\Omega} \qquad [10]$$

The following IP quantity is the incident power computed with grasp8.

$$IP = \frac{\iint_{\Omega_S} f_n(q,j).d\Omega}{\iint_{4p} f_n(q,j).d\Omega} \qquad [11]$$

On final the power fluctuation is expressed as

$$\Delta P = \frac{\Delta T}{2} * l^2 * I * IP \qquad [12]$$

The detector efficiency and the surface emissivity have to be taken into account ($\eta = 1$ for the LFI and $\eta = 0.3$ for the HFI )

$$\Delta P = \frac{\Delta T}{2} * l^2 * I * IP * h * e \qquad [13]$$

The integral I is numerically computed as follow :

$$I = \int_{f_1}^{f_2} \frac{\partial B(q,j,f,T)}{\partial T} df = \sum_{i=1}^{N} \frac{\partial}{\partial T}(B(q,j,f,T)).\Delta f \qquad [14] \text{ with } \begin{cases} \Delta f = \dfrac{f_2 - f_1}{N} \\ \\ f_i = f_1 + i.\Delta f \end{cases}$$

ALCATEL ALENIA SPACE
An Alcatel/Finmeccanica company

REFERENCE : H-P-3-ASP-AN-323

DATE : 12/2/2007

ISSUE : 3

Page : 19/126

Numerical computation of I.

$$I = \sum_{i=1}^{N} \frac{\partial}{\partial T}(B(\theta, \varphi, f, T)).\Delta f \qquad [15]$$

The former quantity is computed for all frequencies and for different average surface temperatures (fig 3-1).

| Central frequency (GHz) | Lowest frequency (GHz) | Highest frequency (GHz) | Temperature (K) | I (ISU) |
|---|---|---|---|---|
| 30 | 27 | 30 | 50 | 1.6646E-09 |
| 30 | 27 | 30 | 80 | 1.6647E-09 |
| 30 | 27 | 30 | 150 | 1.6647E-09 |
| 100 | 90 | 110 | 50 | 6.1608E-08 |
| 100 | 90 | 110 | 80 | 6.1638E-08 |
| 100 | 90 | 110 | 150 | 6.1652E-08 |
| 353 | 317.7 | 388.3 | 50 | 2.6857E-06 |
| 353 | 317.7 | 388.3 | 80 | 2.7016E-06 |
| 353 | 317.7 | 388.3 | 150 | 2.7090E-06 |
| 857 | 771.3 | 942.7 | 50 | 3.6656E-05 |
| 857 | 771.3 | 942.7 | 80 | 3.7948E-05 |
| 857 | 771.3 | 942.7 | 150 | 3.8559E-05 |

Figure 3.3-1 : Numerical integration results.

The numerical result is varying with the frequency but not with the average temperature. This is explained by looking at the Planck's law behavior and at its associated derivative. The derivative curves are quasi identical over the Planck average temperature range. (see fig 3-2 to 3-5)
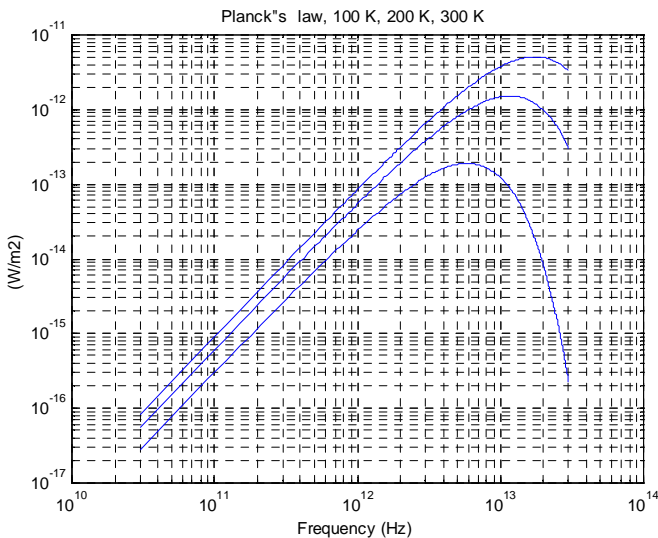


Figure 3.3-2 : Planck's law over a wide frequency domain.
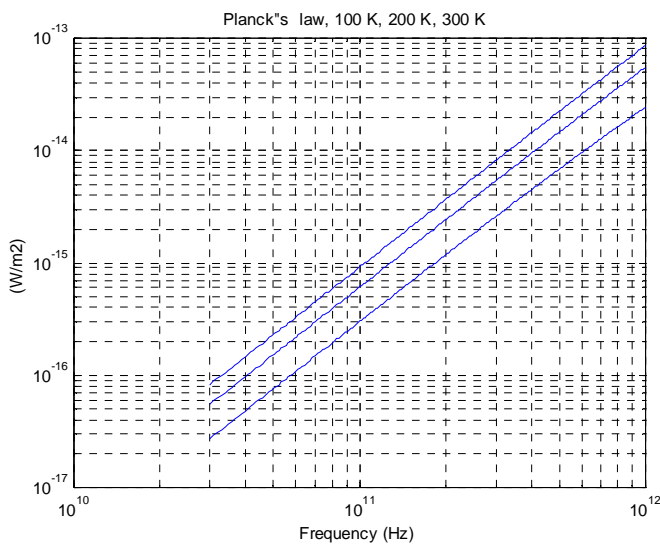
Figure 3.3-3 : Planck's law over the 30 –1000 GHz domain for 100, 200 and 300 K.
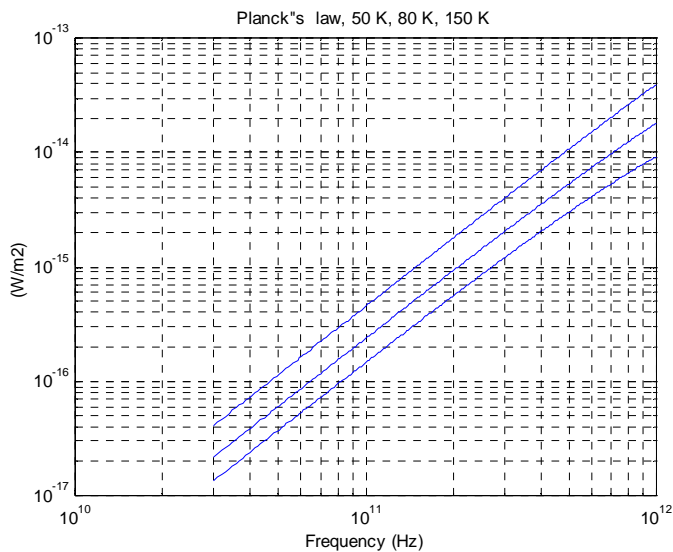


Figure 3.3-4  : Planck's law over the 30 –1000 GHz domain for 50, 80 and 150 K.
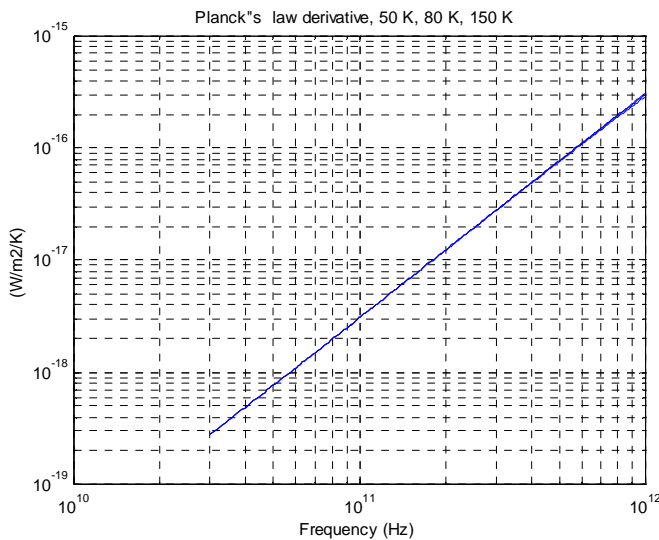
Figure 3.3-5 : Planck's law derivative over the 30 –1000 GHz domain for 50, 80 and 150 K

As a conclusion the power reaching a detector is expressed as :

$$\Delta P = \frac{\Delta T}{2} * \lambda^2 * I * IP * \eta * \varepsilon$$

where η is the detector efficiency  (η=1 for the LFI and η=0.3 for the HFI )

IP is the incident power of RF coupling factor from the thermal source to the detector.

ε is the surface emissivity of the thermal source

λ is the wavelength of the observation channel

ΔT is the physical thermal deviation of the thermal source.

I is the Numerical integration over the channel bandwidth of the thermal derivative of the Planck's law.

| Central frequency (GHz) | I (ISU) |
|---|---|
| 30 | 1.6646E-09 |
| 100 | 6.1652E-08 |
| 353 | 2.7090E-06 |
| 857 | 3.8559E-05 |

## 3.4 Sensitivity analysis method of the temperature fluctuation.

The former section has shown how to convert a temperature fluctuation into power fluctuation. Now it is necessary to perform the conversion for each surface of the spacecraft and to sum up all contribution.

The sensitivity analysis is performed so as to determine what are the most critical surface element wrt the performance. The first phase is then to compute the maximum theoretical fluctuation allowed for each surface considered alone.

The second phase is to weight all the obtain temperature so as to obtain a total power performance equal to the requirement

### 3.4.1 first phase : method to compute the maximum theoretical fluctuation temperature for each surface element.

The total power reaching a detector is the linear sum of all the elementary power of each surface of the spacecraft.

$$\Delta P_{total} = \sum_{i=1}^{n\_surface} \Delta P_{surface(i)} \qquad [1]$$

$$\Delta P_{total} = \sum_{i=1}^{n\_surface} \frac{\Delta T_{surface(i)}}{2} * I^2 * I * IP_{surface(i)} * h * e_{surface(i)} \qquad [2]$$

n_surface :  number of fluctuating surfaces considered on the spacecraft.

Under this assumption the power allocation for each surface is the following :

$$\Delta P_{surface(i)} = a_i * \Delta P_{total} \quad [3]$$

$$\text{with} \quad \sum_{i=1}^{n\_surface} a_i = 1$$

The temperature allocation consists in  computing the temperature of each considered surface alone. This means that the considered surface will induce a power at detector level equal to the requirement. The procedure is then :

$$\Delta P_{total} = \frac{ASD_{requirement}}{\sqrt{t_{obs}}} \quad [4] \qquad \text{with} \qquad t_{obs} = 3600 \cdot \frac{FWHM[arc\min]}{2.5\,arc\min} \quad [5]$$

Then

$$\Delta T_{surface\_alone} = 2 * \Delta P_{total} /(I^2 * I * IP_{surface} * h * e_{surface}) \quad [6]$$

Then in order to take into account the other surfaces, this temperature has to be weighted.

3.4.2  second phase : method to weight the maximum theoretical fluctuation temperature for each surface element.

The sum of each individual surface contribution has to generate an amount of power at detector level lower than the requirement. Hence the weighted temperature fluctuation of each surface is

$$\Delta T_{surface} = a_i * \Delta T_{surface\_alone} \quad [7]$$

$$\text{with} \quad \sum_{i=1}^{n\_surface} a_i = 1$$

Rem the weighting coefficient are the same as the one used in former section:

## 3.5  RF coupling factor evaluation

### 3.5.1  Overall amount of relative power evaluation.

The TICRA RF expertise study (reference document [RD 1]) is producing the incident power or RF coupling factor from the structural element to the detector. The computed  values are detailed in table 2-1. Those RF coupling factor have not been recomputed for the new baffle configuration as far as the values are already very low and provide significant margin. Anyhow those value are an update wrt the PDR configuration.

The values presented in these tables correspond to the relative incident power exchanged between the detector and the corresponding element. The computation have been performed at 30 and 100 GHz only. At 857 GHz there's numerically no RF power exchanged between the detector and any of the spacecraft elements. This is due to the location in the center of the Focal plane unit of the 857 GHz and to its gaussian radiation pattern. Hence there's no self spacecraft emission at 857 GHz.

As a worst case  the 353 GHz incident power numerical value are considered to be the ones at 100 GHz.

The following table shows a significant difference between the relative power exchanged with a structural element inside or outside the baffle cavity.

| Structural element | Method used in analysis | Total relative power. Field from the 30 GHz LFI27 feed. | Total relative power. Field from the HFI_100_1 feed at 100 GHz |
|---|---|---|---|
| Baffle A | 1 | 0.000168 | 0.000457 |
| Baffle B | 1 | 0.000310 | 0.000536 |
| Baffle C | 1 | 0.000249 | 0.000220 |
| Baffle D | 1 | 0.000081 | 0.000111 |
| Baffle E | 1 | 0.000183 | 0.000164 |
| Baffle F | 1 | 0.000674 | 0.000404 |
| Baffle G | 1 | 0.000417 | 0.000304 |
| Baffle H | 1 | 0.000085 | 0.000178 |
| FPU | 1 | 0.000047 | 0.000124 |
| Hexagon side 2 | 1 | 0.000002 | 7.4E-7 |
| Groove 3 | 1 and 2 | 1.09E-7 (Method 1) | 1.95E-8 (Method 1) |
| Solar array | 2 | 5.5E-13 | 1.1E-14 |
| SVM shield | 2 | 4E-13 | 3.5E-15 |
| Side A of the SVM box | 2 | 8.6E-15 | 2.4E-18 |

table 2-3.5-1 : output of the TICRA RF expertise.

## 3.5.2 Relative power evaluation passing through the MLI.

The SVM is covered by a MLI for thermal purposes. This MLI is composed of 15 layers made of Aluminium with a thickness of 800 angströms (0.08$^e$-6 m). From the RF point of view these successive layers of thin metallic sheet have a frequency dependent behavior wrt the frequency range. The MLI has a transmission coefficient decreasing with the frequency.

This sub section introduces the detailed computation of the relative power passing through the MLI and going to the structural top of the SVM. In that case the emissivity of the structural element is 0.95.

The fist step consists in computing the equivalent number of skin depth (thickness) at each frequency.

| Frequency (GHz) | 30 | 100 | 353 | 857 |
|---|---|---|---|---|
| skin depth (m) | 4.770E-07 | 2.610E-07 | 1.390E-07 | 8.900E-08 |
| MLI thickness | 8.00E-08 | 8.00E-08 | 8.00E-08 | 8.00E-08 |
| Number of layer | 15 | 15 | 15 | 15 |
| total thickness (m) | 1.20E-06 | 1.20E-06 | 1.20E-06 | 1.20E-06 |
| Equivalent number of thickness | 2.52 | 4.60 | 8.63 | 13.48 |

The second step consists in computing the RF power attenuation knowing that for 1 skin depth the attenuation is $10 \times \log(e) = 10 / \ln(10) = 4.3$ dB.

| Power attenuation for 1 skin depth (dB) | 4.3 | 4.3 | 4.3 | 4.3 |
|---|---|---|---|---|
| Total power attenuation (dB) | 10.82 | 19.77 | 37.12 | 57.98 |

On final each relative power is computed through the MLI.
Rem : The relative power at 353 GHz is assumed to be the same as the one at 100 GHz (conservative approach).

| | 30 GHz | 100 GHz | 353 GHz |
|---|---|---|---|
| **Solar Array** | | | |
| Solar array top of MLI | 5.50E-13 | 1.10E-14 | 1.10E-14 |
| Solar array structural face (below the MLI) | 4.56E-14 | 1.16E-16 | 2.13E-18 |
| **SVM shield** | | | |
| SVM shield top of MLI | 4.00E-13 | 3.50E-15 | 3.50E-15 |
| SVM shield structural face (below the MLI) | 3.31E-14 | 3.69E-17 | 6.79E-19 |
| **SVM walls** | | | |
| Side A of SVM box top of MLI | 8.60E-15 | 2.40E-18 | 2.40E-18 |
| Side A of SVM structural face (below the MLI) | 7.12E-16 | 2.53E-20 | 4.66E-22 |

ALCATEL ALENIA SPACE
An Alcatel/Finmeccanica company

REFERENCE : H-P-3-ASP-AN-323

DATE : 12/2/2007

ISSUE : 3

Page : 27/126

## 3.6 Self spacecraft emission evaluation

### 3.6.1 Methodology to check the compliance with the specifications.

To check compliance with the specifications, which are given in terms of ASD [W/Hz$^{1/2}$], the following must be compared:

$$\Delta P_{\det ector} < \frac{ASD}{\sqrt{t_{obs}}} \qquad \qquad \Delta P = \frac{\Delta T}{2} * I^2 * I * IP * h * e$$

where:

$$t_{obs} = 3600 \cdot \frac{FWHM\,[arc\min]}{2.5\,arc\min}$$

$\Delta T$ is obtained by computing the ASD of the temporal thermal law over 7200 s.

Then $\Delta T = \dfrac{ASD(T(t))}{\sqrt{t_{obs}}}$

Hence the following value has to be compared to the requirements.

$$ASD(Power) = \frac{1}{2} * I^2 * I * IP * h * e * ASD(T(t))$$

## 3.6.2 Self spacecraft emission for Planck .

For each structural element of the SVM a time domain thermal law has been computed and Fourier transformed for the QR. The reference documents RD2 contain the thermal QR analysis..

For the PLM elements, the direct component at 1/60 Hz has been used.

The following table displays the comparison of the computed thermal deviation obtained at 1/60 Hz. The ASD thermal performance expressed in K/Hz^1/2 is divided by the observation defined for each channel. Then the corresponding ΔT at 1/60Hz is displayed for each channel.

In the following table the input for the PLM elements (PR, SR , groove 3) are not changed since the CDR. The other ones have been updated according to [RD 2].

| | ASD requirement at 1/60 Hz (K/Hz^1/2) | ASD performance at 1/60 Hz (K/Hz^1/2) | DT 1/60 Hz 30 GHz (mK) | DT 1/60 Hz 100 GHz (mK) | DT 1/60 Hz 353 GHz (mK) | DT 1/60 Hz 857GHz (mK) |
|---|---|---|---|---|---|---|
| PR circular central part | | | 0.2 | 0.2 | 0.2 | 0.2 |
| PR Upper part (moon limited part) | | | 1.3 | 1.3 | 1.3 | 1.3 |
| PR circular outer part | | | 1.1 | 1.1 | 1.1 | 1.1 |
| SR | | 6.00E-07 | 2.89E-03 | 5.00E-03 | 7.07E-03 | 7.07E-03 |
| BAFFLE | | | 45 | 5.00E-03 | 5.00E-03 | 45 |
| GROOVE 3 (baffle floor inside the optical cavity) | | | 45 | 45 | 45 | 45 |
| MLI OF THE SVM UPPER PANEL (+X Face) | 0.01 | 1.48E-06 | 6.78E-03 | 1.23E-02 | 1.74E-02 | 1.74E-02 |
| GROOVE 3 (outside the optical cavity) | 0.01 | 1.10E-04 | 5.05E-01 | 9.17E-01 | 1.30E+00 | 1.30E+00 |
| MLI of the SVM lateral panel (side of SVM box) | 0.01 | 1.02E-07 | 4.68E-04 | 8.50E-04 | 1.20E-03 | 1.20E-03 |
| Solar array +X face of the MLI | 0.01 | 2.81E-07 | 1.29E-03 | 2.34E-03 | 3.31E-03 | 3.31E-03 |

Table 3.6-1 : spacecraft temperature results from thermal analysis (see RD2)

The following tables display the ASD computed using the data coming from the thermal analysis. Only the surface element inside the optical cavity are taken into account. This choice is justified because the impact of the element oustide the optical cavity is many order of magnitude lower than the one inside the optical cavity.

A system contingency is defined as 20% of the requirement This system contingency is then summed up in order to obtain the total performance.

| | F (GHz) | λ mm | Eta | I(SI) | tobs (s) |
|---|---|---|---|---|---|
| | 30 | 10 | 1 | 1.66E-09 | 47520 |
| | | | | | |
| | | | | | |
| | | | | | |
| | | | | | |
| | | DT | Emissivity | | ASD |
| | | Performance | of the | IP | Performance |
| | | at 1/60 Hz | surface | | (W/Hz^0,5) |
| | | μK | | | |
| PR circular central part | | 0.2000 | 0.02 | 2.58E-01 | 4.67E-20 |
| PR Upper part | | 1.3000 | 0.02 | 6.14E-04 | 7.22E-22 |
| PR Circular outer part | | 1.1000 | 0.02 | 2.58E-01 | 2.57E-19 |
| SR | | 0.0029 | 0.02 | 1.00E+00 | 2.62E-21 |
| Baffle | | 45.0000 | 0.05 | 2.17E-03 | 8.83E-20 |
| Groove 3 (baffle floor inside the optical cavity) | | 45.0000 | 0.05 | 2.00E-06 | 8.14E-23 |
| | | | | | |
| | | | | | |
| system contingency (20%) | | | | | 6.80E-19 |
| TOTAL ASD (W/Hz^0,5) | | | | | 1.08E-18 |
| ASD SPEC (W/Hz^0,5) | | | | | 3.40E-18 |

table 3.6-2 : 30 GHz channel ASD performance display (worst case component at 1/60 Hz).

| | F (GHz) | l mm | Eta | I(SI) | tobs (s) |
|---|---|---|---|---|---|
| | 100 | 3.00E+00 | 0.3 | 6.16E-08 | 14400 |
| | | | | | |
| | | | | | |
| | | | | | |
| | | DT | Emissivity | | ASD |
| | | Performance | of the | IP | Performance |
| | | at 1/60 Hz | surface | | (W/Hz^0,5) |
| | | mK | | | |
| PR circular central part | | 0.2 | 2.00E-02 | 0.258 | 1.14428E-19 |
| PR Upper part | | 1.3 | 2.00E-02 | 0.000614 | 1.77009E-21 |
| PR Circular outer part | | 1.1 | 2.00E-02 | 0.258 | 6.29355E-19 |
| SR | | 0.005 | 0.02 | 1 | 1.1088E-20 |
| Baffle | | 45 | 0.05 | 0.0021700 | 4.87234E-20 |
| Groove 3 (baffle floor inside the optical cavity) | | 45 | 0.05 | 0.0000020 | 4.49064E-23 |
| | | | | | |
| | | | | | |
| system contingency (20%) | | | | | 4.2E-19 |
| TOTAL ASD (W/Hz^0,5) | | | | | 1.22541E-18 |
| ASD SPEC (W/Hz^0,5) | | | | | 2.1E-18 |

table 3.6-3 : 100 GHz HFI channel ASD performance display (worst case component at 1/60 Hz).

| | F (GHz) | l mm | Eta | I(SI) | tobs (s) |
|---|---|---|---|---|---|
| | 353 | 8.50E-01 | 0.3 | 2.70E-06 | 7200 |
| | | | | | |
| | | | | | |
| | | | | | |
| | | DT | Emissivity | | ASD |
| | | Performance | of the | IP | Performance |
| | | at 1/60 Hz | surface | | (W/Hz^0,5) |
| | | mK | | | |
| PR circular central part | | 0.2 | 2.00E-02 | 0.258 | 6.40588E-20 |
| PR Upper part | | 1.3 | 2.00E-02 | 0.000614 | 9.90925E-22 |
| PR Circular outer part | | 1.1 | 2.00E-02 | 0.258 | 3.52323E-19 |
| SR | | 0.00707 | 0.02 | 1 | 8.77705E-21 |
| Baffle | | 45 | 0.05 | 0.00217 | 1.21228E-19 |
| Groove 3 (baffle floor inside the optical cavity) | | 45 | 0.05 | 0.000002 | 1.1173E-22 |
| | | | | | |
| | | | | | |
| system contingency (20%) | | | | | 4.2E-19 |
| TOTAL ASD (W/Hz^0,5) | | | | | 9.67E-19 |
| ASD SPEC (W/Hz^0,5) | | | | | 2.1E-18 |

table 3.6-4 : 353 GHz  channel ASD performance display (worst case component at 1/60 Hz).

As far as there's no RF power exchanged between the detector and the spacecraft surfaces there's no self spacecraft emission level at 857 GHz from a numerical point of view.

As a conclusion the self spacecraft emission level is well below the requirements.

# 4. SELF SPACECRAFT EMISSION LEVEL CONCLUSIONS.

The section 3.6.2 shows two main results. The first one is that th e self spacecraft emission level is driven by the PLM elements contained inside the baffle cavity. The synthesis table (3.6-2 & 3.6-3 & 3.6-4) show a performance lower than the requirement which is recalled hereafter :

\*\*\*\*\*\*\*\*\*\*\*\*\*\*\*\*\*\*\*\*\*\*\*\*\*\*\*\*\*\*\*\*\*\*\*\*\*\*\*\*\*\*\*\*\*\*\*\*\*\*\*\*\*\*\*\*\*\*

The ASD ( in Watts / √Hz ) of each frequency component  between
0.01 Hz and 100 Hz shall be such that :

| Frequency [ GHz ] | ASD [ Watt / √Hz ] |
|---|---|
| 30 | < 3.4 E-18 X |
| 100 ( LFI ) | < 1.1 E-17 X |
| 100 ( HFI ) | < 2.1 E-18 X |
| 353 | < 1.8 E-18 X |
| 857 | < 2.2 E-17 X |

**Note :**

X is equal to one for any frequency component  fo  of the fluctuation source synchronous with the Planck S/C spinning rate ( i.e. multiple of f.spin = 1 / 60 Hz ).

Otherwise , X = ( B * t.obs * Delta.f ) , where  Delta.f = fo – k * f.spin and k is chosen to minimise Delta.f .
t.obs = 3600 * FWHM / 2.5 arcmin  , and FWHM is the angular resolution of the antenna radiation pattern in arc minutes .

# 5. ANALYSIS OF THE RESULTS OF THE 4 PI COMPUTATIONS WITH THE BAFFLE EXTENSION USING INSTRUMENT FEED MODEL (4PI-EXT BAF-INST FEED)

This section presents the re-run of the TICRA grasp file where the gaussian feed models have been replaced by the computed radiation pattern of the actual feed (QM or FM). No other parameters have been changed. The feeds are located at the same position with the same polarization orientation at detector level for the polarized detector. In other word all geometrical elements are defined in [RD 5] and the RF feed models are defined in [RD 6] and [RD 7].

In addition for each frequency, two computations have been performed : one for each polarization of the detector in the focal plane in line with the detector orientation provided by the instruments.

Then the sub area where the Moon is located (half cone angle of 32° along the spacecraft spin axis) is extracted. The maximum directivity within this area is labelled the Edge of Cone (EOC) directivity. This directivity is then compared to the maximum on axis gain in order to obtain the achieved rejection.

The same process is applied for the Earth and Sun.

The modeling are performed using the up to date available data (see [RD 6] and [RD 7]). Hence the following data have been used :
- 30 GHz LFI detector radiation pattern (see [RD 6]) , dual orthogonal polarization
- 100 GHz HFI horn pattern (see [RD 7]) , dual orthogonal polarization
- 353 GHz HFI horn pattern (see [RD 7 ])
- 857 GHz no computation as far as multi moded horn characteristic is not available.

On final a table summarizes the performances for the rejection toward Earth Sun and Moon.

## 5.1  30 GHz Pattern analysis(4pi-ext baf-inst feed)

The following figure (fig 5.1-1) displays the 4 PI radiation pattern of the LFI 30 GHz radiation pattern inserted in the Planck geometry. The computation is  performed as explained in  (RD 8]. The numerical computation is performed as different sequence of ray combination or physical optics local computations. Then all elementary pattern are recombined so as to provide the 4 Pi radiation pattern. As visible on the following figure a sub pattern (see square shape) located between phi values of 90° to 105° and theta values of 97.5° to 122.5° is badly located. The error is not located in the computation itself but in the parameters setting of the different pattern window size. Unfortunatelly the investigation are not over for the release of this document.

Anyhow all pattern corresponding to all elementary ray combination are computed and ready to be recombined.
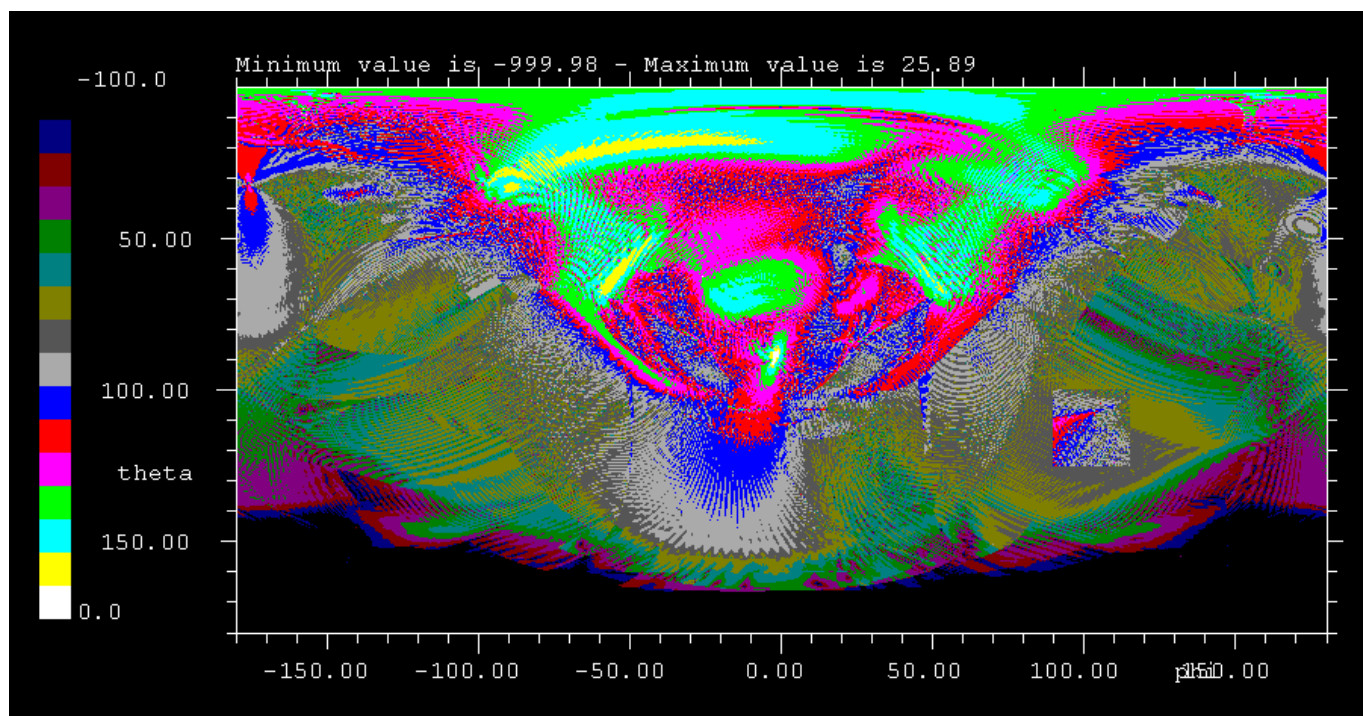


Figure 5.1-1 : 4PI diagram , phi : -180°, 180° / theta : 0,+180° / levels in directivity displayed from -100 dBi  to +0 dBi  (first component, Xpol)
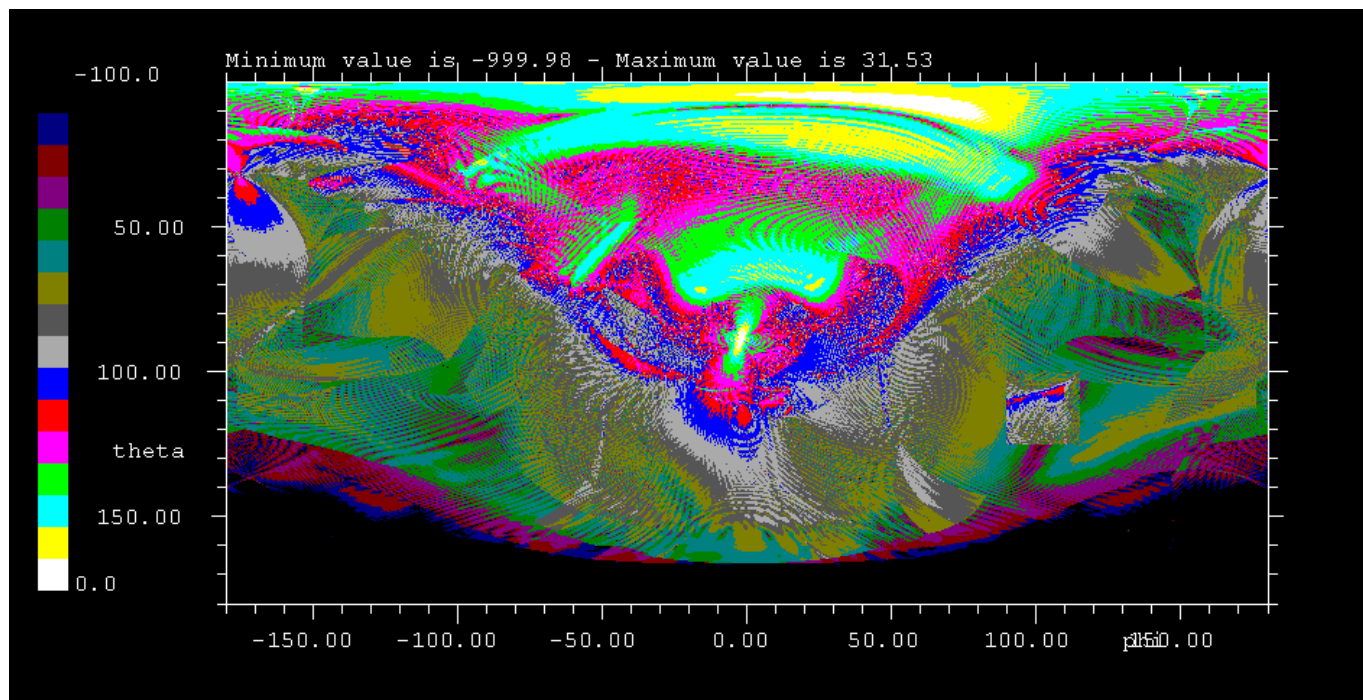
Figure 5.1-2 : 4PI diagram , phi : -180°, 180° / theta : 0,+180° / levels in directivity displayed from -100 dBi to +0 dBi (second component, co-pol)
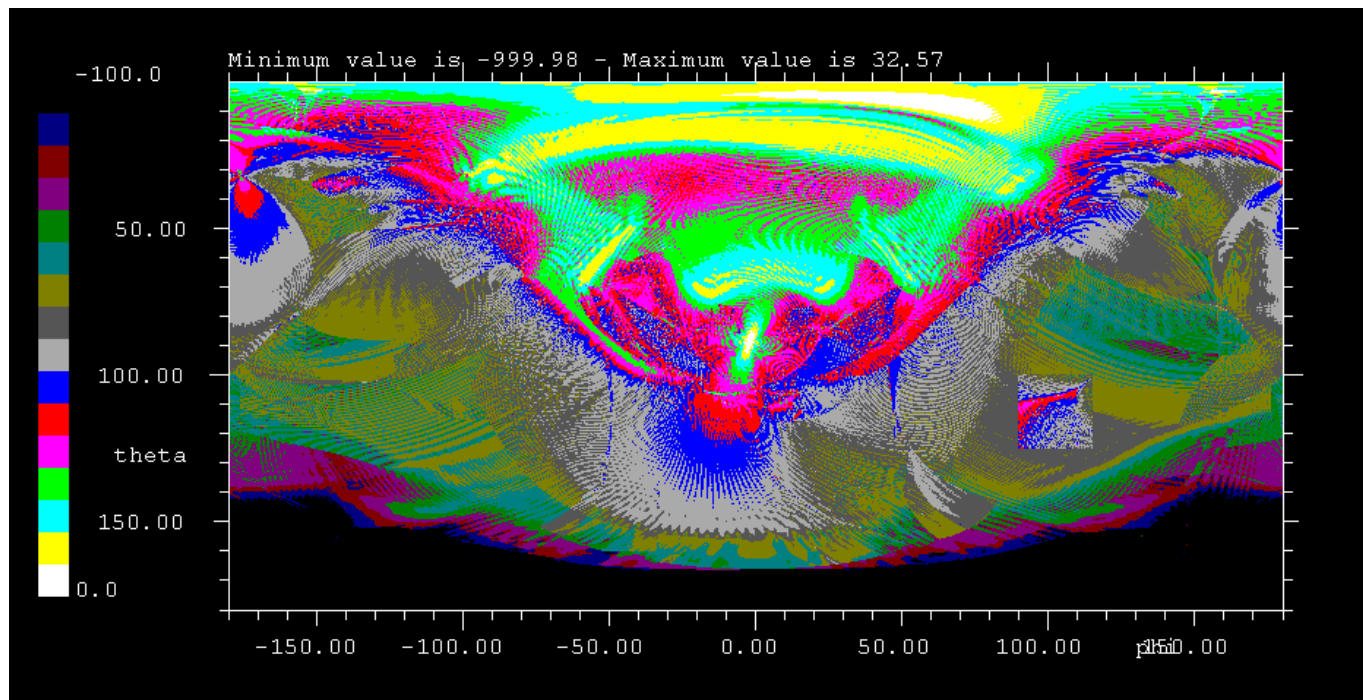


Figure 5.1-3 : 4PI diagram , phi : -180°, 180° / theta : 0,+180° / levels in directivity displayed from -100 dBi to +0 dBi (local major/minor component)

## 5.2 100 GHz Pattern analysis(4pi-ext baf-inst feed) 1$^{st}$ detector polarisation orientation

The detector phase center is located in the RDP coordinate such that :

x:-47.57 mm, y:-32.966 mm, z: 14.847 mm

The X_axis vector of the detector coordinate system is :
x_axis  (x:  0.99540745  , y:-0.00331985, z:-0.09567128)
The Y_axis vector :
y_axis  (x:-0.00331985, y: 0.99760016  , z:-0.06915857)
The Z_axis vector :
z_axis : (x :0.09567128 , y: 0.06915857  , z:-0.99300760)

For the 1$^{st}$ detector polarization orientation, the polarization vector of the feed is oriented along the Y axis.
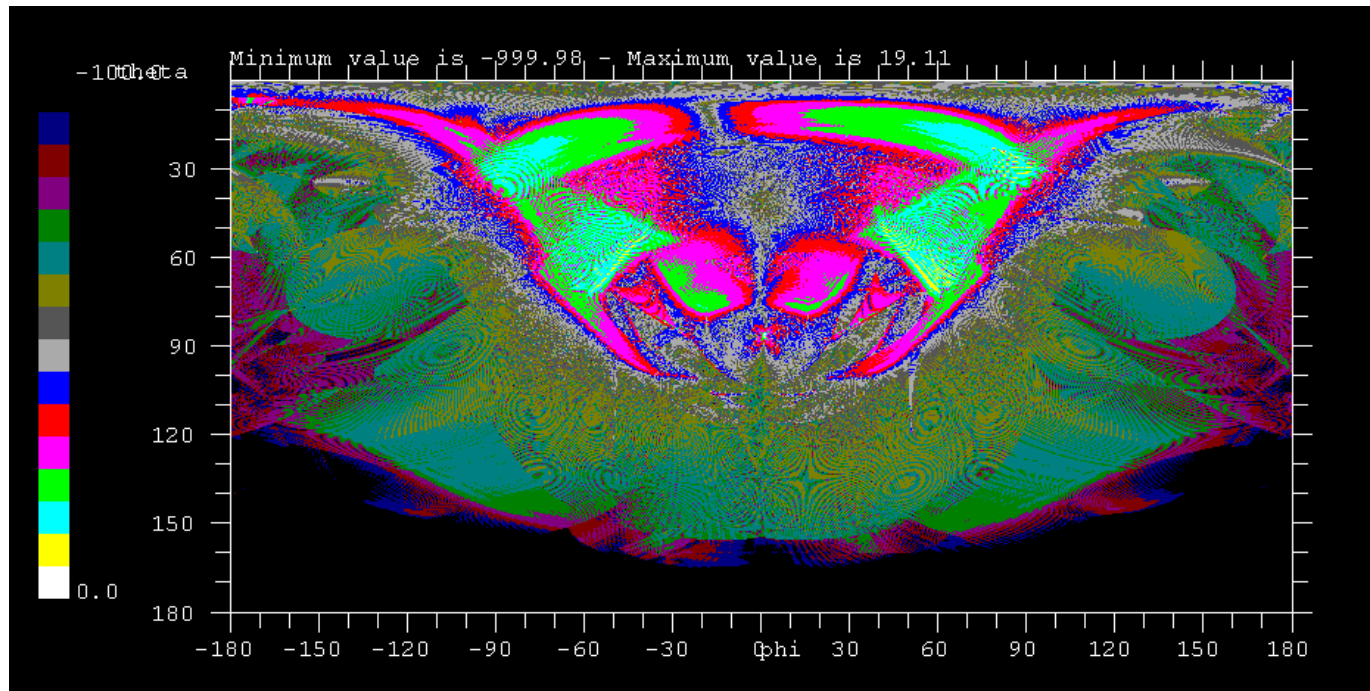


Figure 5.2-1 : 4PI diagram , phi : -180°, 180° / theta : 0,+180° / levels in directivity displayed  from -100 dBi   to +0 dBi   (first component, Xpol)
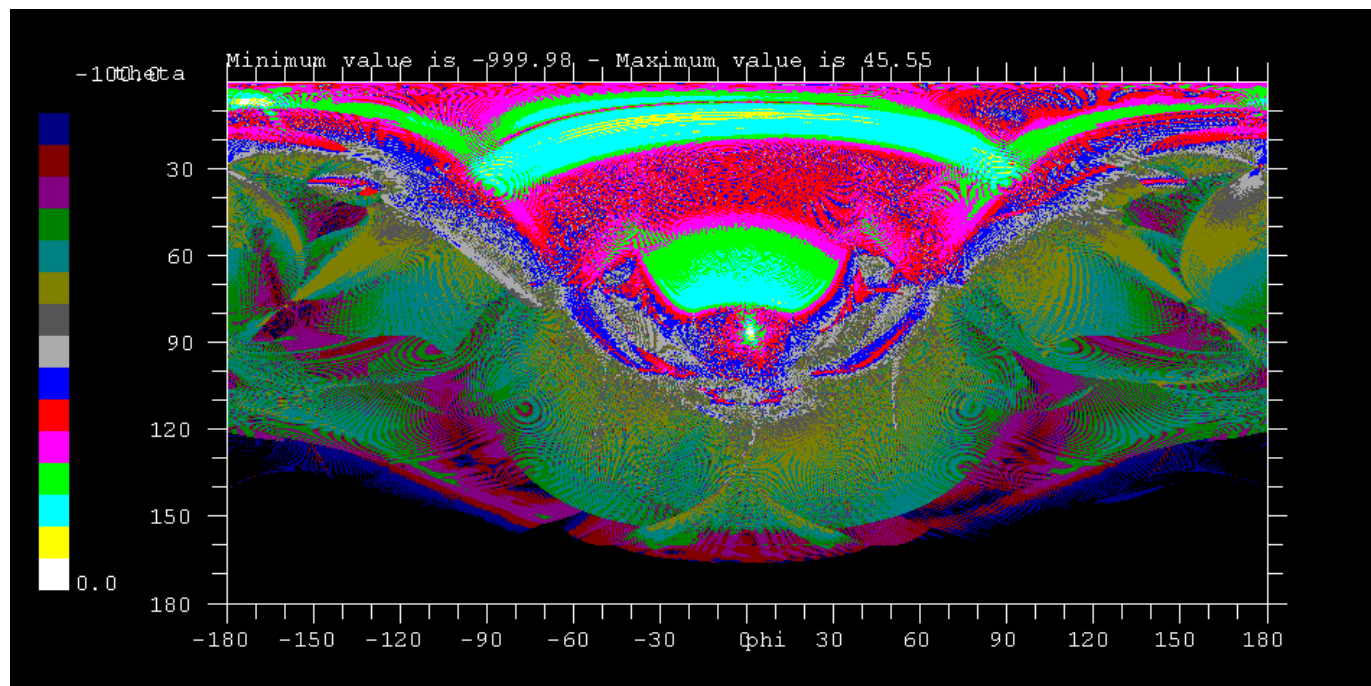
Figure 5.2-2 : 4PI diagram , phi : -180°, 180° / theta : 0,+180° / levels in directivity displayed from -100 dBi to +0 dBi (second component, co-pol)
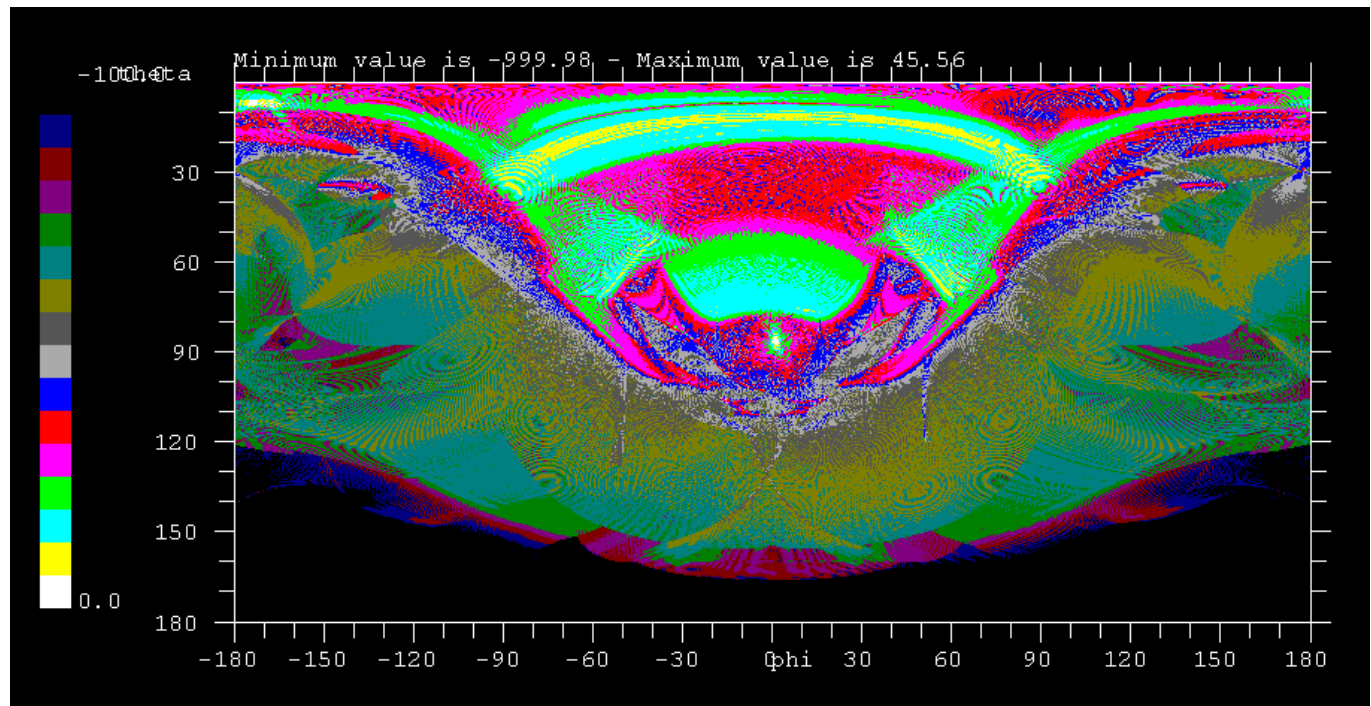


Figure 5.2-3 : 4PI diagram , phi : -180°, 180° / theta : 0,+180° / levels in directivity displayed from -100 dBi to +0 dBi (local major/minor component)
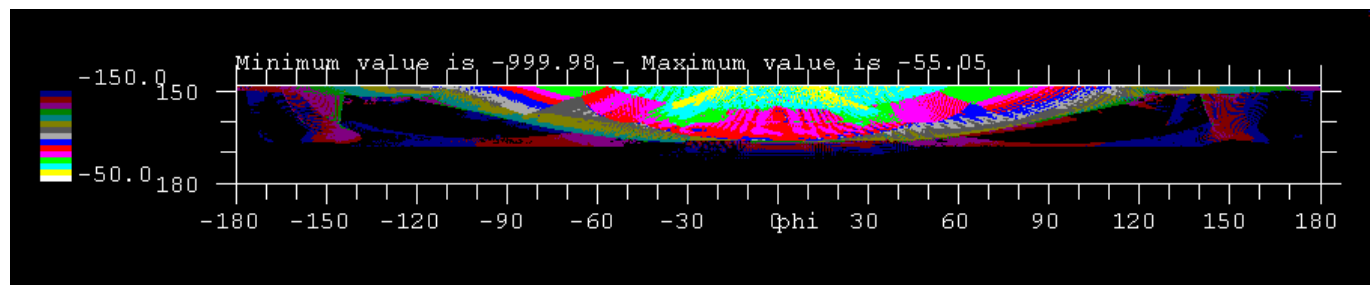
Figure 5.2-4 : Moon area    phi : -180°, 180° / theta : +148°,+180° / levels in directivity displayed from -150 dBi  to -50 dBi
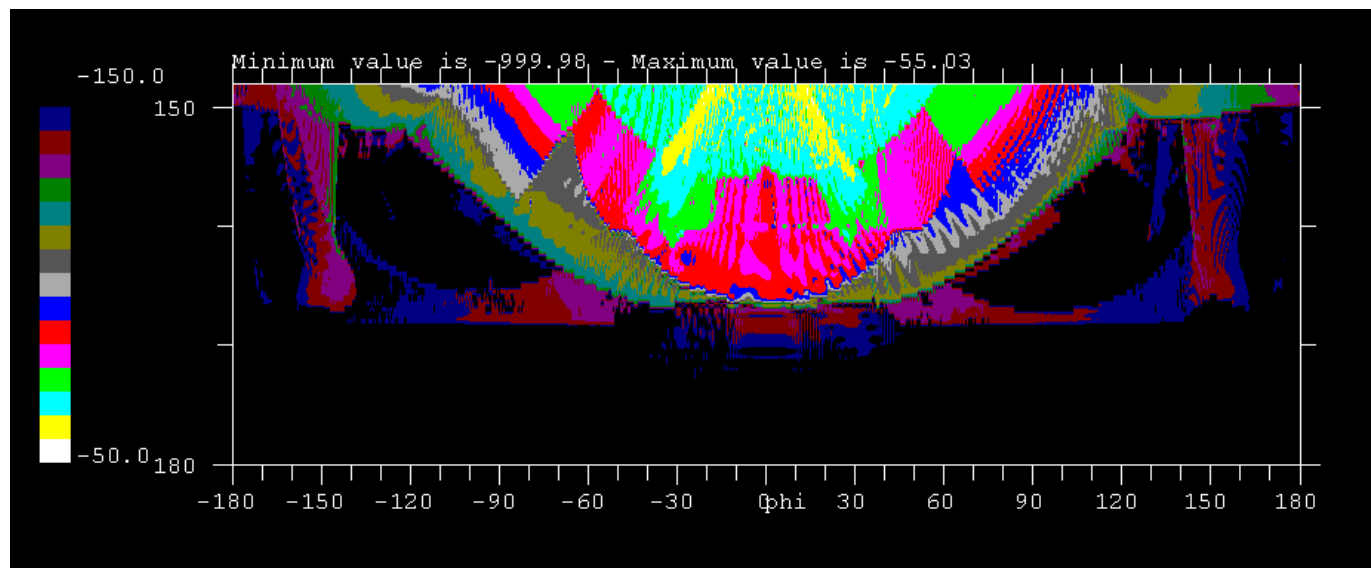


Figure 5.2-5 : enlarged Moon area    phi : -180°, 180° / theta : +148°,+180° / levels in directivity displayed from -150 dBi  to -50 dBi (local major/minor component)
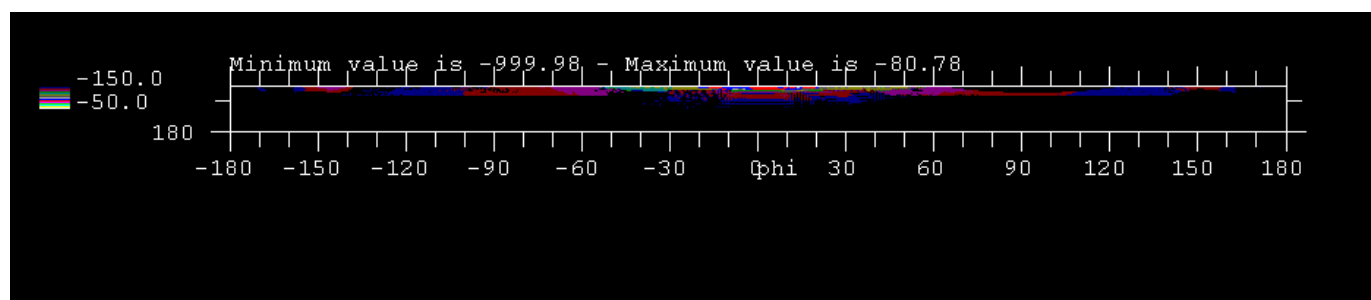


Figure 5.2-6 : Earth area    phi : -180°, 180°  /  theta : +165°,+180°  / levels in directivity displayed  from -150 dBi to -50dBi (local major/minor component)
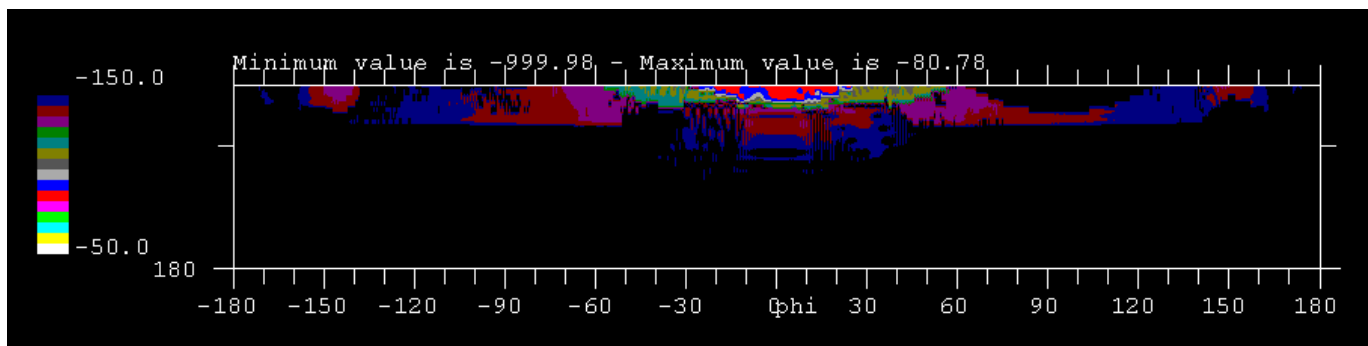
Figure 5.2-7 : Enlarged Earth area phi : -180°, 180° / theta : +165°,+180° / levels in directivity displayed from -150 dBi to -50dBi (local major/minor component)
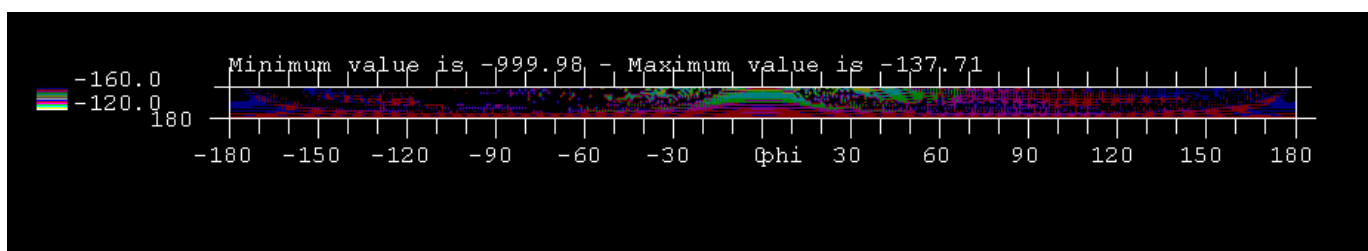


Figure 5.2-8 : Sun area phi : -180°, 180° / theta : +170°,+180° / levels in directivity displayed from -1600 dBi to -120dBi (local major/minor component
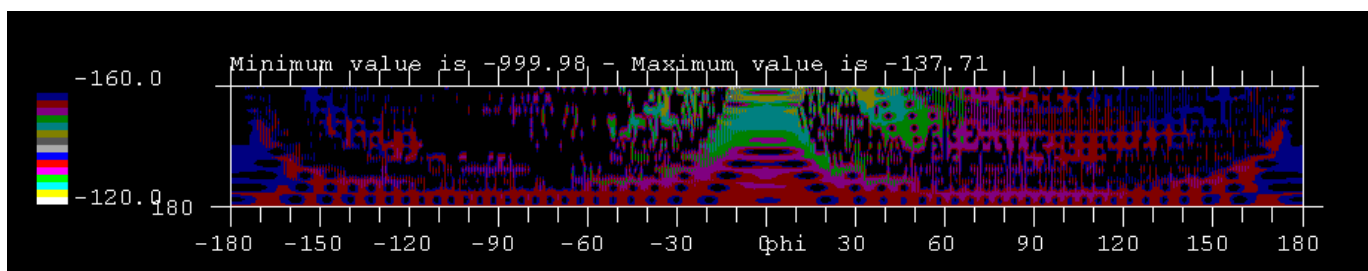


Figure 5.2-9 : Sun area phi : -180°, 180° / theta : +170°,+180° / levels in directivity displayed from -160 dBi to -120dBi (local major/minor component

Only the main lobe area is over the -65 dB rejection.

## 5.3 100 GHz Pattern analysis(4pi-ext baf-inst feed) 2nd detector polarisation orientation

The detector phase center is located in the RDP coordinate such that :

x:-47.57 mm, y:-32.966 mm, z: 14.847 mm

The X_axis vector of the detector coordinate system is :
x_axis  (x:  0.99540745 , y:-0.00331985, z:-0.09567128)
The Y_axis vector :
y_axis  (x:-0.00331985, y: 0.99760016  , z:-0.06915857)
The Z_axis vector :
z_axis : (x :0.09567128 , y: 0.06915857  , z:-0.99300760)

For the 2nd  detector polarization orientation, the polarization vector of the feed is oriented along the X axis.
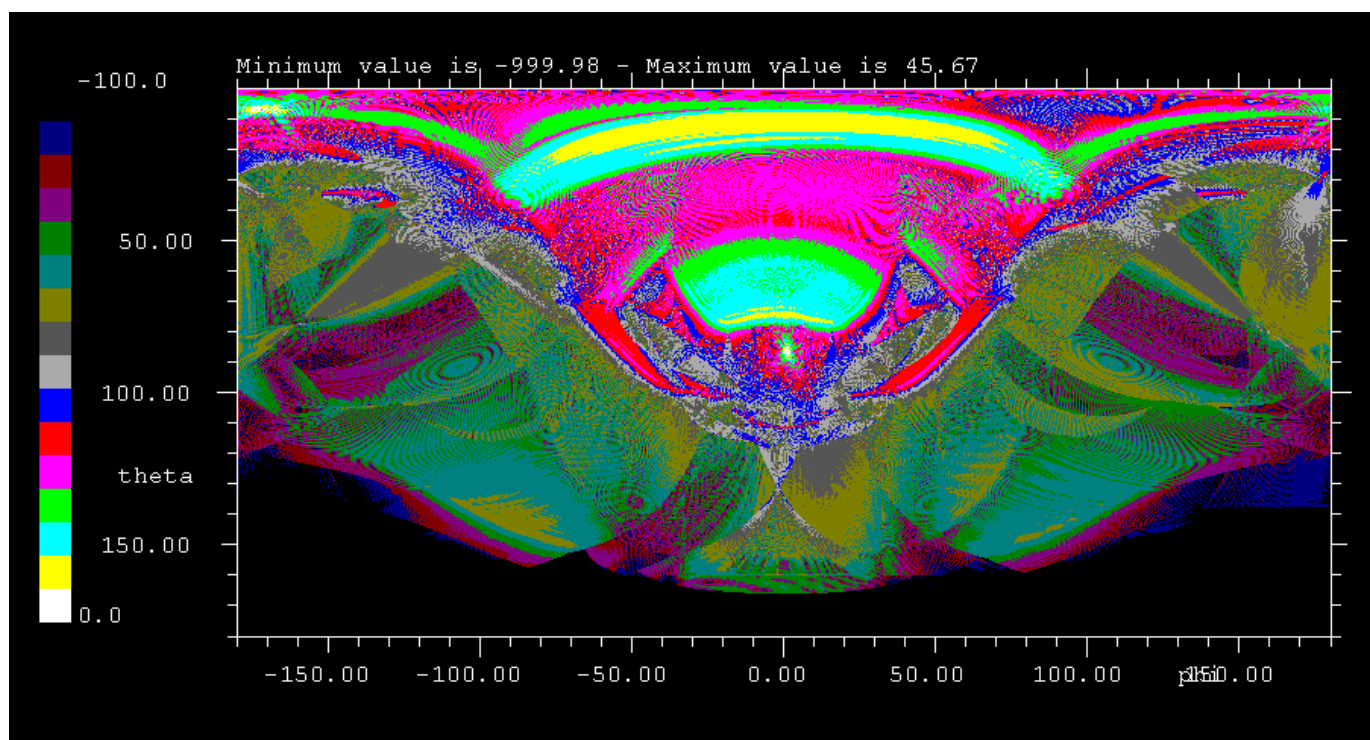


Figure 5.3-1 : 4PI diagram , phi : -180°, 180° / theta : 0,+180° / levels in directivity displayed from -100 dBi  to +0 dBi  (first component, Xpol)

ALCATEL ALENIA SPACE
An Alcatel/Finmeccanica company
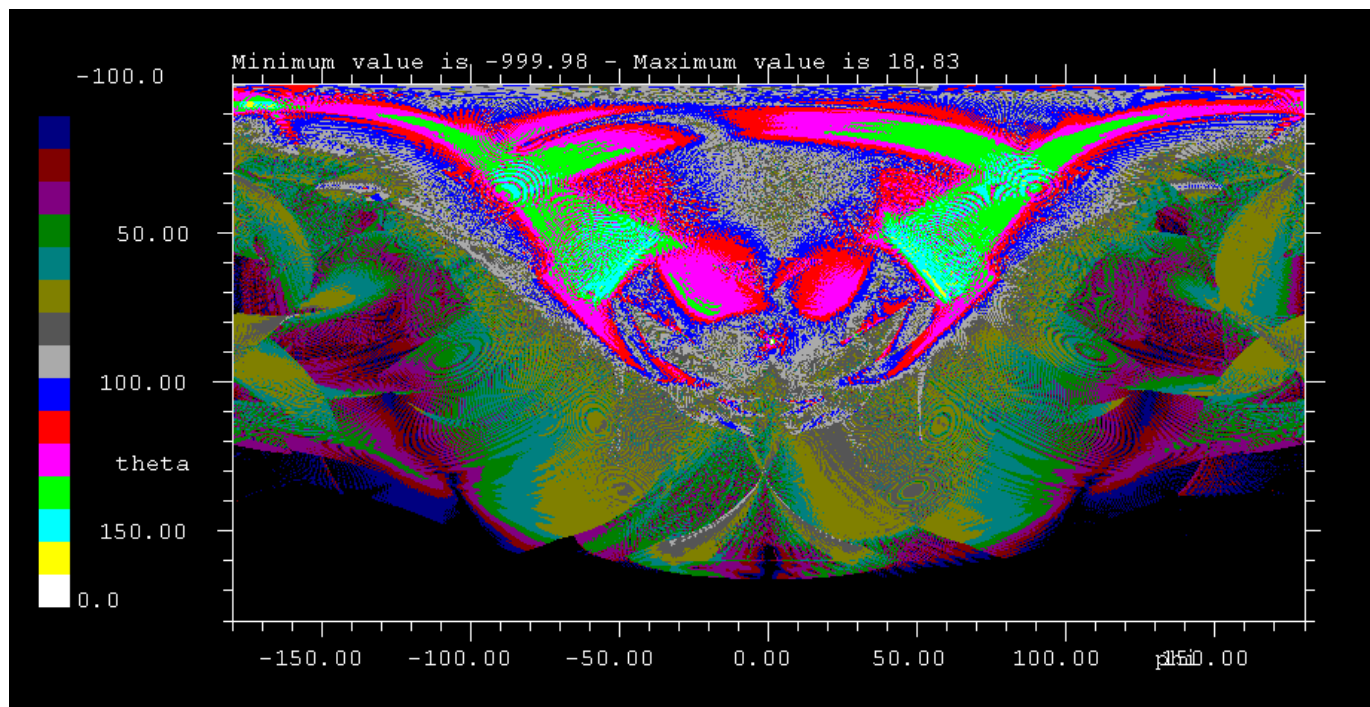


Figure 5.3-2 : 4PI diagram , phi : -180°, 180° / theta : 0,+180° / levels in directivity displayed from -100 dBi to +0 dBi (second component, co-pol)
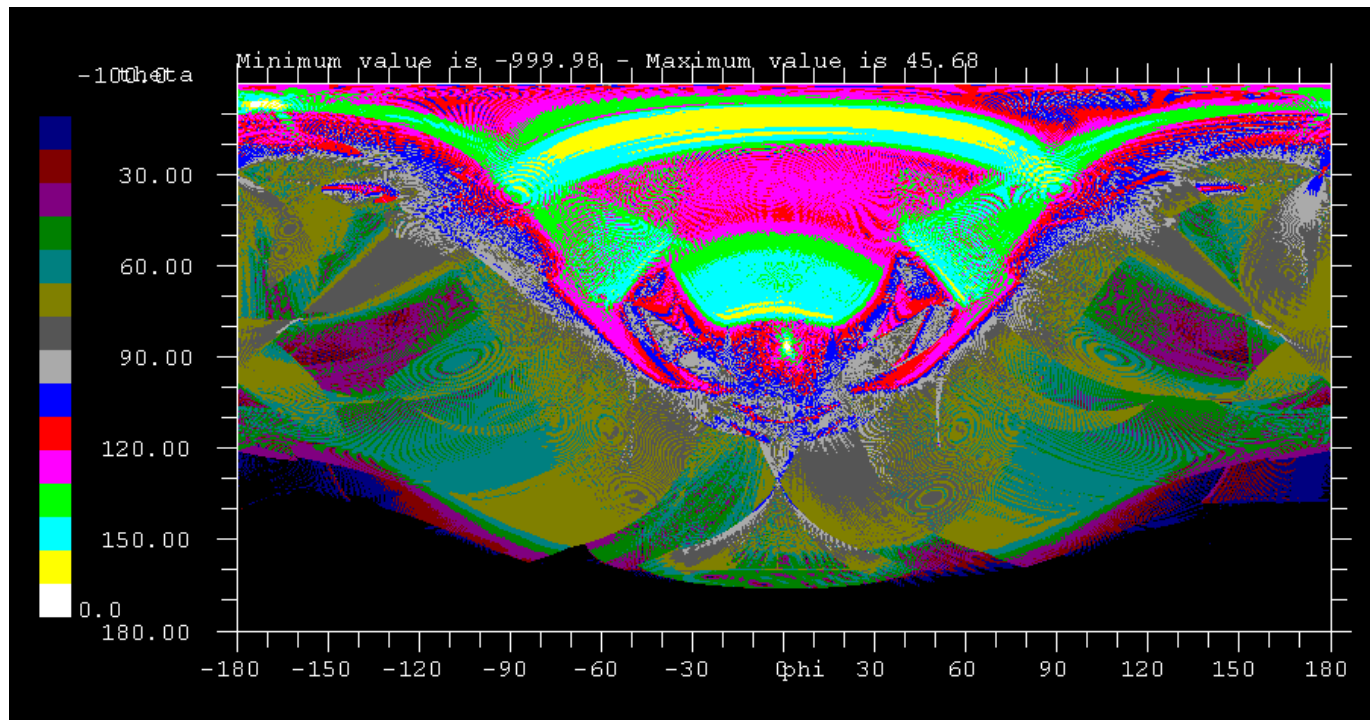


Figure 5.3-3 : 4PI diagram , phi : -180°, 180° / theta : 0,+180° / levels in directivity displayed from -100 dBi to +0 dBi (local major/minor component)
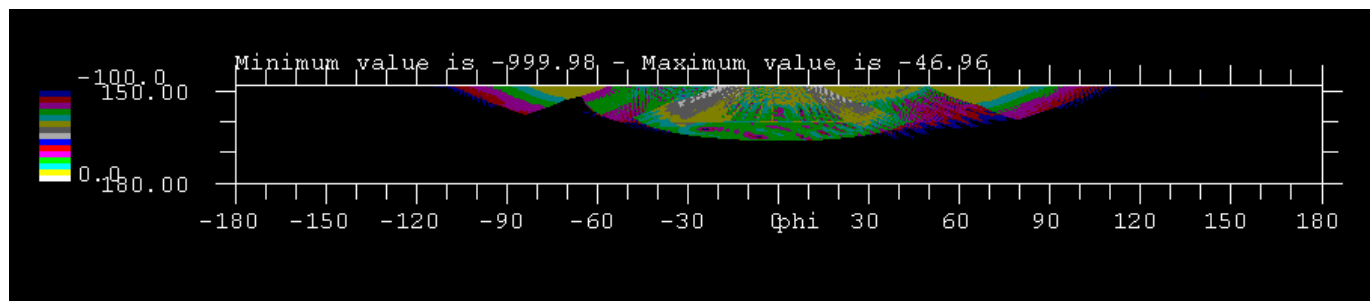
Figure 5.3-4 : Moon area       phi : -180°, 180° / theta : +148°,+180° / levels in directivity displayed from -150 dBi  to -50 dBi
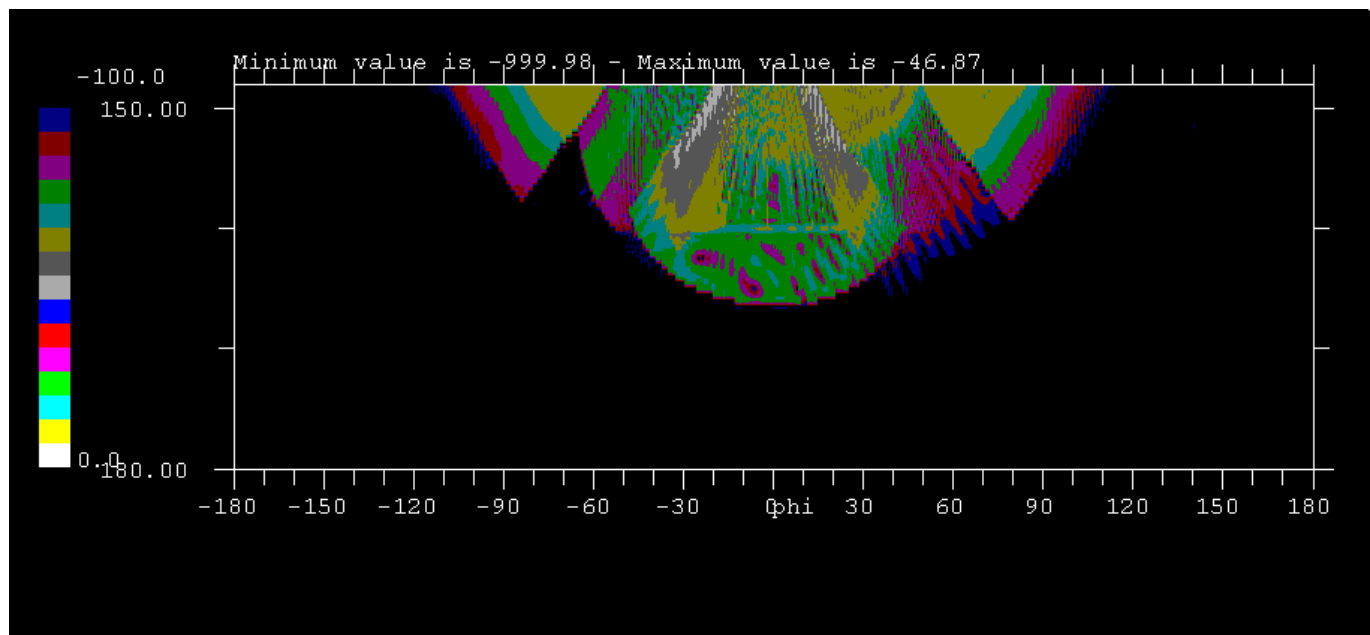


Figure 5.3-5 : enlarged Moon  area phi : -180°, 180° / theta : +148°,+180° / levels in directivity displayed from -100 dBi to 0 dBi (local major/minor component)
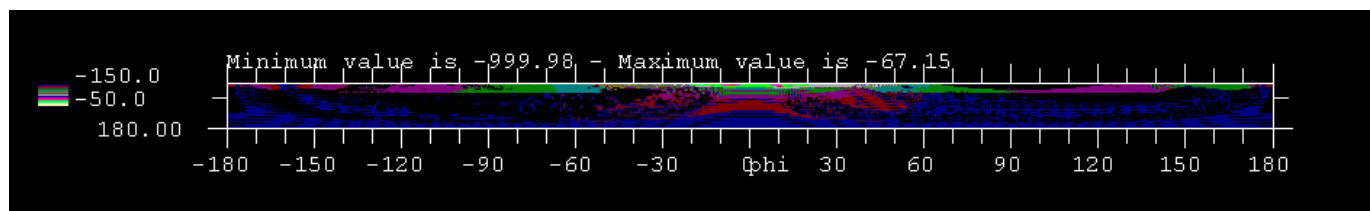


Figure 5.3-6 : Earth area       phi : -180°, 180° / theta : +165°,+180° / levels in directivity displayed  from -150 dBi to -50dBi (local major/minor component)
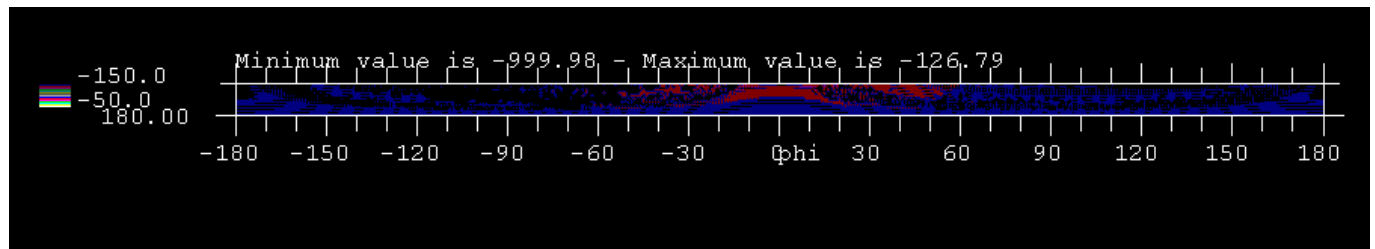
Figure 5.3-7 : Sun area phi : -180°, 180° / theta : +170°,+180° / levels in directivity displayed from -150 dBi to -50dBi (local major/minor component

## 5.4 100 GHz pattern preliminary comparison

As far as the 100 GHz 4 pi pattern have been computed for two orthogonal polarization orientations at the focal plane level, it is then possible to compare the difference on the overall pattern.

The comparison is performed on the pattern expressed in local major/minor polarisation component. Only the major axis of polarisation ellipse is displayed and compared.

The comparison consists in computing the ratio between the major polarization axis of each pattern. The first pattern is computed as described in section 5.2 for the first polarization orientation of the detector. The second pattern is computed for the orthogonal polarization orientation (see section 5.3).

The pattern difference is performed by computing the linear ratio for each direction between the first and second pattern. Then the display is performed in dB. For graphical purpose the ratio has been performed twice (fist / second) then (second / first). This is useful to obtain only coloured pixel of interest on the plots. For instance the pattern difference is plotted over a dB range (eg ratio variation from -20 dB to -10 dB and +10 dB to +20 dB). In both cases the values over the upper limit are plotted in black pixels and the values below the lower limit are plotted as red pixels. Then all red pixels have to be disgarded or considered as black for graphical readibility.

The figure 5.4-1 shows that very few pixels are impacted by more than 30 dB gain variation. Such variation can be attributed to the coarse meshing of 0.5° by 0.5°. The highest variation are obtained in the Earth Sun and Moon cone are (theta values varying from 148° to 180°).

The figure 5.4-3 displays some quasi continuous area (not only isolated pixel) where the gain variation is between (+10 dB and +20 dB) and (-20 dB and -10 dB). This area is located between phi=-150° and phi=-100° and theta=70° to theta=90°.

On final the figure 5.4-4 and 5.4-5 show that almost all pattern direction are affected by the polarization detector orientation change  by a value of 10 dB.

As a conclusion a raw result is that the detector polarization rotation by 90° generate a pattern global pattern difference of 10 dB on the far out side lobes.

ALCATEL ALENIA SPACE
An Alcatel/Finmeccanica company

REFERENCE : H-P-3-ASP-AN-323

DATE : 12/2/2007

ISSUE : 3

Page : 44/126
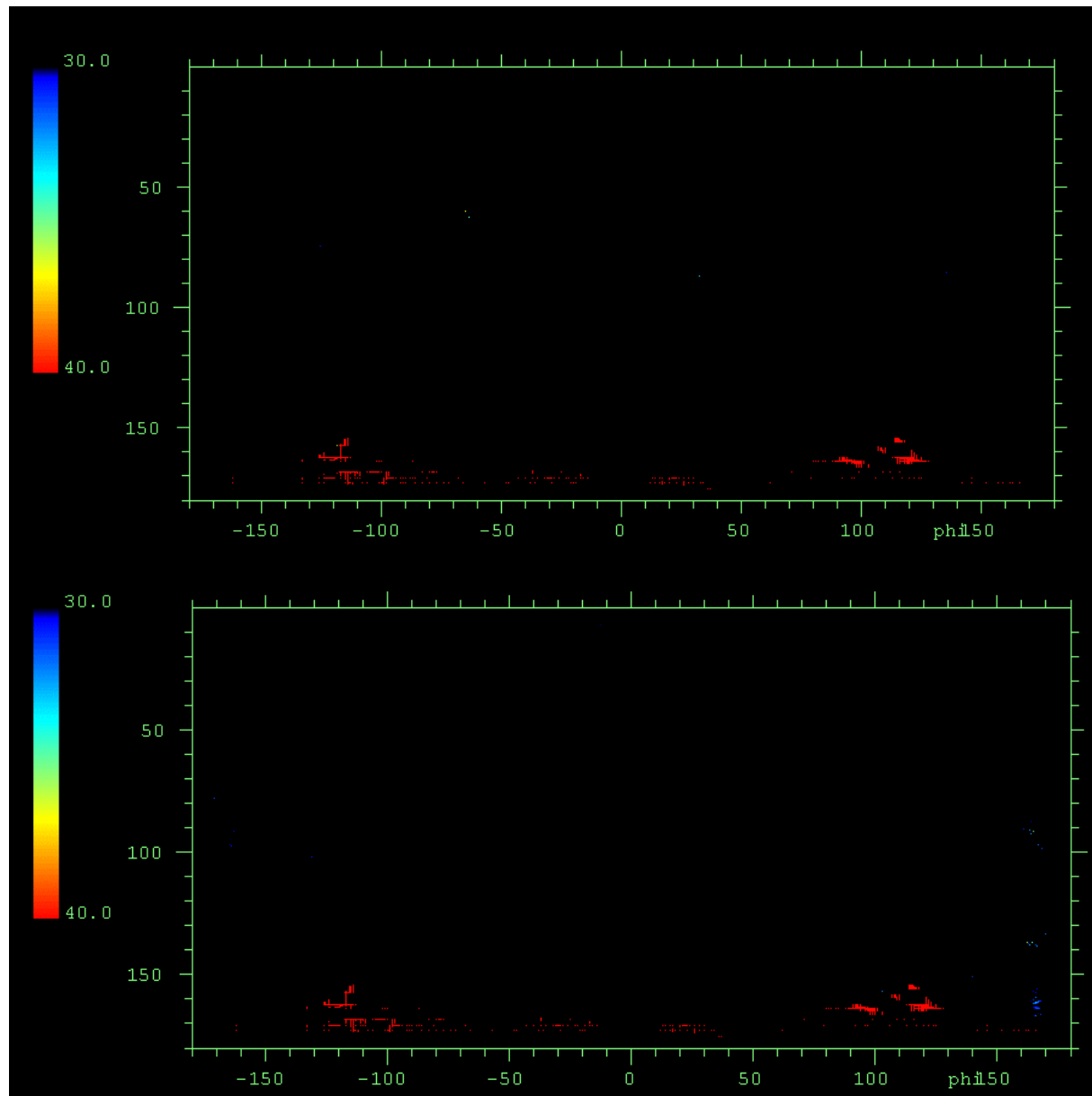
Figure 5.4-1 : local area modified by more than 30 dB (red pixels to be disgarded)

ALCATEL ALENIA SPACE
An Alcatel/Finmeccanica company

REFERENCE : H-P-3-ASP-AN-323

DATE : 12/2/2007

ISSUE : 3

Page : 45/126
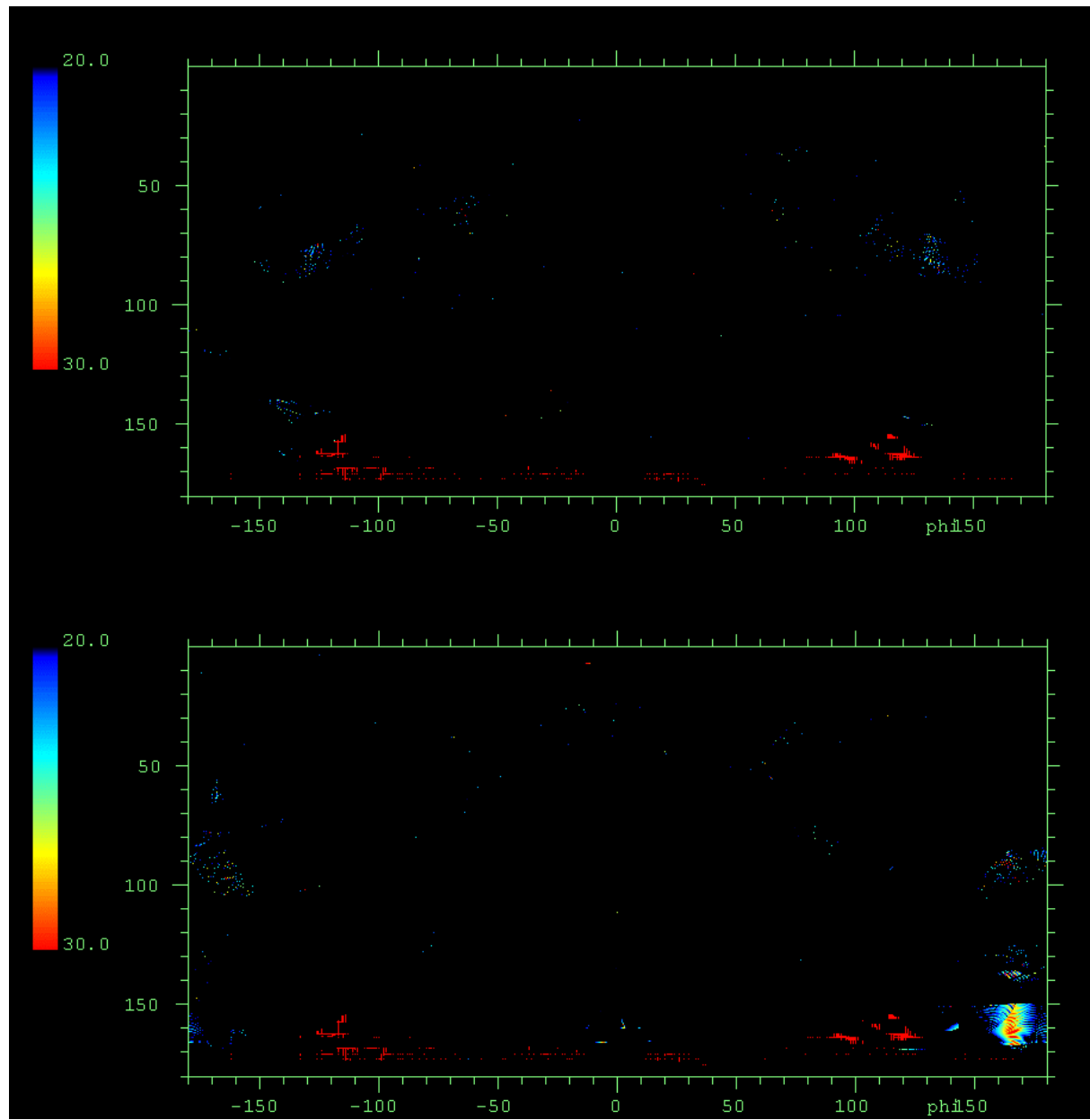
Figure 5.4-2 : local area modified by more than 20 dB (red pixels to be disgarded).
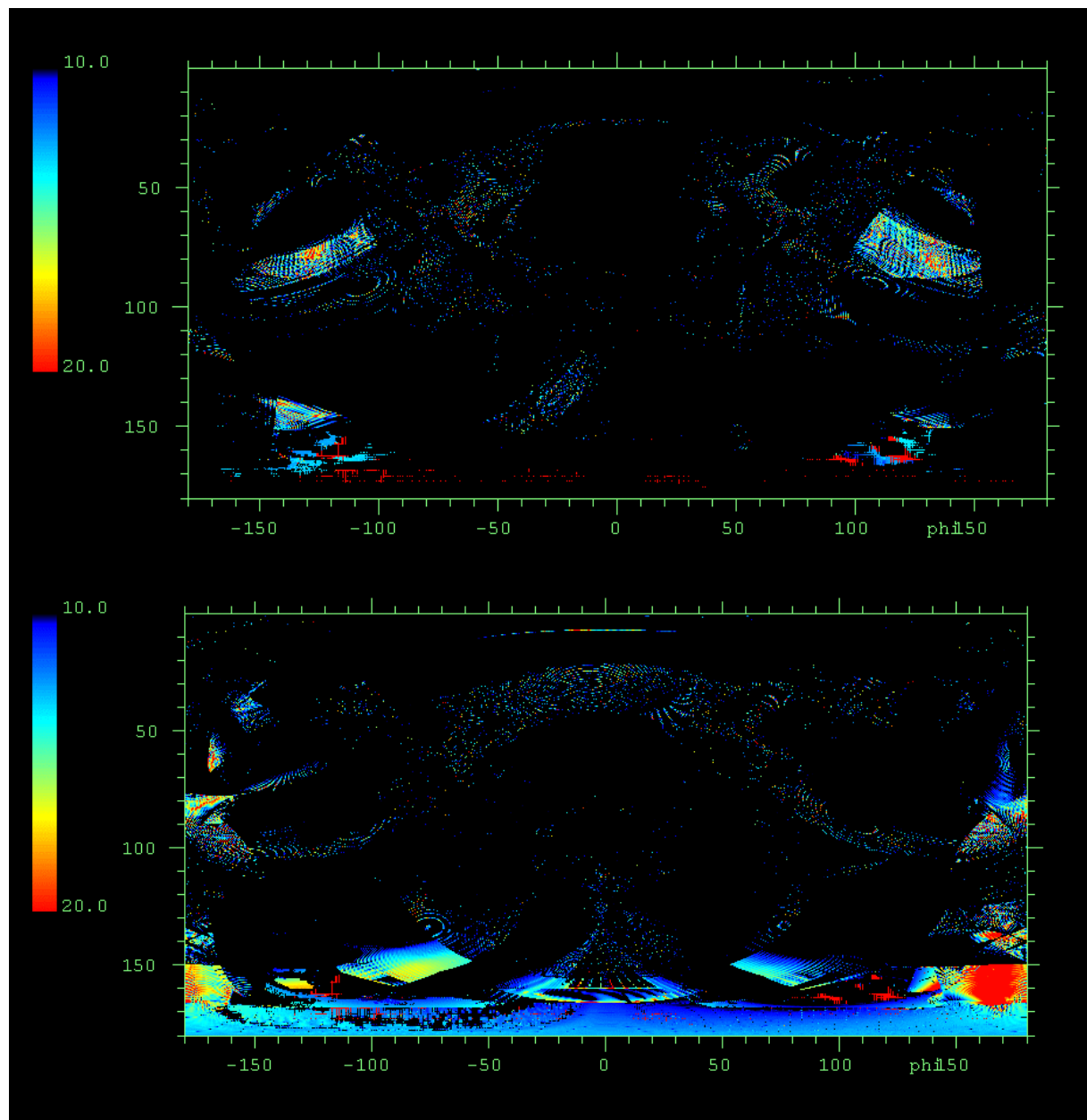
Figure 5.4-3 : local area modified by more than 10 dB   and  no  more  than  20  dB  (red pixels to be disgarded)
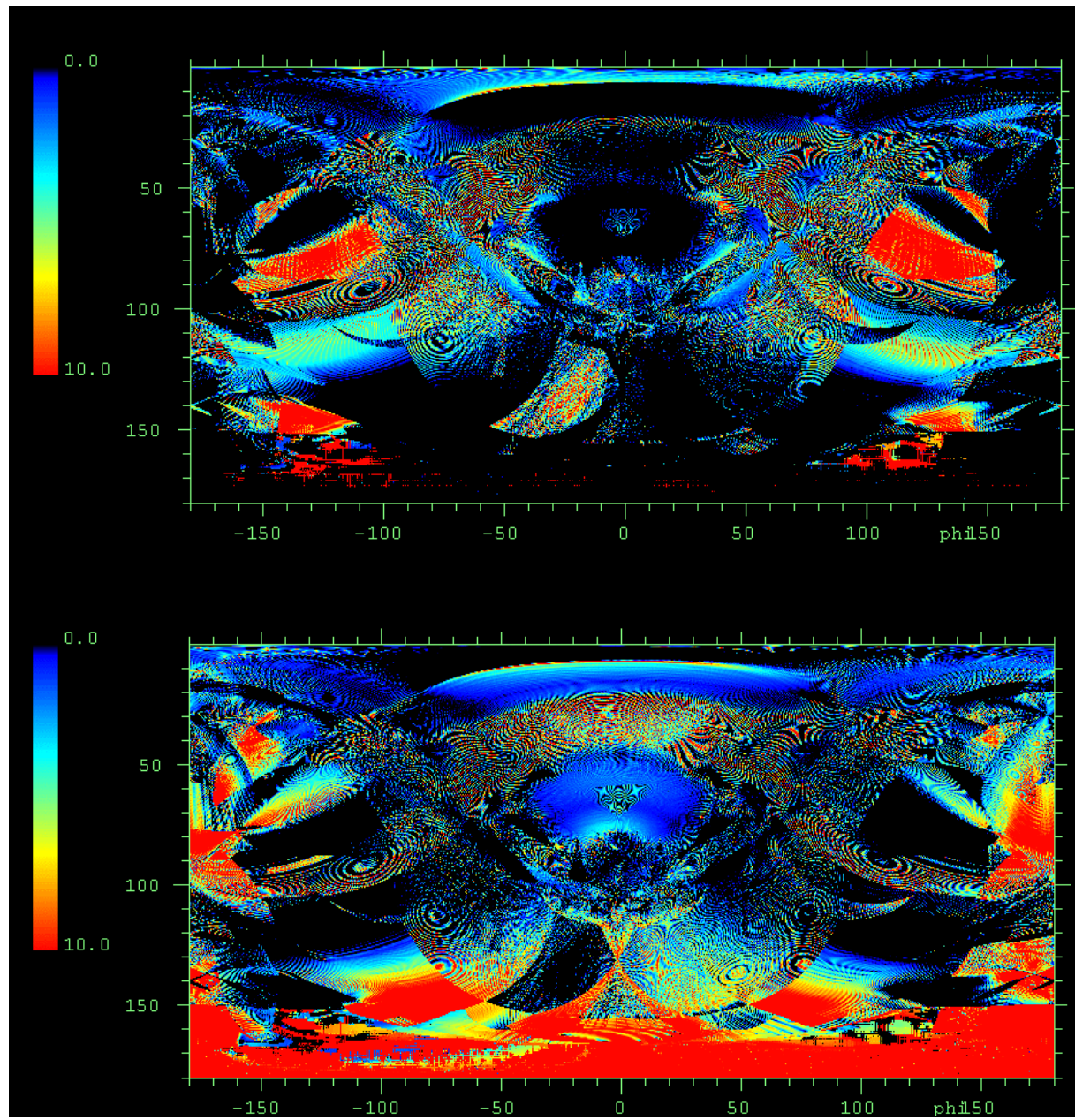
Figure 5.4-4 local area modified by more than 10 dB (red pixels to be disgarded).
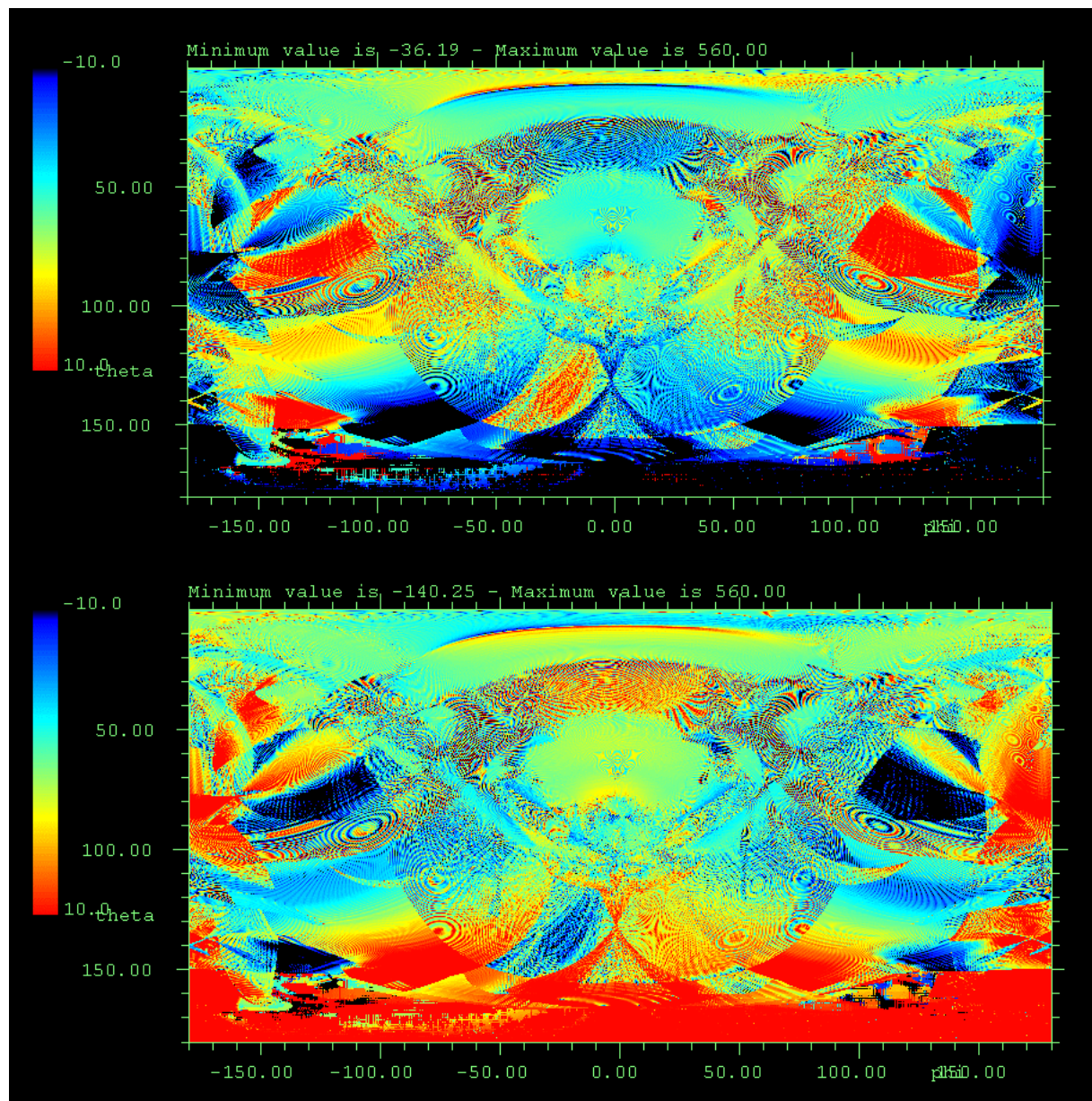
Figure 5.4-5 :local area modified by no more than 10 dB (red pixels to be disgarded).

ALCATEL ALENIA SPACE
An Alcatel/Finmeccanica company

## 5.5  353 GHz Pattern analysis(4pi-ext baf-inst feed)
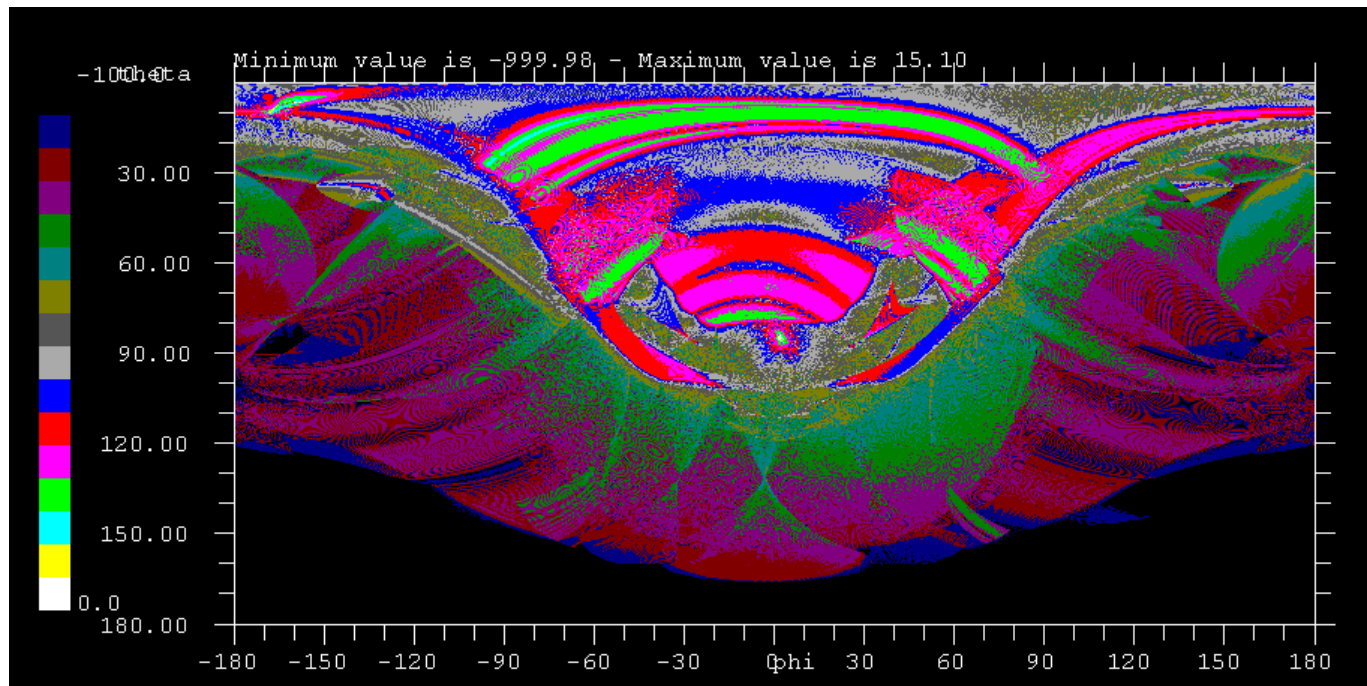


Figure 5.5-1 : 4PI diagram , phi : -180°, 180° / theta : 0,+180° / levels in directivity displayed from -100 dBi  to +0 dBi  (local major/minor component)
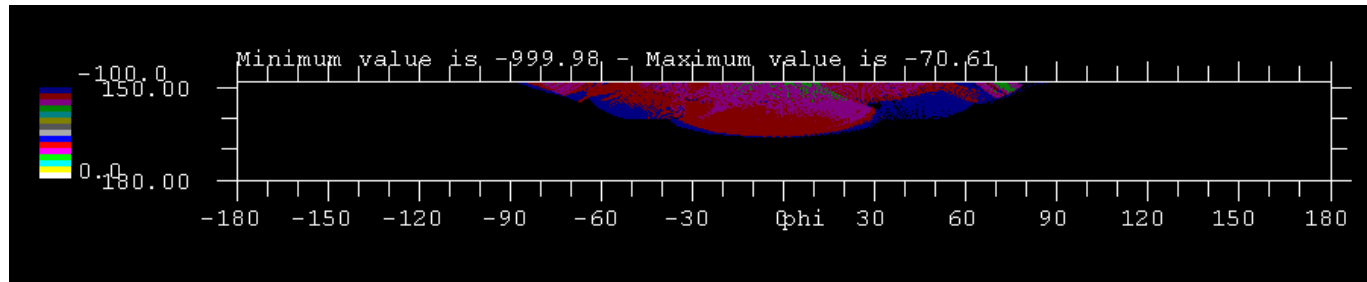


Figure 5.5-2 : Moon area        phi : -180°, 180° / theta : +148°,+180° / levels in directivity displayed from -100 dBi  to -0 dBi
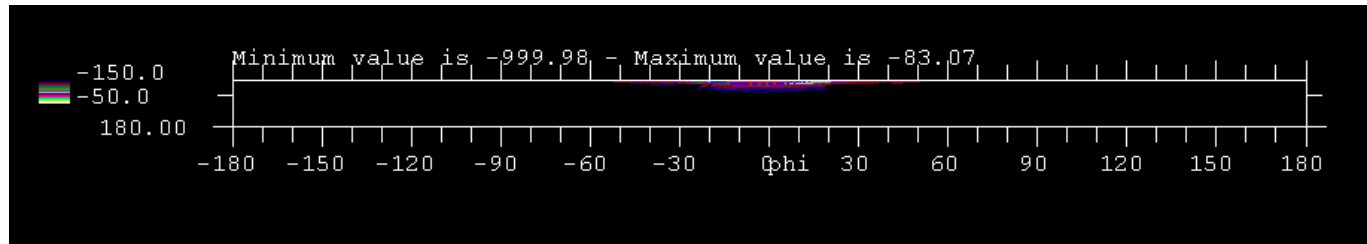


Figure 5.5-3 : Earth area        phi : -180°, 180° /  theta : +165°,+180°  / levels in directivity displayed  from -150 dBi to -50dBi (local major/minor component)
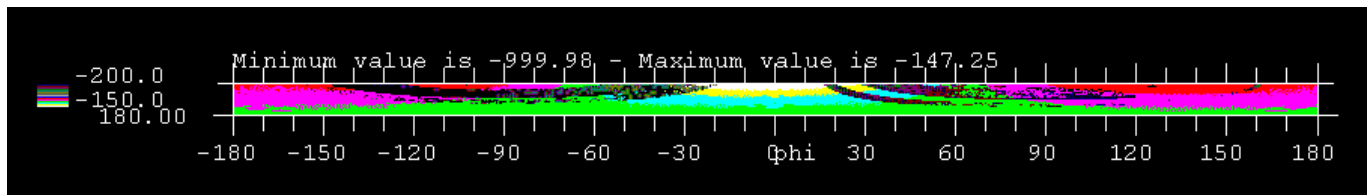
Figure 5.5-4 : Sun  area phi : -180°, 180°  /  theta : +170°,+180°  / levels in directivity displayed  from -150 dBi  to -50dBi (local major/minor component

INTENTIONALLY LEFT BLANK.

# 6. FAR OUT SIDE LOBE PERFORMANCE SYNTHESIS.

## 6.1 Performance toward Earth Sun and Moon of the Planck Spacecraft with perfect reflector surfaces

The following table shows that a nice margin is obtained for the rejection toward the Earth Sun and Moon for the Planck spacecraft equipped with ideal ellipsoidal reflector with no dust and no moon illumination of the primary.

| 30 GHz | Rejection (dB) with baffle extension & instrument feed models (polarization 1) | Rejection (dB) with baffle extension & instrument feed models (polarization 2) |
|---|---|---|
| Moon | -93 | -83 |
| Earth | -110 | -107 |
| Sun | -155 | -147 |

| 100 GHz | Rejection (dB) with baffle extension & instrument feed models polarization 1 | Rejection (dB) with baffle extension & instrument feed models polarization 2 |
|---|---|---|
| Moon | -116 | -107 |
| Earth | -141 | -128 |
| Sun | -198 | -187 |

| 353 GHz | Rejection (dB) with baffle extension & instrument feed models |
|---|---|
| Moon | -139 |
| Earth | -152 |
| Sun | -216 |

| 857 GHz | Rejection (dB) with baffle extension & gaussian feed | Rejection (dB) with baffle extension & instrument feed models |
|---|---|---|
| Moon | -170 | NA(*) |
| Earth | -187 | Na(*) |
| Sun | -259 | NA(*) |

(*) not applicable because multi moded computation of the horn not available

Table 6.1-1 : rejection performance synthesis.

## 6.2 Quilting or Grating lobe impact on the far out side lobe level.

The [RD 9] contains the analysis of the reflector quilting. The quilting is a regular distortion of the reflectors surfaces. This is in fact a regular array of spacing higher than the wavelength hence the grating lobe are recombined in the real angular domain of the pattern. The quilting on the secondary reflector is equivalent to an array as well as the quilting of the primary. Hence it can be found two arrays of grating lobe around each main lobe.

The grating lobes induced by the reflector quilting have no impact on the rejection performance. The only visible grating are the ones close to the main beam 4th order of grating. For greater order the grating lobes are merged among the natural side lobe level.

## 6.3 Impact of dust contamination on the far out side lobe level.

All the details of the dust contamination analysis is provided in [RD 15] and revisited also in [RD 16]

This section presents only the performance budget and details the margins.

The numerical model in [RD 15] is based upon the computation of the BRDF and the BRDF variation with the incident angle. The BRDF values have been computed using a given contamination level as well as a given dust composition (see [RD 15]).

No computation have been performed at 30 GHz as far as the effect is negligible. In addition RF test on the RFDM and RFQM (see [RD 10] ) have shown no impact on the measurement.

The following table presents the rejection performance synthesis with the specification and also with the goals. It can be seen that even with the very worst case conservative dust model, the rejection requirement are met. Anyhow the goals toward the sun are not always met. Now the revisited model shows positive margins for all requirements (spec and goals). The measurement on the RFQM allow to obtain the minimum measurable signal in the rejection area at 320 and 100 GHz. As far as the levels measured inthe CATR are lower than the modified level with the nominal dust, it is then possible to say that the first dust model described in [RD 15] is too pessimistic and can be disgarded for any further analysis. It is also possible to say that the revisited dust model is conservative .

For the contamination level of the reflector taking into account the contamination value of 225 ppm per day, for the polarization 1 campaign the reflectors had a level of 225*16 = 4000 ppm and of 13000 ppm for the second polarization campaign.   So the dust numerical model has been used with 5000 ppm and the minimum very low level signal have been measured at 320 GHz with the worst level of contamination. This means that the dust model is pessimistic even with best case input parameter. As a conclusion the dust contamination numerical model can be disregarded.

| Spec (dB) | Margin worst case model of (RD 15) /spec (dB) | Margin with the revisited model (RD 16) / goals (dB) |
|---|---|---|
| -78 | 31 | 23 |
| -85 | 26 | 28 |
| -98 | 17 | 44 |
| | | |
| Goal (dB) | Margin worst case model of (RD 15) / Goal (dB) | Margin with the revisited model (RD 16) / Goal (dB) |
| -95 | 13 | 6 |
| -109 | 1 | 4 |
| -122 | -7 | 20 |

Table 6.3-1 : margin @857 GHz  wrt the requirements and the goals.

| Spec (dB) | Margins worst case model of (RD 15)  /spec (dB) | Margins with the revisited model (RD 16) / goals (dB) | Margins measured on the RFQM (see [RD 10]) (Nota constant level limited by the dynamic measured at –115 dB /max) |
|---|---|---|---|
| -72 | 31 | 31 | 43 |
| -79 | 20 | 36 | 36 |
| -92 | 5 | 48 | 23 |
| Goal (dB) | Margins / Goal (dB) | Margins with the revisited model (RD 16) / Goal (dB) | |
| -81 | 22 | 22 | 34 |
| -95 | 4 | 20 | 20 |
| -108 | -10 | 32 | 7 |

Table 6.3-2 : margin @353 GHz wrt the requirements and the goals.

| Spec (dB) | Margins worst case model of (RD 15) /spec (dB) | Margins with the revisited model (RD 16) / goals (dB) | Margins measured on the RFQM (see [RD 10]) (Nota constant level limited by the dynamic measured at −110 dB /max) |
|---|---|---|---|
| -72 | 10 | 14 | 38 |
| -79 | 17 | 19 | 31 |
| -92 | 9 | 34 | 18 |
| Goal (dB) | Margins / Goal (dB) | Margins with the revisited model (RD 16) / Goal (dB) | |
| -81 | 1 | 5 | 29 |
| -95 | 1 | 3 | 15 |
| -108 | -7 | 18 | 2 |

Table 6.3-3 : margin @100 GHz wrt the requirements and the goals.

## 6.4 Final performance rejection toward Earth Sun and Moon.

The following table synthesizes all contributors to the rejection modification. The nominal performance is the one of the Planck spacecraft with ideal reflector, the baffle extension and the computed feed model. This nominal performance is degraded by different contributor. In fact the only contributor of importance is the dust contamination at the highest frequency. The far out side lobe are then dominated by the dust effect. In the following table the total rejection is obtained as the maximum of the different rejection computed alone (ie total rejection = max (rejection with no dust , rejection from dust model). As a conclusion, positive margin are obtained at all frequencies wrt the requirements and goals.

30 GHz

| | Rejection with no dust (dB) | Rejection from dust model | Rejection from grating lobes | Total rejection (dB) | Rejection requirement (dB) | | Margin / requirement (dB) |
|---|---|---|---|---|---|---|---|
| Moon | -83 | NA | NA | -83 | -71 | | 12 |
| Earth | -107 | NA | NA | -107 | -78 | | 29 |
| Sun | -147 | NA | NA | -147 | -91 | | 56 |

100 GHz

| | Rejection with no dust (dB) | Rejection from dust model | Rejection from grating lobes | Total rejection (dB) | Rejection requirement (dB) | Rejection goal (dB) | Margin / requirement (dB) | Margin / goal (dB) |
|---|---|---|---|---|---|---|---|---|
| Moon | -107 | -107 | NA | -107 | -71.5 | -73 | 36 | 34 |
| Earth | -128 | -110 | NA | -110 | -78.5 | -86 | 32 | 24 |
| Sun | -187 | -126 | NA | -126 | -91.5 | -99 | 35 | 27 |

353 GHz

| | Rejection with no dust (dB) | Rejection from dust model | Rejection from grating lobes | Total rejection (dB) | Rejection requirement (dB) | Rejection goal (dB) | Margin / requirement (dB) | Margin / goal (dB) |
|---|---|---|---|---|---|---|---|---|
| Moon | -139 | -115 | NA | -115 | -72 | -81 | 43 | 34 |
| Earth | -152 | -115 | NA | -115 | -79 | -95 | 36 | 20 |
| Sun | -216 | -140 | NA | -140 | -92 | -108 | 48 | 32 |

857 GHz

| | Rejection with no dust (dB) Gaussian feed | Rejection from dust model | Rejection from grating lobes | Total rejection (dB) | Rejection requirement (dB) | Rejection goal (dB) | Margin / requirement (dB) | Margin / goal (dB) |
|---|---|---|---|---|---|---|---|---|
| Moon | -170 | -101 | NA | -101 | -78 | -95 | 23 | 6 |
| Earth | -187 | -113 | NA | -113 | -85 | -109 | 28 | 4 |
| Sun | -259 | -142 | NA | -142 | -98 | -122 | 44 | 20 |

Table 6.4-1 : Final performance rejection comparison wrt to the requirements and the goals.

# 7. MAIN LOBE PERFORMANCE ANALYSIS

## 7.1 Introduction

The purpose of this chapter is to establish the Planck Telescope RF Performance analysis. This section is an update of the Planck CDR RF Analysis.

- In the first part the hypotheses and the input data used to perform the analysis are reviewed: telescope geometry, feed definitions, orientation and positions.

- In the second part, the hypotheses, the method of analysis applied for main lobes simulation is presented as well as discussions on convergence and on the performance estimation.

- The third part gives the description of the RF budget, which is based on two types of data: deterministic and random. The origin of these data are recalled as well as, in some cases, the process applied to convert them in a usable form for GRASP8.

- The fourth part gives the final budget of the telescope.

## 7.2 Hypotheses and data used for RF Budget

### 7.2.1 Planck telescope geometry

The geometry of the telescope is shown in Figure 7.2-1. The telescope is composed of two reflectors in a gregorian off-axis configuration.  M1 and M2 are located at the vertex of the ellipsoids and the RDP is the coordinate system of the FPU (Focal Plane Unit). Two additional coordinate systems OM1C and OM2C are introduced and are the coordinates systems associated with the mechanical interface of the reflectors and are defined in [RD11].
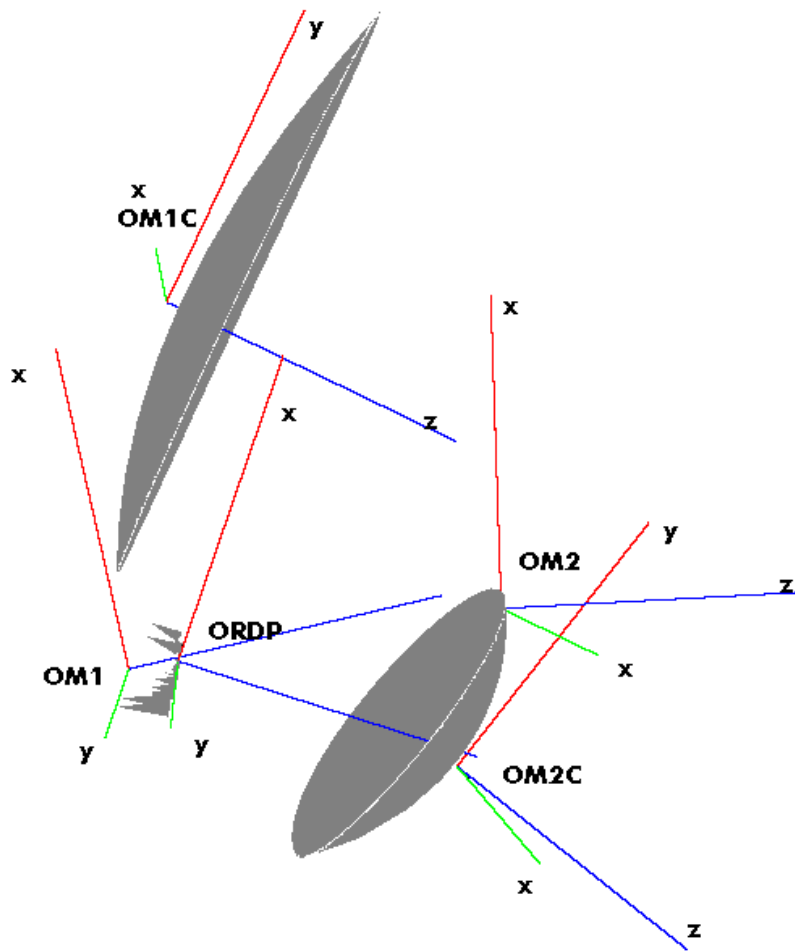


Figure 7.2-1 Planck Telescope coordinate systems

## 7.2.2 Horns definition

The FPU (focal plane unit) is composed of two type of horns: LFI (low frequency instruments) and HFI (High frequency instruments). The HFI horns are placed at the center of the FPU and are surrounded by the LFI horns.
The operating frequency of the horns is defined by their center frequency. LFI includes three types of horns defined by their center frequencies: 30, 44 and 70 and HFI includes six types defined by their center frequencies: 100, 143, 217, 353, 545 and 857 GHz.

For the analysis of the Planck performance, the feed model used is a gaussian beam defined by a far-field taper (apodization) as given in Table 7.2-1 :

| Frequency | Angle 30 dB from Peak (°) |
|---|---|
| 30 GHz  (LFI-30-27 to LFI-30-28) | 23.6 |
| 44 GHz (LFI-44-23 to LFI-44-26) | 23.6 |
| 70 GHz (LFI-70-18 to LFI-70-22) | 21.9 |
| | |
| 100 GHz (HFI-100-1 to HFI_100_4) | 26.8 |
| 143 GHz (HFI-143-1 to HFI_100_8) | 23.7 |
| 217 GHz (HFI-217-1 to HFI_100_8) | 21.8 |
| 353 GHz  (HFI-353-1 to HFI_353_8) | 19.4 |
| 545 GHz  (HFI-545-1 to HFI_545_4) | 19.4 |
| 857 GHz (HFI-857-1 to HFI_857_4) | 19.4 |

Table 7.2-1 Taper of Horns

The feed radiation patterns are defined according to Table 7.2-1 in Grasp8 model.

## 7.2.3  Horns position in the ORDP plane

### 7.2.3.1  LFI Horns

The horns positions used for the analysis are the ones given (see Table 7.2-2 ). 11 detectors are defined by their working  center frequencies between 30 GHz to 70 GHz. The positions are given in the ORDP coordinate system ($X_{rdp}$, $Y_{rdp}$, $Z_{rdp}$) and their orientation by the cosine directors.

| Detectors N# | Xrdp mm | Yrdp mm | Zrdp mm | Ux | Uy | Uz | Ux | Uy | Uz | Ux | Uy | Uz | frequency GHz |
|---|---|---|---|---|---|---|---|---|---|---|---|---|---|
| LFI_70_18 | -76.38 | -69.37 | 14.54 | 0.936379 | 0.299574 | -0.182891 | -0.320318 | 0.942398 | -0.096346 | 0.143494 | 0.1488 | 0.978401 | 70 |
| LFI_70_19 | -92.41 | -43.29 | 18.66 | 0.922853 | 0.32965 | -0.19918 | -0.342171 | 0.939123 | -0.031084 | 0.176808 | 0.096839 | 0.97947 | 70 |
| LFI_70_20 | -101.86 | -17.69 | 20.86 | 0.912768 | 0.359322 | -0.194275 | -0.359717 | 0.932423 | 0.034501 | 0.193544 | 0.038393 | 0.98034 | 70 |
| LFI_70_21 | -101.86 | 17.69 | 20.86 | 0.912768 | -0.359322 | -0.194275 | 0.359717 | 0.932423 | -0.034501 | 0.193544 | -0.038393 | 0.98034 | 70 |
| LFI_70_22 | -92.41 | 43.29 | 18.66 | 0.922853 | -0.32965 | -0.19918 | 0.342171 | 0.939123 | 0.031084 | 0.176808 | -0.096839 | 0.97947 | 70 |
| LFI_70_23 | -76.38 | 69.37 | 14.54 | 0.936379 | -0.299574 | -0.182891 | 0.320318 | 0.942398 | 0.096346 | 0.143494 | -0.1488 | 0.978401 | 70 |
| LFI_44_24 | -138.41 | 0. | 21.29 | 0.9666 | 0.0 | -0.256289 | 0. | 1. | 0. | 0.256289 | 0. | 0.9666 | 44 |
| LFI_44_25 | 55.32 | 133.27 | -17.90 | -0.262536 | -0.923175 | -0.280755 | 0.958343 | -0.283384 | 0.035667 | -0.112488 | -0.259696 | 0.959117 | 44 |
| LFI_44_26 | 55.32 | -133.27 | -17.90 | -0.262536 | 0.923175 | -0.280755 | -0.958343 | -0.283384 | -0.035667 | -0.112488 | 0.259696 | 0.959117 | 44 |
| LFI_30_27 | -136.95 | 54.94 | 18.60 | 0.910601 | -0.314901 | -0.267661 | 0.331426 | 0.943315 | 0.017731 | 0.246905 | -0.104856 | 0.96335 | 30 |
| LFI_30_28 | -136.95 | -54.94 | 18.60 | 0.910601 | 0.314901 | -0.267661 | -0.331426 | 0.943315 | -0.017731 | 0.246905 | 0.104856 | 0.96335 | 30 |

Table 7.2-2 LFI Horns positions and orientations

The overview of the LFI horns is shown in the Figure 7.2-2.

Figure 7.2-2: LFI horns in the ORDP plane

**ALCATEL ALENIA SPACE**
An Alcatel/Finmeccanica company

## 7.2.3.2  HFI Horns

The positions of the horns are given in the ORDP coordinate system ( $X_{rdp}$, $Y_{rdpf}$, $Z_{rdp}$)  (see Table 7.2-3) .

| Detectors N# | Xrdp mm | Yrdp mm | Zrdp mm | Ux | Uy | Uz | Ux | Uy | Uz | Ux | Uy | Uz | frequency GHz |
|---|---|---|---|---|---|---|---|---|---|---|---|---|---|
| HFI_100_1 | -47.57 | -32.966 | 14.847 | 0.995407 | -0.003320 | -0.095675 | -0.003320 | 0.997600 | -0.069161 | 0.095675 | 0.069161 | 0.993007 | 100 |
| HFI_100_2 | -55.114 | -10.622 | 16.831 | 0.993785 | -0.001245 | -0.111314 | -0.001245 | 0.999750 | -0.022304 | 0.111314 | 0.022304 | 0.993535 | 100 |
| HFI_100_3 | -55.114 | 10.622 | 16.831 | 0.993785 | 0.001245 | -0.111314 | 0.001245 | 0.999750 | 0.022304 | 0.111314 | -0.022304 | 0.993535 | 100 |
| HFI_100_4 | -47.57 | 32.966 | 14.847 | 0.995407 | 0.003320 | -0.095675 | 0.003320 | 0.997600 | 0.069161 | 0.095675 | -0.069161 | 0.993007 | 100 |
| HFI_143_1 | 33.184 | -39.106 | -1.28 | 0.997576 | 0.002875 | 0.069528 | 0.002875 | 0.996591 | -0.082449 | -0.069528 | 0.082449 | 0.994167 | 143 |
| HFI_143_2 | 35.142 | -16.019 | -0.572 | 0.997306 | 0.001247 | 0.073346 | 0.001247 | 0.999423 | -0.033937 | -0.073346 | 0.033937 | 0.996729 | 143 |
| HFI_143_3 | 34.424 | 16.013 | -0.39 | 0.997415 | -0.001221 | 0.071848 | -0.001221 | 0.999423 | 0.033940 | -0.071848 | -0.033940 | 0.996838 | 143 |
| HFI_143_4 | 33.912 | 41.141 | -1.613 | 0.997466 | -0.003090 | 0.071078 | -0.003090 | 0.996232 | 0.086673 | -0.071078 | -0.086673 | 0.993698 | 143 |
| HFI_143_5 | 48.96 | -32.843 | -4.919 | 0.994759 | 0.003545 | 0.102182 | 0.003545 | 0.997603 | -0.069112 | -0.102182 | 0.069112 | 0.992362 | 143 |
| HFI_143_6 | 50.593 | -8.581 | -4.455 | 0.994421 | 0.000958 | 0.105483 | 0.000958 | 0.999835 | -0.018119 | -0.105483 | 0.018119 | 0.994256 | 143 |
| HFI_143_7 | 49.882 | 8.578 | -4.263 | 0.994576 | -0.000945 | 0.104011 | -0.000945 | 0.999835 | 0.018122 | -0.104011 | -0.018122 | 0.994411 | 143 |
| HFI_143_8 | 49.672 | 32.856 | -5.108 | 0.994608 | -0.003596 | 0.103642 | -0.003596 | 0.997602 | 0.069120 | -0.103642 | -0.069120 | 0.992210 | 143 |
| HFI_217_1 | -31.18 | -27.749 | 12.776 | 0.997992 | -0.001858 | -0.063313 | -0.001858 | 0.998281 | -0.058579 | 0.063313 | 0.058579 | 0.996273 | 217 |
| HFI_217_2 | -29.527 | -8.754 | 13.236 | 0.998168 | -0.000561 | -0.060502 | -0.000561 | 0.999828 | -0.018533 | 0.060502 | 0.018533 | 0.997996 | 217 |
| HFI_217_3 | -30.307 | 8.752 | 13.362 | 0.998071 | 0.000576 | -0.062081 | 0.000576 | 0.999828 | 0.018535 | 0.062081 | -0.018535 | 0.997899 | 217 |
| HFI_217_4 | -30.399 | 27.756 | 12.651 | 0.998090 | 0.001813 | -0.061746 | 0.001813 | 0.998280 | 0.058603 | 0.061746 | -0.058603 | 0.996370 | 217 |
| HFI_217_5 | -16.174 | -34.288 | 9.791 | 0.999467 | -0.001184 | -0.032614 | -0.001184 | 0.997369 | -0.072487 | 0.032614 | 0.072487 | 0.996836 | 217 |
| HFI_217_6 | -14.291 | -15.164 | 10.422 | 0.999569 | -0.000473 | -0.029368 | -0.000473 | 0.999481 | -0.032197 | 0.029368 | 0.032197 | 0.999050 | 217 |
| HFI_217_7 | -15.051 | 15.16 | 10.563 | 0.999522 | 0.000498 | -0.030916 | 0.000498 | 0.999482 | 0.032174 | 0.030916 | -0.032174 | 0.999004 | 217 |
| HFI_217_8 | -15.412 | 34.298 | 9.651 | 0.999517 | 0.001128 | -0.031062 | 0.001128 | 0.997367 | 0.072508 | 0.031062 | -0.072508 | 0.996884 | 217 |
| HFI_353_1 | -3.268 | -58.369 | 5.117 | 0.999987 | -0.000308 | -0.005009 | -0.000308 | 0.992474 | -0.122458 | 0.005009 | 0.122458 | 0.992461 | 353 |
| HFI_353_2 | -0.512 | -39.964 | 6.325 | 1.000000 | -0.000011 | -0.000262 | -0.000011 | 0.996427 | -0.084458 | 0.000262 | 0.084458 | 0.996427 | 353 |
| HFI_353_3 | -0.073 | -23.141 | 7.308 | 1.000000 | 0.000003 | 0.000122 | 0.000003 | 0.998792 | -0.049138 | -0.000122 | 0.049138 | 0.998792 | 353 |
| HFI_353_4 | 1.231 | -5.905 | 7.552 | 0.999997 | 0.000016 | 0.002562 | 0.000016 | 0.999921 | -0.012547 | -0.002562 | 0.012547 | 0.999918 | 353 |
| HFI_353_5 | 0.409 | 10.332 | 7.649 | 1.000000 | -0.000010 | 0.000908 | -0.000010 | 0.999758 | 0.021980 | -0.000908 | -0.021980 | 0.999758 | 353 |
| HFI_353_6 | 0.451 | 27.097 | 6.996 | 0.999999 | -0.000038 | 0.001309 | -0.000038 | 0.998347 | 0.057477 | -0.001309 | -0.057477 | 0.998346 | 353 |
| HFI_353_7 | -1.536 | 42.928 | 6.29 | 0.999997 | 0.000101 | -0.002234 | 0.000101 | 0.995885 | 0.090631 | 0.002234 | -0.090631 | 0.995882 | 353 |
| HFI_353_8 | -2.513 | 58.387 | 4.964 | 0.999994 | 0.000212 | -0.003456 | 0.000212 | 0.992469 | 0.122496 | 0.003456 | -0.122496 | 0.992463 | 353 |
| HFI_545_1 | 12.049 | -58.768 | 1.867 | 0.999650 | 0.001635 | 0.026421 | 0.001635 | 0.992370 | -0.123281 | -0.026421 | 0.123281 | 0.992020 | 545 |
| HFI_545_2 | 14.698 | -40.242 | 3.022 | 0.999512 | 0.001329 | 0.031201 | 0.001329 | 0.996378 | -0.085027 | -0.031201 | 0.085027 | 0.995890 | 545 |
| HFI_545_3 | 13.702 | 43.225 | 3.004 | 0.999572 | -0.001337 | 0.029230 | -0.001337 | 0.995828 | 0.091238 | -0.029230 | -0.091238 | 0.995400 | 545 |
| HFI_545_4 | 12.784 | 58.788 | 1.703 | 0.999609 | -0.001729 | 0.027922 | -0.001729 | 0.992366 | 0.123312 | -0.027922 | -0.123312 | 0.991975 | 545 |
| HFI_857_1 | 15.072 | -23.799 | 3.974 | 0.999501 | 0.000798 | 0.031581 | 0.000798 | 0.998724 | -0.050492 | -0.031581 | 0.050492 | 0.998225 | 857 |
| HFI_857_2 | 16.357 | -6.442 | 4.207 | 0.999420 | 0.000233 | 0.034060 | 0.000233 | 0.999906 | -0.013691 | -0.034060 | 0.013691 | 0.999326 | 857 |
| HFI_857_3 | 15.568 | 9.909 | 4.332 | 0.999474 | -0.000342 | 0.032430 | -0.000342 | 0.999778 | 0.021065 | -0.032430 | -0.021065 | 0.999252 | 857 |
| HFI_857_4 | 15.617 | 27.287 | 3.672 | 0.999462 | -0.000950 | 0.032788 | -0.000950 | 0.998324 | 0.057862 | -0.032788 | -0.057862 | 0.997786 | 857 |

Table 7.2-3 Positions of HFI horns

The overview the HFI horns in the focal plane is shown in Figure 7.2-3 and Figure 7.2-4.

Figure 7.2-3: HFI horns in the ORDP plane



Figure 7.2-4 Detectors view in the focal Plane

## 7.3 Main lobes computation

### 7.3.1 Introduction

The telescope performance evaluation is defined in term of main lobe gain degradation. The gain degradation evaluation is based on different type of inputs (displacement of the reflector and feeds, distortion of the surface.). In order to achieve the computation with a given accuracy and in a reasonable computation time, the convergence parameters and the method of analysis must be optimized and adjusted. These last points are detailed in the following sections.

### 7.3.2 Requirements

The requirements for the Planck telescope performance are recalled in the followig table :

| Frequency | Max reduction in gain |
|---|---|
| GHz | dB |
| 30 | 0,5 |
| 44 | 0,5 |
| 70 | 0,5 |
| 100 | 0,5 |
| 143 | 0,5 |
| 217 | 1 |
| 353 | 1 |
| 545 | 1,4 |
| 857 | 2,5 |

Table 7.3-1 Telescope specification : Gain degradation

PTPE-035 The telescope shall achieve a Gain at the defined position of the detectors and operational conditions that do not reduce the theoretical value by more than see Table 7.3-1.

### 7.3.3 Quantification in terms of directivity degradation

Directivity degradation:

The horns are placed in the focal plane but not at the focus point. As a consequence, according to the usual definition of the cross-polarisation, the co-polarisation direction is given by the feed horn polarisation. Hence in order to obtain the diagram in co-polarisation and cross-polarisation, the coordinate system of the uv pattern of the telescope main lobe must be re-computed for each horn and each displacement. So as to avoid this additional computation, which could become heavy with regards to the number of detectors and displacements to analyse, the directivity degradation is computed through the power diagram.

The term $E_x$ given by Grasp8 is normalized to a square root of power ($P=|E|^2$).

Component 1:

$$\left|E_1\right| = \sqrt{E_{1r}^{\ 2} + E_{1i}^{\ 2}}$$

Component 2:

$$\left|E_2\right| = \sqrt{E_{2r}^{\ 2} + E_{2i}^{\ 2}}$$

Directivity in term of principal component

$$D_{dB} = 20\log_{10}(\sqrt{\left|E_1\right|^2 + \left|E_2\right|^2})$$

### 7.3.4 Simulation Tool

For the computation of the RF performance, a method of simulation with a good accuracy must be chosen to reach enough sensitivity to evaluate the impact of small disturbances. More precisely, the computation will have to take into account small displacements (translations and rotations) and surface deformations of small magnitude (a few microns).

As long as small disturbances could have a great impact on directivity, it is necessary ensure the numerical convergence of the results. For instance, according to the Ruze formula, at 857 GHz few microns of surface error could have a large impact in directivity degradation:

| delta rms | delta directivity (dB) |
|---|---|
| 1 | 0,005 |
| 2 | 0,02 |
| 3 | 0,05 |
| 4 | 0,09 |
| 5 | 0,14 |
| 6 | 0,20 |
| 7 | 0,27 |

Table 7.3-2 Surface error and gain degradation by Ruze

Thus, the sensitivity in directivity that one must be able to reach would be less than 0.01 dB.

Two types of data have to be considered in the computation: Impact of BFE displacement and distortion (rotation, translation, conicity and radius variations) and surface errors on the reflectors.

### 7.3.4.1 Main lobe and displacement computations

There are two ways to simulate the telescope performance: MGTD (multi-geometrical-theory of diffraction) and PO (physical optics) or a hybrid between the two methods. In the case of main lobe computation the use of PO is more accurate but time-consuming even if a pattern grid is reduced and centered on the main beam. In the purpose of determining the reflector surface discretisation parameters for physical optics, a convergence study on the directivity computation have been performed with an accuracy better than 0.01 dB.

Generally used for fast computation away from the main lobes, full MGTD method is not correct for main lobe computation because of caustic problem. Anyway, it is possible to use MGTD on the sub reflector and PO on the main reflector.

The advantage of doing this is to be faster than the full PO and this approach will gain in accuracy as long as the theory of geometrical diffraction is based on higher frequency approximation.

A preliminary comparison study is summarised in the Table 7.3-3 for LFI and HFI horns. The comparison between the two computations MGTD - PO (Reflection on the sub and PO on the main) and PO-PO is shown. The last column gives the difference in directivity in dB.

One can notice that at higher frequencies there is no difference in directivity (less than 0.006 dB up to 100 GHz). At lower frequencies the difference remains small, around 0.024 dB at 30 GHz, 0.022 dB at 44 GHz and 0.012 dB at 70 GHz). These results are in line with the fact that GTD method is accurate at high frequencies. Therefore, in the case of perfect reflectors, MGTD with PO could be used for the computation of the impact of displacement at higher frequencies.

## 7.3.4.2  Impact of deformation on surface

When the surface deformation has to be taken into account (high frequency distortion), full Physical Optics method (PO) must be chosen for computation, as it is the only way to handle the distortion on the surface. This means that the surface must be represented in one of the following formats:

1) Cloud of points (x, y, z) representative of the reflector surface

2) Equation of the conic (BFE) surface + distortion expanded in term of Zernike polynomials

3) Equation of conic (BFE) surface + distortion in term z-axis deviation from the perfect surface (x,y,$\Delta$z)

In the first format, the grid must be dense enough to avoid any additional grating lobes. These latter could occur if the magnitude of the distortion is important. Moreover, the grid must be close to a regular grid to minimize interpolating errors. Obviously, a compromise must be found with regards to the accuracy and computation time.

If the second format is used, one must ensure higher order Zernike polynomials in the expansion so as to be representative of high frequency distortion. This method could not be applied for deformations, which have a high spatial periodicity as quilting and random surface errors.

If the third format is used, the distortion must be expanded in Z-axis deviation (could be a constraint when measurement gives radial distortion). However, the advantage of this format is to apply interpolation only on the distortion file instead of on the complete surface of the reflector as when the first format is used. Therefore, this last format will be used for simulating the high frequency distortion.

| detector | GTD-PO | PO-PO | delta G |
|----------|--------|-------|---------|
| LFI_70_18 | 57,2117 | 57,2209 | -0,0092 |
| LFI_70_19 | 57,3694 | 57,3820 | -0,0126 |
| LFI_70_20 | 57,4513 | 57,4629 | -0,0117 |
| LFI_70_21 | 57,4513 | 57,4629 | -0,0117 |
| LFI_70_22 | 57,3694 | 57,3820 | -0,0126 |
| LFI_70_23 | 57,2117 | 57,2205 | -0,0088 |
| LFI_44_24 | 54,2521 | 54,2739 | -0,0217 |
| LFI_44_25 | 52,4603 | 52,4583 | 0,0020 |
| LFI_44_26 | 52,4603 | 52,4583 | 0,0020 |
| LFI_30_27 | 50,9666 | 50,9898 | -0,0232 |
| LFI_30_28 | 50,9666 | 50,9898 | -0,0232 |
| HFI_100_1 | 61,5997 | 61,6052 | -0,0056 |
| HFI_100_2 | 61,6568 | 61,6627 | -0,0059 |
| HFI_100_3 | 61,6568 | 61,6627 | -0,0059 |
| HFI_100_4 | 61,5997 | 61,6052 | -0,0056 |
| HFI_143_1 | 63,3077 | 63,3124 | -0,0046 |
| HFI_143_2 | 63,3577 | 63,3624 | -0,0047 |
| HFI_143_3 | 63,3654 | 63,3695 | -0,0041 |
| HFI_143_4 | 63,2852 | 63,2876 | -0,0024 |
| HFI_143_5 | 63,1215 | 63,1234 | -0,0019 |
| HFI_143_6 | 63,1942 | 63,1973 | -0,0031 |
| HFI_143_7 | 63,2046 | 63,2087 | -0,0040 |
| HFI_143_8 | 63,1083 | 63,1104 | -0,0021 |
| HFI_217_1 | 66,7002 | 66,7007 | -0,0005 |
| HFI_217_2 | 66,7143 | 66,7157 | -0,0014 |
| HFI_217_3 | 66,7186 | 66,7210 | -0,0024 |
| HFI_217_4 | 66,6984 | 66,6997 | -0,0013 |
| HFI_217_5 | 66,6210 | 66,6231 | -0,0020 |
| HFI_217_6 | 66,6246 | 66,6260 | -0,0014 |
| HFI_217_7 | 66,6289 | 66,6295 | -0,0006 |
| HFI_217_8 | 66,6173 | 66,6190 | -0,0018 |
| HFI_353_1 | 69,2531 | 69,2474 | 0,0057 |
| HFI_353_2 | 69,6751 | 69,6708 | 0,0043 |
| HFI_353_3 | 69,7500 | 69,7470 | 0,0031 |
| HFI_353_4 | 69,7265 | 69,7246 | 0,0019 |
| HFI_353_5 | 69,7339 | 69,7341 | -0,0002 |
| HFI_353_6 | 69,7432 | 69,7409 | 0,0023 |
| HFI_353_7 | 69,6462 | 69,6429 | 0,0034 |
| HFI_353_8 | 69,2464 | 69,2408 | 0,0055 |
| HFI_545_1 | 71,8578 | 71,8516 | 0,0062 |
| HFI_545_2 | 72,9061 | 72,9011 | 0,0050 |
| HFI_545_3 | 72,8181 | 72,8126 | 0,0055 |
| HFI_545_4 | 71,8342 | 71,8288 | 0,0053 |
| HFI_857_1 | 76,6257 | 76,6232 | 0,0025 |
| HFI_857_2 | 76,6672 | 76,6642 | 0,0031 |
| HFI_857_3 | 76,6807 | 76,6769 | 0,0038 |
| HFI_857_4 | 76,5524 | 76,5492 | 0,0032 |

Table 7.3-3 Convergence between PO-PO and MGTD (reflection)-PO

### 7.3.4.3 Pattern windowing

A remark concerning the window size used for the pattern computation. The windows are optimized in order to reduce the computation time. The typical window is defined so as to cover the −3 dBmax with a 51*51 points grid (see Figure 7.3-1.



HFI_100          HFI_143          HFI_217

HFI_353          HFI_545          HFI_857
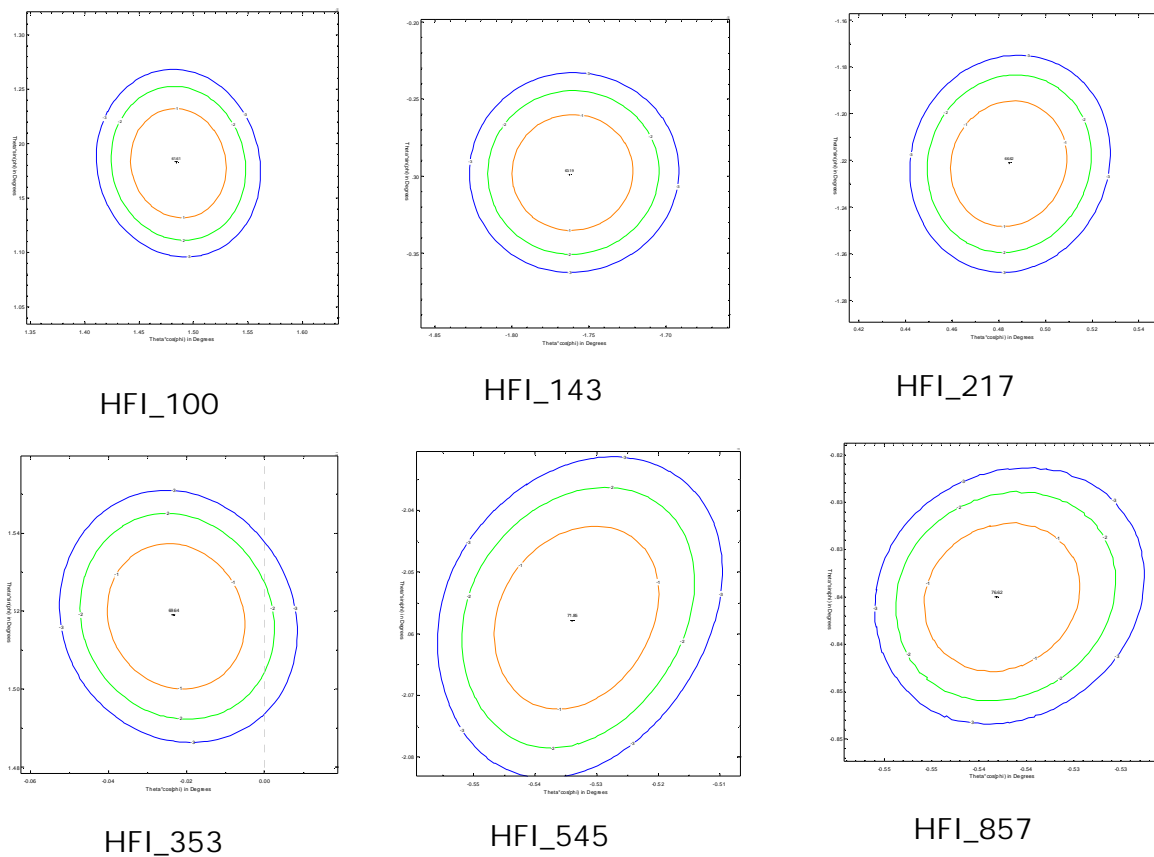
Figure 7.3-1 Patterns HFI examples.

.

## 7.3.5 LFI radiation pattern

The radiation patterns for LFI horns are shown in Figure 7.3-2. The contour levels correspond to -3 dB below the maximum.
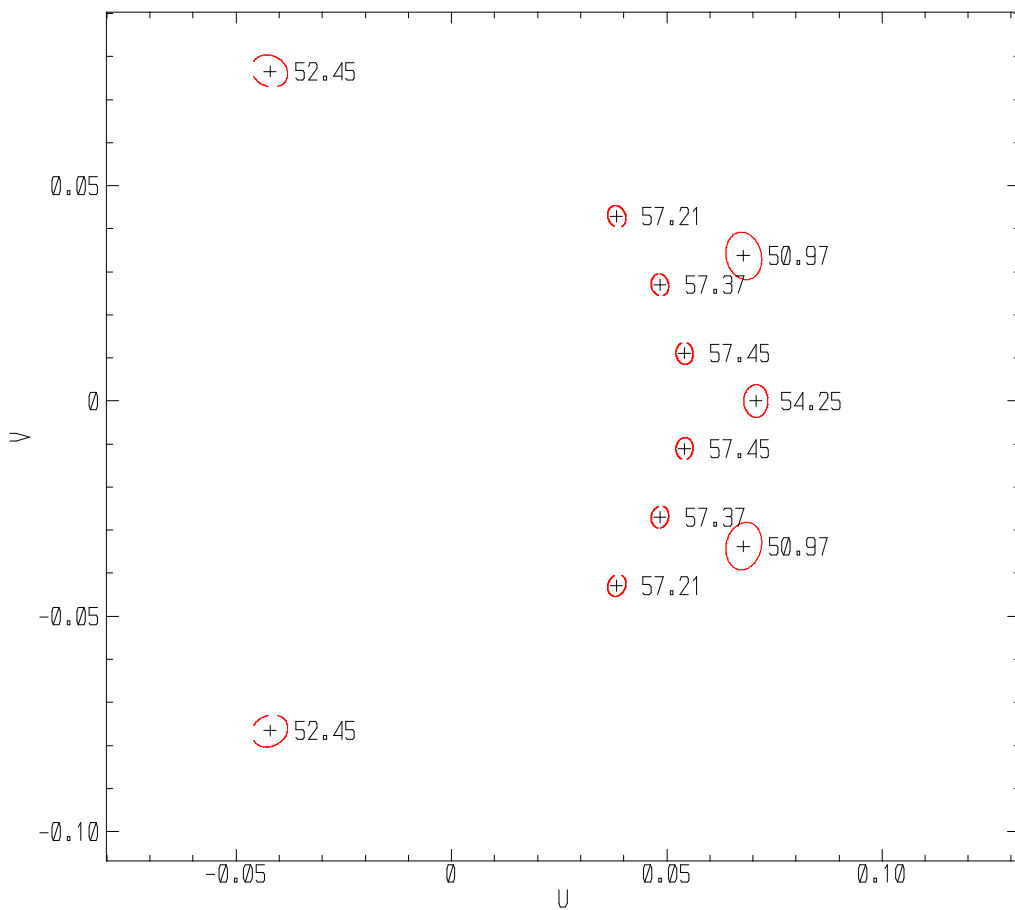


Figure 7.3-2: Radiation pattern of the telescope for LFI horns

## 7.3.6  HFI radiation pattern

In the same way the radiation patterns for HFI horns are plotted in Figure 7.3-3. The contour levels correspond to –3 dB and –6 dB.
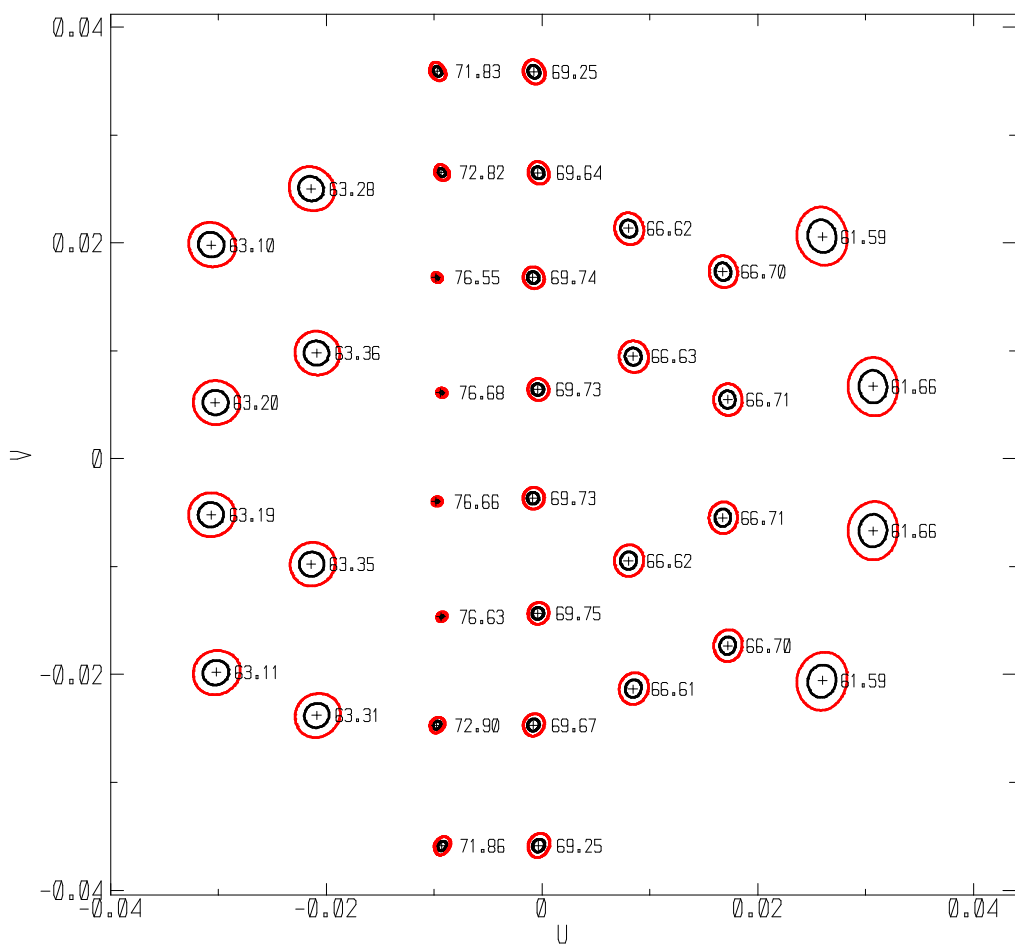


Figure 7.3-3. Radiation pattern of the telescope for HFI horns

## 7.4 Contributors analysis

This part presents the identification of the contributors and their conversion in terms of RF performance degradations. For this purpose, it is necessary to decompose each contributor and to define the best way to insert them in the numerical RF model.

The major part of the inputs for the budget comes from [RD20], [RD21] and [RD22] where the mechanical impact of the contributors have been quantified by simulations (under several load cases of random contributors), surface measurements (videogrammetry, interferometry) and other parts from a specific analysis or allocations.

### 7.4.1 Contributors identification

Two types of contributors could be identified : deterministic (signed) and statistic (not signed) contributors (see Figure 7.4-1).
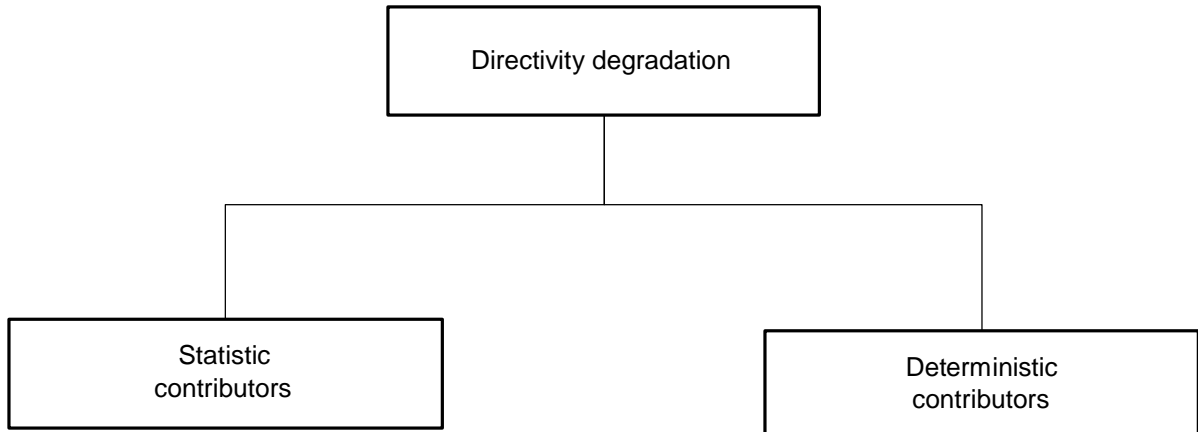


Figure 7.4-1 Contributors identification

For statistic contributors the degradation of the performance will be obtained by a quadratic summation of each degradation and for the deterministic contributors by a summation.

Each contributor is divided into several sub-contributors in order to identify precisely the origin (see [RD23]).

## 7.4.2 Deterministic contributor

The deterministic case at operational is composed of two parts :
- a "deterministic load case"
- others deterministic estimated cases.

The "deterministic load case" (boxes 1, 2, 3, 4, 5 in figure 7.4-2) is built through a numerical model which includes a major part of the contributors.
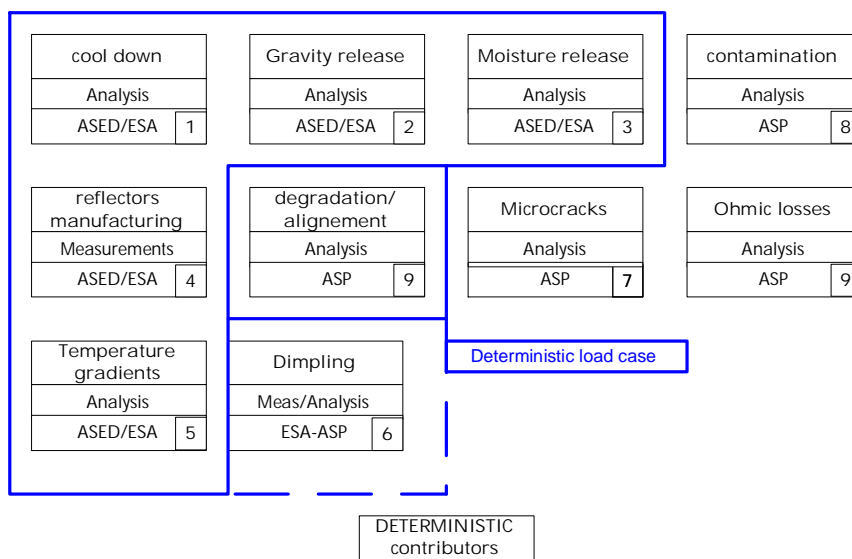


Figure 7.4-2 deterministic contributors

The numerical model must be representative of the telescope at operational. The model is built with different data from measurements, analysis (extrapolation at operational) and optimisation results. The methodology used to establish the geometrical configuration at operational is detailed in [RD6]-[RD7] [RD8] and is recalled in the following steps:

1) Measurement of BFE by videogrammetry (ESA) of reflector surface shape at 100 k and extrapolation to 55 k by analysis.
2) Optimisation of the best geometrical configuration according to these two BFE. (Alcatel)
3) Alignment measurement, deviation measured and extrapolated at operational from configuration defined in 2)
4) Measurements of sub reflector surface shape (high frequency distortion) by interferometry
5) Measurement of RFQM Mould measurement analysis for the main reflector (ESA/ASED) (nota : this set of data has not been updated for the QR analysis).

6) Additional contributor at operational

ALCATEL ALENIA SPACE
An Alcatel/Finmeccanica company

REFERENCE : H-P-3-ASP-AN-323

DATE : 12/2/2007

ISSUE : 3

Page : 76/126

The numerical model is constructed from step 1 to 6 . This model is used to estimate the performance degradation for the deterministic load case. This degradation (calculated with the deterministic load case) must be added to the three others contributors appearing outside the blue contour (see Figure 7.4-2). The dashed contour of the "dimpling contributor" means that the "dimpling or quilting" contributor has only been considered for the sub reflector (measured and estimated at 55 K) and is included in the deterministic load case. An allocation will be taken for the main reflector in the final budget.

## 7.4.2.1 Input for deterministic load case

The deterministic load case is obtained by a summation of sub level contributors and is defined by one set of parameters (BFE distortion+ HF distortion + displacements and rotation).

The deterministic load case is defined in following the data format:

1) BFE defined by $\Delta R$ and $\Delta K$ from the initial conics defining the main and the sub reflectors.
2) Position of the BFE vertex in OM1 and OM2 ($T_x$, $T_y$, $T_z$, $R_x$, $R_y$)
3) Defocus of the ORDP plane ($T_x$, $T_y$, $T_z$)
4) Residual distortion (also mentioned as HF -high frequency distortion)

The parameters refer to deviation, displacement and rotation from the theoretical model.

## 7.4.2.2  FM Reflector BFE shape

The shape of the reflectors have been measured and interpolated to 55 k (operational temperature) ( [RD21].

The measurements have been performed by videogrammetry. The clouds of points has been best fitted by a conic and allowed to calculate the BFE of each surface (main and sub reflectors). The values obtained for conicity and radius of curvature defining the BFE are given in Figure 7.4-1. The parameters, interfoci and vertex-focus distance defining the conic is given in Table 7.4-2. The optical configuration can be reconstructed by positioning the real surface defined by the last parameters.

| mm | | primary | reflector | | secondary | reflector | |
|---|---|---|---|---|---|---|---|
| | | measured | theory | delta | measured | theory | delta |
| radius of curvature (mm) | R | 1439,115 | 1440 | -0,885 | 643,78 | 643,972 | -0,192 |
| conicity | K | -0,86738 | -0,869417 | 0,002037 | -0,21514 | -0,215424 | 0,000284 |

Table 7.4-1 BFE measured by videogrammetry

| | | | Primary | reflector | (mm) | | | |
|---|---|---|---|---|---|---|---|---|
| a | a | | b | b | | c | c | |
| measured | theory | delta | measured | theory | delta | measured | theory | delta |
| 10851,4176 | 11027,4691 | -176,0515 | 3951,7639 | 3984,9160 | -33,1521 | 10106,2766 | 10282,2916 | -176,0150 |
| vertex-focus | distance | | | | | interfoci | distance | |
| a-c | a-c | | | | | 2*c | 2*c | |
| 745,1410 | 745,1776 | -0,0365 | | | | 20212,5531 | 20564,5831 | -352,0300 |
| | | | secondary | reflector | mm | | | |
| a | a | | b | b | | c | c | |
| measured | theory | delta | measured | theory | delta | measured | theory | delta |
| 820,2482 | 820,7898 | -0,5416 | 726,6769 | 727,0252 | -0,3483 | 380,4573 | 380,9597 | -0,5024 |
| vertex-focus | distance | | | | | interfoci | distance | |
| a-c | a-c | delta | | | | 2*c | 2*c | delta |
| 439,7909 | 439,8302 | -0,0392 | | | | 760,9145 | 761,9194 | -1,0048 |

Table 7.4-2 Deviation of the actual surface/ theory

The comparison with the theoretical values shows significant discrepancies. The reflector cannot be placed at the theoretical location without degrading the performance. Another optical configuration has been defined.

### 7.4.2.3 Realignment

As previously mentioned, the surfaces of the reflectors present significant deviations with the theoretical ones. According to the alignment method proposed in (RD7), the positions of the reflectors and of the FPU have been optimised in order to improve the image quality by CODE V. The values obtained which ameliorate the optical arrangement are given in Table 7.4-3.

| Optimisation results by Code V | Tx | Ty | Tz | Rx | Ry | Rz | coordinate system |
|---|---|---|---|---|---|---|---|
| | mm | mm | mm | deg | deg | deg | |
| Primary reflector | -0,64 | 0 | 0,015 | 0 | 0,0493 | 0 | OM1 |
| secondary reflector | 0,25 | 0 | -0,04 | 0 | 0,0324 | 0 | OM2 |
| FPU | 0 | 0 | 2,82 | 0 | 0 | 0 | ORDP |

Table 7.4-3 Optimisation results

### 7.4.2.4 Reflector high frequency surface distortion

### 7.4.2.4.1 Main reflector

For the main reflector, the residual surface distortion is given in the format of a cloud of point x, y, $\Delta z$ where $\Delta z$ is the deviation of the surface from the ideal reflector in the z-direction. This surface distortion is plotted in

The distortions are obtained from analysis (Contraves simulation and QM mould measurements). In fact this surface has not been updated since the CDR, the measurement of this surface by interferometry is not available yet. Therefore, a hypothesis has been taken to perform the computation: the order of magnitude of the distortions remains unchanged and their impacts on gain degradation remain representative of the flight model (see map in figure 7.4-3).
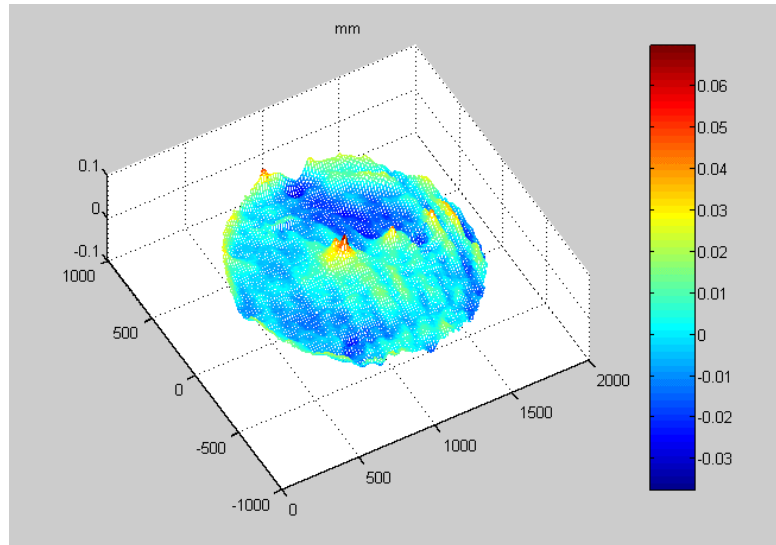
Figure 7.4-3 Residual deformations on the main reflector (unity in figure: mm)

### 7.4.2.4.2  Sub reflector

The surface of the sub reflector has been measured by interferometry. The data contained in [RD 21] is a cloud of points providing the distortion along the normal at 798558 point on the surface. The cloud of points has been measured in the plane of the reflector in OM2C (mechanical coordinate system) see Figure 7.4-4.

 In this state, this data cannot be exported in GRASP8 and need to be re-processed:

- First the distortion must be defined in the coordinate system associated with the definition of the reflector OM2  (more precisely in sub reflector coordinate system which is the OM2 coordinate system (vertex) translated at the focus point and rotated of 180°).

-  Secondly, the distortion must be expressed as deviation in the z-axis where the z-axis belongs to the coordinate system of the perfect conic definition.
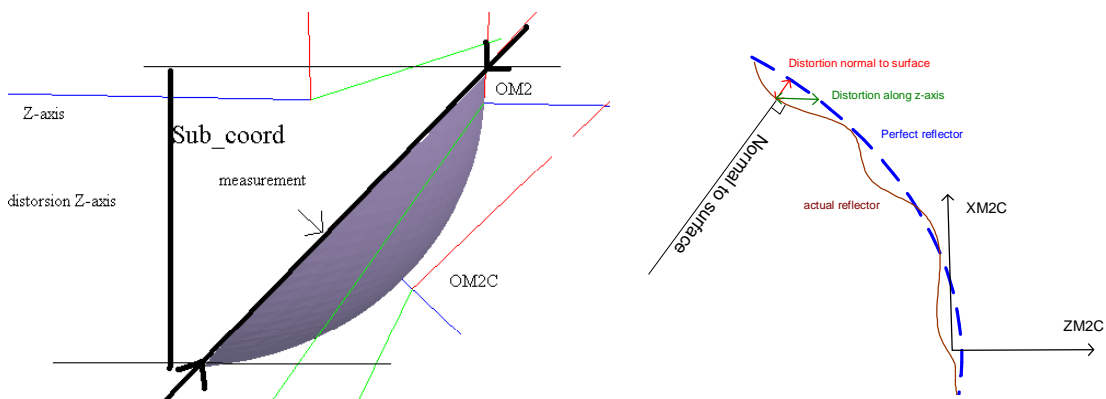


Figure 7.4-4 Sub reflector coordinate systems

The process used to fulfil these two conditions is described in the flow chart of Figure 7.4-5 and the result of this process is depicted in Figure 7.4-5.
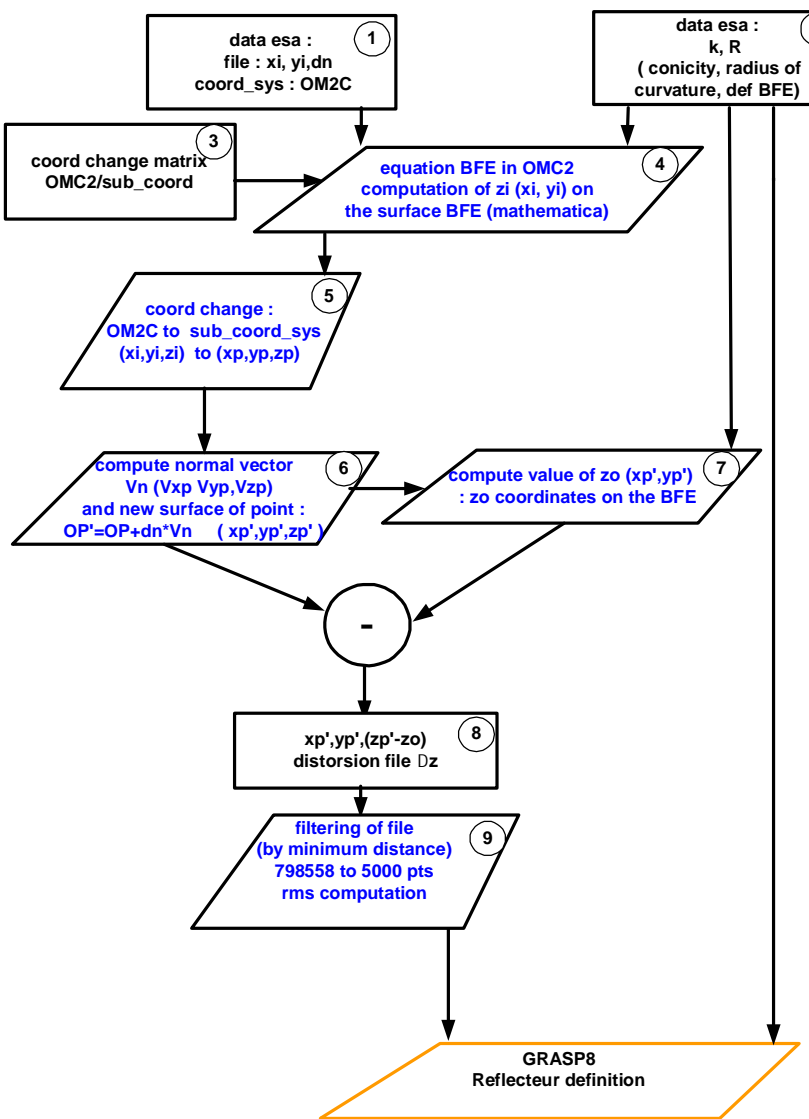
Figure 7.4-5 Process flow chart for the sub reflector distortion file

1: data from [RD21] contains 798558 points.
2: data recalled in Table 7.4-1.
3: data coordinate change matrix   [RD20]
4: computation of the conic expression in OM2 and zi-coordinate computation
5: change coordinate system (xi, yi, zi) to (xp, yp, zp)
6: gradient computation: normal vector: real surface shape of the reflector (xp', yp', zp')
7: computation of the zo coordinates on the BFE.
8: subtract distortion file (xp', yp', zp'-zo)
9: filtering the distortion file: 798558 points to 5000 points (minimum  distance 4.5 mm)

sub_filtre

delta_sub_N50_45s.sfc
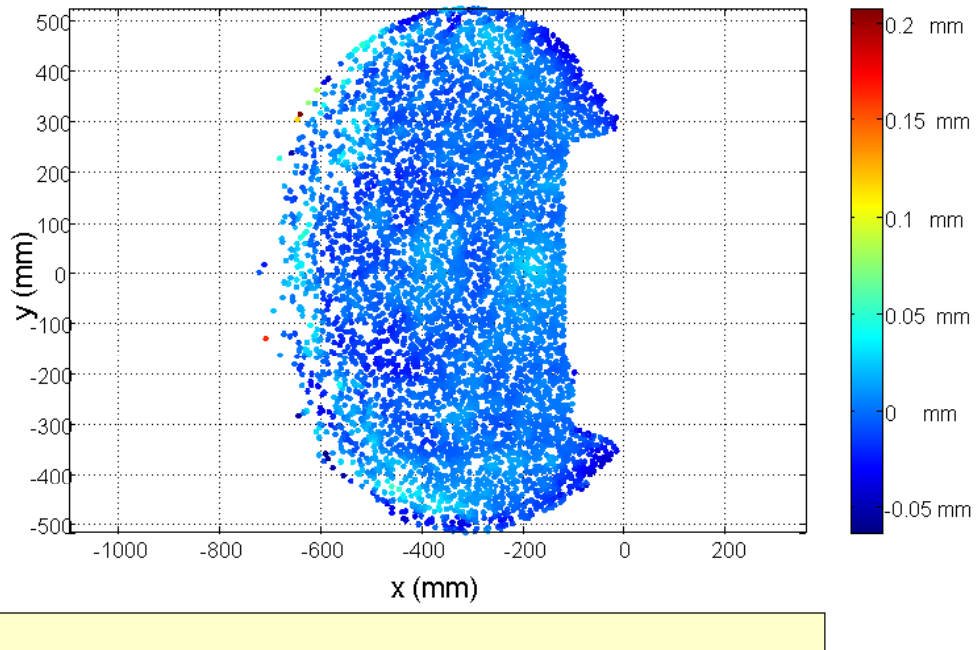


Figure 7.4-6 Residual deformations on the sub reflector (unity in figure mm)

### 7.4.2.5 Degradation (real structure)

As described in the previous chapter, the optimization of the geometrical configuration allows to define a goal for positioning the real reflectors and the FPU. The residual of this achievement is given in Table 7.4-4.

| microns microncorad | Tx | Ty | Tz | Rx | Ry | dR | dK | coordinate system |
|---|---|---|---|---|---|---|---|---|
| PR | 0 | 0 | 0 | 0 | 0 | 151 | -0,00012 | OM1 |
| SR | -1107 | -33 | -11 | 497 | -1246 | 118 | -0,00005 | OM2 |
| FPU | 0 | 0 | 500 | 0 | 0 | | | ORDP |

Table 7.4-4 Real case degradation

This degradation will be added to the deterministic model.

### 7.4.2.6 Others contributors

The impact of others contributors detailed in [RD23 ] is given in Table 7.4-5.

| microns/micron rad valeur delta | Tx | Ty | Tz | rx | ry | dR | dK | coordinate system |
|---|---|---|---|---|---|---|---|---|
| primary reflector | 0,9 | -7,8 | 202,3 | -2,09 | 267,01 | -18,5 | 4,00E-05 | OM1 |
| secondary reflector | 104,8 | -11,8 | 43,3 | -1,3 | 167,91 | 14,7 | 5,30E-06 | OM2 |

Table 7.4-5 Other contributors

ALCATEL ALENIA SPACE
An Alcatel/Finmeccanica company

REFERENCE : H-P-3-ASP-AN-323

DATE : 12/2/2007

ISSUE : 3

Page : 84/126

### 7.4.2.7 Global deterministic case

The establishment of the deterministic load case could be followed in the steps:

Case O: impact of BFE deviation (configuration theoretical):  Table 7.4-1.

Case 1  : impact of BFE deviation +realignment (by optimization) :  Table 7.4-1 and Table 7.4-3

Case 2 : impact of BFE deviation + realignment (by optimization) + HF distortion : Table 7.4-1, Table 7.4-3,  Figure 7.4-3 and Figure 7.4-6.

Case 3  : impact of BFE deviation +realignment (by optimization) +HF distortion +others contributors: Table 7.4-1+Table 7.4-3+Table 7.4-5 +

Figure 7.4-3+Figure 7.4-6  (see also Table 7.4-6)

Case 4  : impact of BFE deviation +realignment (by optimization) +HF distortion +otherz contributors +degradation: Table 7.4-1+Table 7.4-3+ Table 7.4-4+ Table 7.4-5

Figure 7.4-3+Figure 7.4-6 (See also Table 7.4-7).

Case 5  : impact of BFE deviation +realignment (by optimization) +HF distortion +  others contributors +degradation (with compensation of defocus of –500 µm compared to real case 4) :Table 7.4-1+Table 7.4-3+ Table 7.4-4+ Table 7.4-5

Figure 7.4-3+Figure 7.4-6 (See also Table 7.4-7).

| microns/micron rad | | | | | | | | coordinate |
|---|---|---|---|---|---|---|---|---|
| valeur delta | Tx | Ty | Tz | rx | ry | dR | dK | system |
| primary reflector | -639,1 | -7,8 | 162,3 | -2,09 | 832,5 | -903,5 | 2,08E-03 | OM1 |
| secondary reflector | 354,8 | -11,8 | 3,3 | -1,3 | 733,4 | -177,3 | 2,89E-04 | OM2 |
| FPU | 0 | 0 | 2820 | 0 | 0 | | | ORDP |

Table 7.4-6  CASE  3 : contributors: BFE BF distortion + realignment +other IO contributors

| microns<br>micronconrad | | Tx | Ty | Tz | Rx | Ry | dR | dK | coordinate<br>system |
|---|---|---|---|---|---|---|---|---|---|
| PR | | -639,1 | -7,8 | 162,3 | -2,09 | 832,5 | -752,5 | 0,001957 | OM1 |
| SR | | -752,2 | -44,8 | -7,7 | 495,7 | -512,6 | -59,3 | 0,000239 | OM2 |
| FPU | | 0 | 0 | 3320 | 0 | 0 | 0 | | ORDP |
| FPU (autre cas) | | | | 2820 | | | | | ORDP |

Table 7.4-7 Contributors: CASE 4 & 5 : BFE BF distortion + realignments +other contributors+degradation (real case)

CASE 0
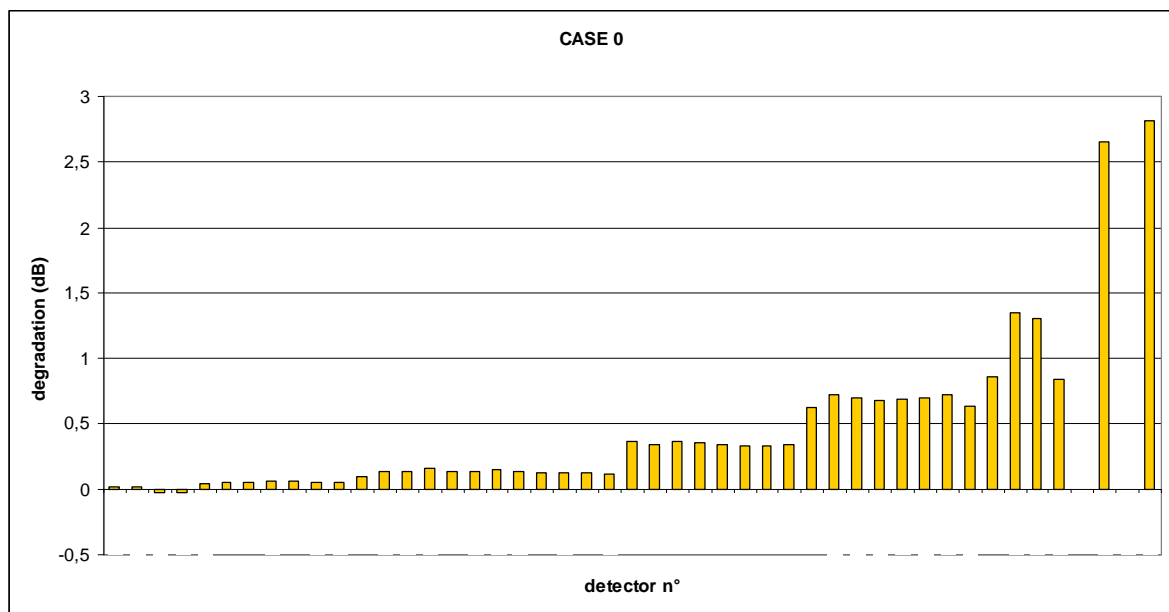
Figure 7.4-7 impact of BFE distortion

CASE 1
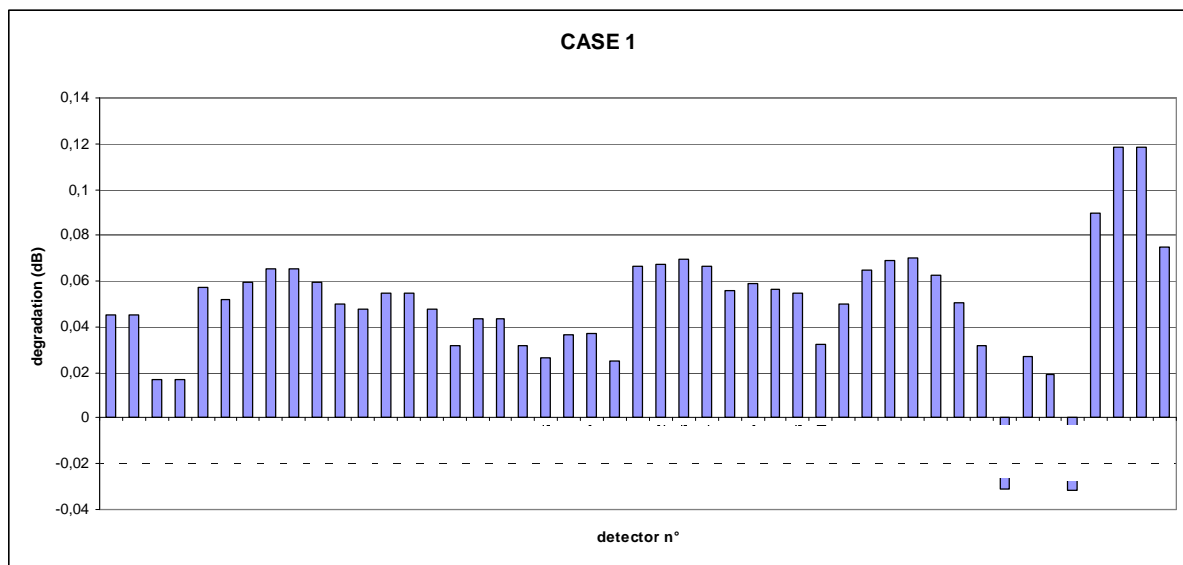
Figure 7.4-8 impact of BFE deviation +realignment
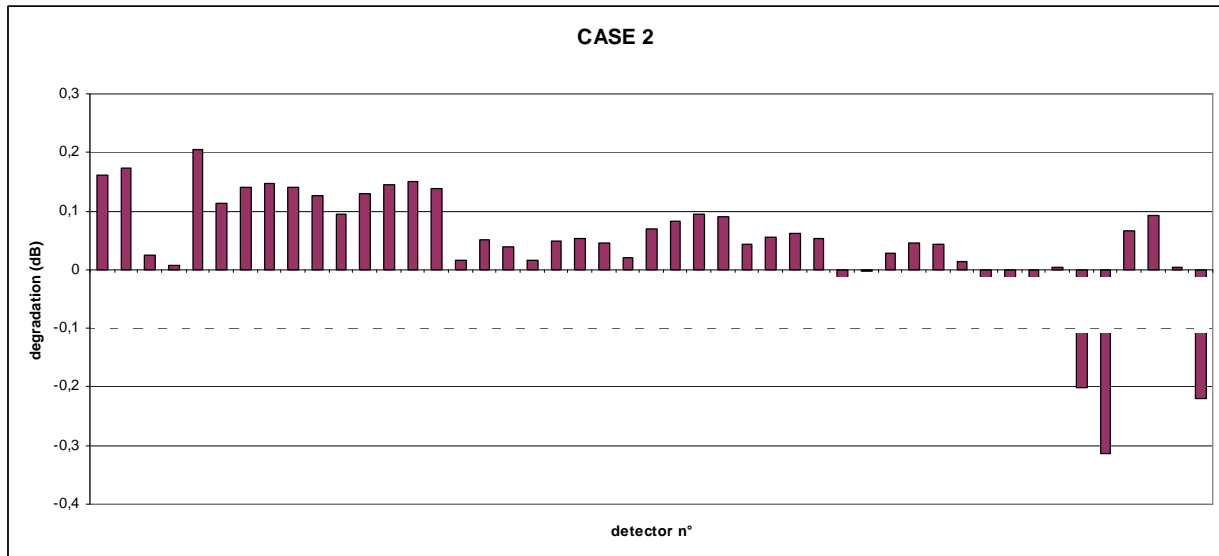
Figure 7.4-9 impact of BFE deviation +realignment (by optimization) +HF distortion
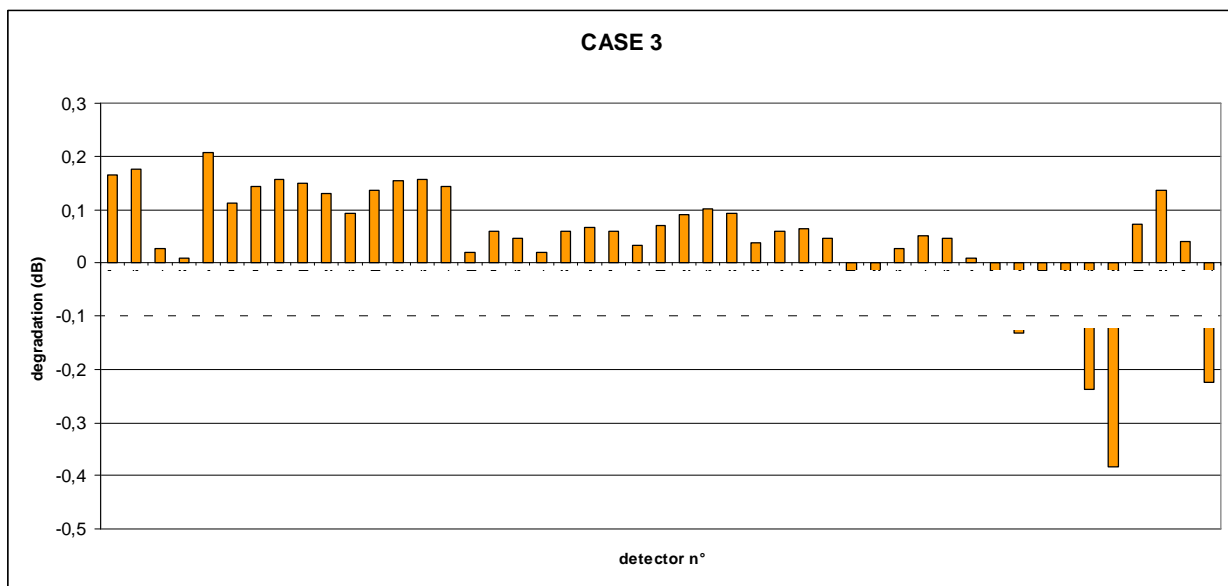


Figure 7.4-10 impact of BFE deviation +realignment (by optimization) +HF distortion +IO contributors
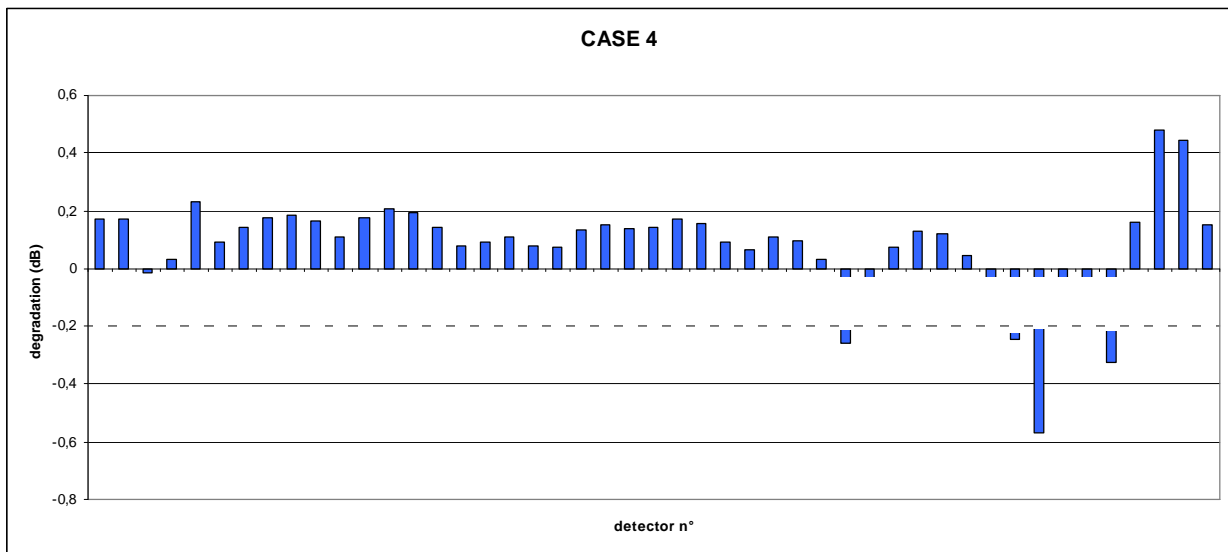
Figure 7.4-11 : impact of BFE deviation +realignment (by optimization) +HF distortion +IO contributors + degradation
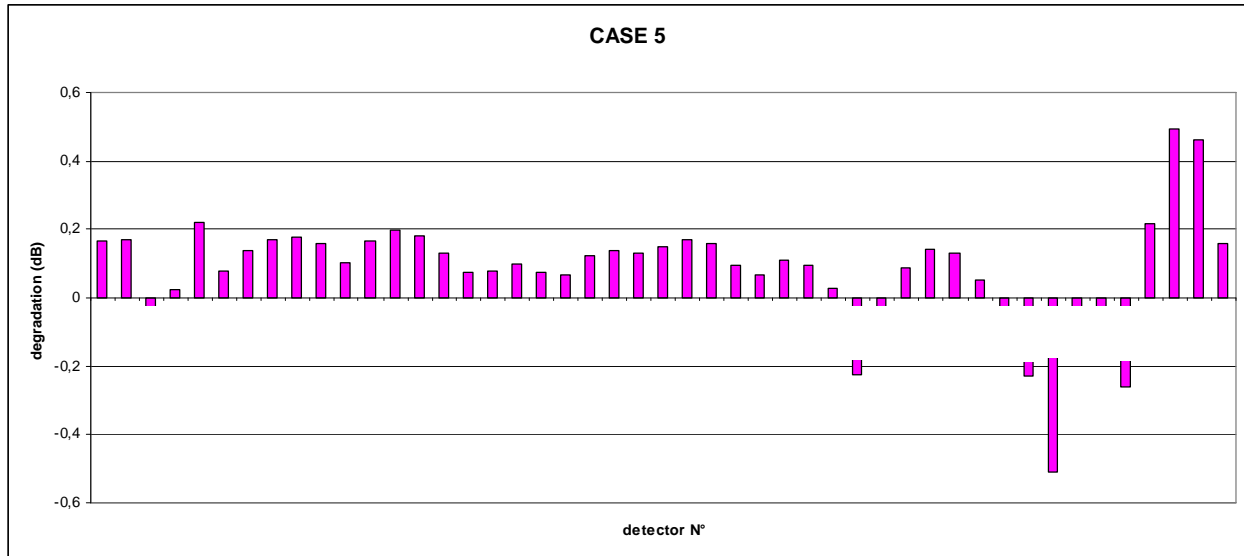


Figure 7.4-12 impact of BFE deviation +realignment (by optimization) +HF distortion +IO contributors+ degradation (with compensation of defocus of –500 compared to real case 4)

ALCATEL ALENIA SPACE
An Alcatel/Finmeccanica company
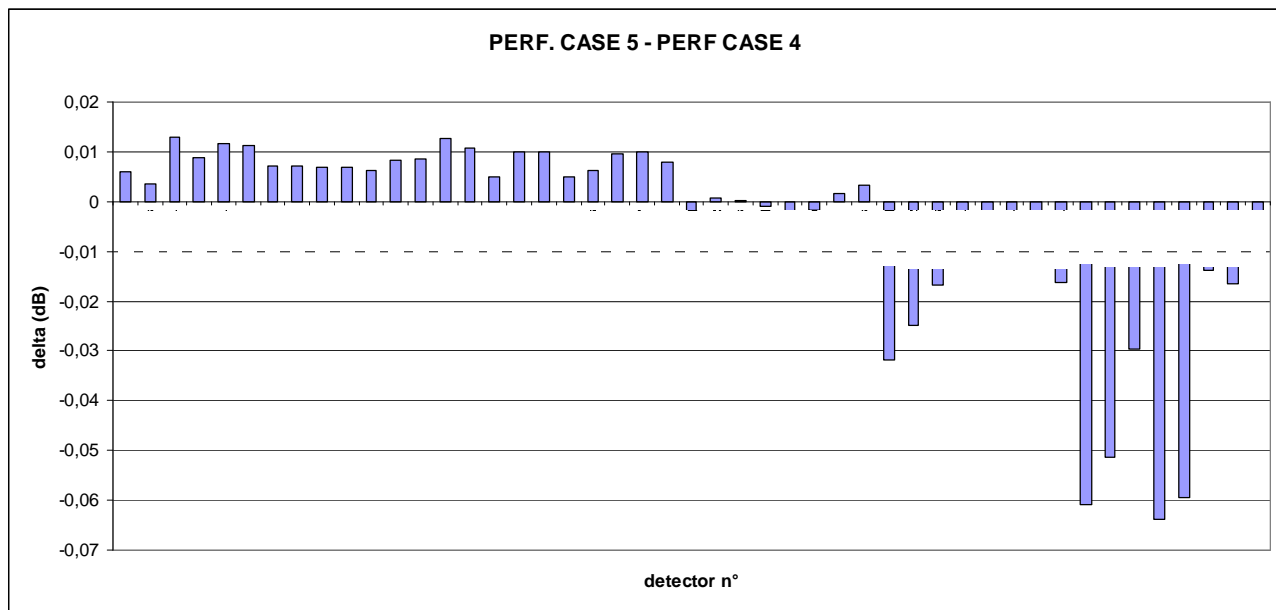


Figure 7.4-13 Improvement if FPU is displaced of -500 microns

CASE 0 : Gain degradation with the flight reflectors: BFE (measured by videogrammetry). The gain degradation is important if any realignment is performed. Moreover a significant depointing angle has been noticed in the patterns, more emphasized at higher frequencies.

CASE 1 : With the flight BFE, the model have been optimised to compensate the surface deviation, the residual gain degradation is around 0.12 dB for HFI-857 horns. The depointing has been corrected.

CASE 2 : The HF surfaces have been added to CASE1, The residual HF distortion degrade the gain at low frequencies and improve the gain at higher frequencies.

CASE 3 : The other IO contributors have been added to CASE 2, one can noticed a slight accentuation in the behaviour observed in CASE2.

CASE 4 : This one constitutes the real case. The alignment-measured data have been inserted in the model.

CASE 5 : This case is an investigation case : a compensation of the FPU by 500 µm translation has been investigated. A realignment of the FPU could improve results for lower frequencies but degrade the budget at higher frequencies.

ALCATEL ALENIA SPACE
An Alcatel/Finmeccanica company

REFERENCE : H-P-3-ASP-AN-323

DATE : 12/2/2007

ISSUE : 3

Page : 90/126

### 7.4.2.8  Other contributors

Some of the contributors could not be calculated directly (be inserted in the numerical model for instance. A specific analysis is  needed in order to evaluate their impact.

### 7.4.2.8.1  Quilting

The quilting has been taken into account for the sub reflector and the measurement of the surface  contain this information. For the main reflector, the reflector surface has not been updated since CDR. As a consequence and to be consequent with the budget, the presence of the quilting must be assesed as for CDR analysis even if his impact is almost negligible.  The results are recalled in the Figure 7.4-14.
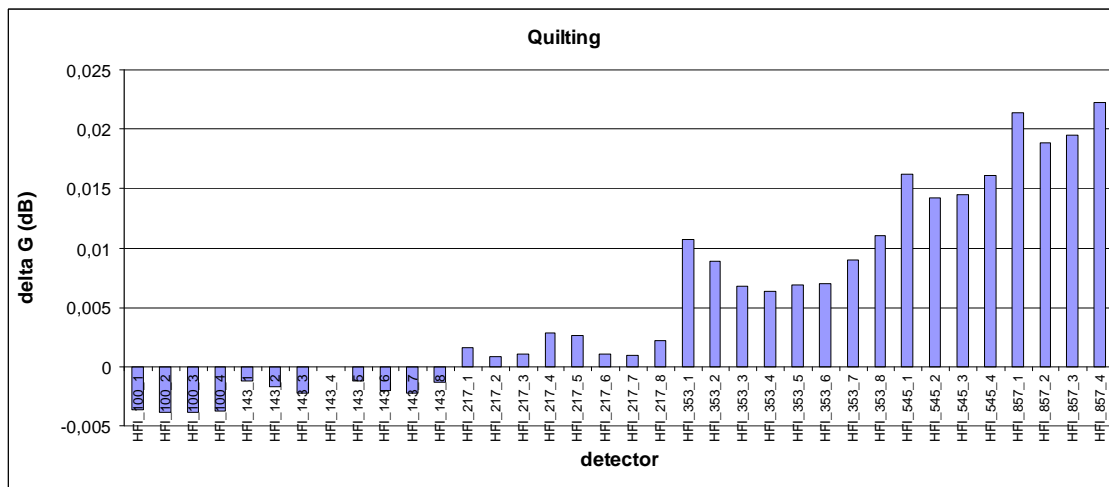


Figure 7.4-14 Degradation due to quilting

The quilting impact is reduced to 0.02 dB at higher frequencies for the two reflectors.  In our case, we have considered an allocation for the main reflector of 0.01 dB for all the detectors.

### 7.4.2.8.2 Ohmic losses

The ohmic losses depend on the surface materials used for the reflectors manufacturing and more precisely on the conductivity of the metal which itself depends on surface finishing and on the nature of the metal. The exact knowledge of the conductivity is difficult to obtain. Some measurement results could be found [1] and [2] up to 377 GHz.

In the scope of the estimation of the ohmic losses, a realistic values for the conductivity has been taken based on the remark in [1]: " the resistivity is twice as high as calculated from nominal DC conductivity" and on the actual quality of the reflector surface: the reflectors are made on pure aluminium.

Based on measurements and empirical assumptions [2][1], the reflection losses at a frequency F (in GHz) in submillimeter frequencies range, for bulk aluminium materials is found to be equal to:

$$L = 0.21 \ \% \ \sqrt{\frac{F}{100}} \tag{1}$$

which correspond to a conductivity of $\sigma = 2 \ 10^{+7}$ S m$^{-1}$ at submillimeter frequencies range ($\sigma = 4 \ 10^{+7}$ S m$^{-1}$ at DC)

For other conductivities the formula found in [1] could be used:

$$L = \frac{10.88.10^{-3}}{30p} \sqrt{\frac{10^{10}}{3s}} \sqrt{\frac{F}{100}} \tag{2}$$

Where F is in GHz.

Different value of conductivity for Aluminium could be found in [1][2] measured at ambient temperature and at frequencies up to 377 GHz. Ohmic losses decrease with temperature and the reflectors are assumed to be at 50 K.

Table 7.4-8 below resumes the values taken for the budget.

---

[1] J. W. Zwart, V. O. Heinen, K. Long and N. Stankiewicz :"Surface resistance measurements at 377 GHz", Int. J. IR and Millimeter Waves, Vol. 17, no. 2, pp. 349-357, Dec. 1996.
[2] J. W. Lamb, "Miscellaneous data on materials for millimetre and submillimetere optics", Int. J. IR and Millimeter Waves, Vol. 17, no. 12, pp. 1997-2034, Dec. 1996.

| frequency (GHz) | delta directivity (dB) |
|---|---|
| 30 | 0,0071 |
| 44 | 0,0086 |
| 70 | 0,0109 |
| 100 | 0,0130 |
| 143 | 0,0156 |
| 217 | 0,0192 |
| 353 | 0,0245 |
| 545 | 0,0305 |
| 857 | 0,0382 |

Table 7.4-8 Gain degradation due to ohmic losses

### 7.4.2.8.3  Roughness

The roughness also intervenes implicitly in the ohmic losses by increasing the surface resistivity, and hence, reducing the efficiency of the reflector surface.

The roughness could be characterised by a peak-to-peak value and a correlation length. As long as this type of contribution is by nature random with small spatial frequency, its impact could not be computed thought the numerical model. Therefore, to estimate the directivity degradation Ruze formula approximated for main peak is used. According to the reflector specification, the surface is assumed to have roughness of 0.2 μm rms.
For a roughness of 0.2 μm rms, it is clearly demonstrated that the roughness has negligible impact (see Table 2-9).

| Frequency | WFE inputs | delta G (dB) (Ruze) |
|---|---|---|
| GHz | (mm) | |
| 30 | 0,2 | NS |
| 44 | 0,2 | NS |
| 70 | 0,2 | NS |
| 100 | 0,2 | NS |
| 143 | 0,2 | NS |
| 217 | 0,2 | NS |
| 353 | 0,2 | NS |
| 545 | 0,2 | NS |
| 857 | 0,2 | 0,0001 |

Table 7.4-9 Gain degradation due to roughness

### 7.4.2.8.4 Micro-cracks effect

Microcracks could be defined as fine slots randomly distributed on the surface of the reflectors.

But for the CDR budget, it has been agreed that there is no microcraks on the reflectors.

### 7.4.2.8.5 Contamination

An allocation is provided on the basis of a 2 µm rms surface error, which is representative of particular contamination:

| Frequency GHz | WFE inputs (mm) | delta G (dB) (Ruze) |
|---|---|---|
| 30 | 2 | NS |
| 44 | 2 | NS |
| 70 | 2 | NS |
| 100 | 2 | 0,0001 |
| 143 | 2 | 0,0002 |
| 217 | 2 | 0,0004 |
| 353 | 2 | 0,0009 |
| 545 | 2 | 0,0023 |
| 857 | 2 | 0,0056 |

Table 7.4-10 Gain degradation due to contamination (NS :not significant)

### 7.4.2.9 Deterministic contributor budget

In Table 2-11 and Figure 2-18, the total budget for the deterministic contributors is presented.

| DETECTOR | deterministic case 4 | deterministic case 5 | quiliting main | ohmic losses | contamination | total with case 4 | total with case 5 |
|---|---|---|---|---|---|---|---|
| | dB | dB | dB | dB | dB | dB | dB |
| LFI_30_27 | 0,1718 | 0,1656 | 0,0100 | 0,0071 | ns | **0,1889** | 0,1827 |
| LFI_30_28 | 0,1715 | 0,1680 | 0,0100 | 0,0071 | ns | **0,1886** | 0,1851 |
| LFI_44_24 | -0,0154 | -0,0284 | 0,0100 | 0,0086 | ns | **0,0032** | -0,0098 |
| LFI_44_25 | 0,0335 | 0,0246 | 0,0100 | 0,0086 | ns | **0,0521** | 0,0432 |
| LFI_44_26 | 0,2322 | 0,2207 | 0,0100 | 0,0086 | ns | **0,2508** | 0,2393 |
| LFI_70_18 | 0,0900 | 0,0786 | 0,0100 | 0,0109 | ns | **0,1109** | 0,0995 |
| LFI_70_19 | 0,1438 | 0,1367 | 0,0100 | 0,0109 | ns | **0,1647** | 0,1576 |
| LFI_70_20 | 0,1763 | 0,1691 | 0,0100 | 0,0109 | ns | **0,1972** | 0,1900 |
| LFI_70_21 | 0,1848 | 0,1780 | 0,0100 | 0,0109 | ns | **0,2057** | 0,1989 |
| LFI_70_22 | 0,1642 | 0,1573 | 0,0100 | 0,0109 | ns | **0,1851** | 0,1782 |
| LFI_70_23 | 0,1096 | 0,1032 | 0,0100 | 0,0109 | ns | **0,1305** | 0,1241 |
| HFI_100_1 | 0,1741 | 0,1659 | 0,0100 | 0,0130 | 0,0001 | **0,1971** | 0,1889 |
| HFI_100_2 | 0,2062 | 0,1977 | 0,0100 | 0,0130 | 0,0001 | **0,2292** | 0,2207 |
| HFI_100_3 | 0,1941 | 0,1812 | 0,0100 | 0,0130 | 0,0001 | **0,2171** | 0,2042 |
| HFI_100_4 | 0,1417 | 0,1308 | 0,0100 | 0,0130 | 0,0001 | **0,1647** | 0,1538 |
| HFI_143_1 | 0,0801 | 0,0750 | 0,0100 | 0,0156 | 0,0002 | **0,1057** | 0,1006 |
| HFI_143_2 | 0,0906 | 0,0805 | 0,0100 | 0,0156 | 0,0002 | **0,1162** | 0,1061 |
| HFI_143_3 | 0,1102 | 0,1002 | 0,0100 | 0,0156 | 0,0002 | **0,1358** | 0,1258 |
| HFI_143_4 | 0,0801 | 0,0750 | 0,0100 | 0,0156 | 0,0002 | **0,1057** | 0,1006 |
| HFI_143_5 | 0,0733 | 0,0668 | 0,0100 | 0,0156 | 0,0002 | **0,0989** | 0,0924 |
| HFI_143_6 | 0,1338 | 0,1242 | 0,0100 | 0,0156 | 0,0002 | **0,1594** | 0,1498 |
| HFI_143_7 | 0,1496 | 0,1396 | 0,0100 | 0,0156 | 0,0002 | **0,1752** | 0,1652 |
| HFI_143_8 | 0,1373 | 0,1293 | 0,0100 | 0,0156 | 0,0002 | **0,1629** | 0,1549 |
| HFI_217_1 | 0,1432 | 0,1520 | 0,0100 | 0,0192 | 0,0004 | **0,1724** | 0,1812 |
| HFI_217_2 | 0,1703 | 0,1695 | 0,0100 | 0,0192 | 0,0004 | **0,1995** | 0,1987 |
| HFI_217_3 | 0,1572 | 0,1570 | 0,0100 | 0,0192 | 0,0004 | **0,1864** | 0,1862 |
| HFI_217_4 | 0,0934 | 0,0942 | 0,0100 | 0,0192 | 0,0004 | **0,1226** | 0,1234 |
| HFI_217_5 | 0,0617 | 0,0661 | 0,0100 | 0,0192 | 0,0004 | **0,0909** | 0,0953 |
| HFI_217_6 | 0,1104 | 0,1121 | 0,0100 | 0,0192 | 0,0004 | **0,1396** | 0,1413 |
| HFI_217_7 | 0,0975 | 0,0959 | 0,0100 | 0,0192 | 0,0004 | **0,1267** | 0,1251 |
| HFI_217_8 | 0,0323 | 0,0291 | 0,0100 | 0,0192 | 0,0004 | **0,0615** | 0,0583 |
| HFI_353_1 | -0,2576 | -0,2257 | 0,0100 | 0,0245 | 0,0009 | **-0,2231** | -0,1912 |
| HFI_353_2 | -0,0600 | -0,0352 | 0,0100 | 0,0245 | 0,0009 | **-0,0255** | -0,0007 |
| HFI_353_3 | 0,0713 | 0,0881 | 0,0100 | 0,0245 | 0,0009 | **0,1058** | 0,1226 |
| HFI_353_4 | 0,1308 | 0,1433 | 0,0100 | 0,0245 | 0,0009 | **0,1653** | 0,1778 |
| HFI_353_5 | 0,1210 | 0,1299 | 0,0100 | 0,0245 | 0,0009 | **0,1555** | 0,1644 |
| HFI_353_6 | 0,0436 | 0,0518 | 0,0100 | 0,0245 | 0,0009 | **0,0781** | 0,0863 |
| HFI_353_7 | -0,0875 | -0,0758 | 0,0100 | 0,0245 | 0,0009 | **-0,0530** | -0,0413 |
| HFI_353_8 | -0,2464 | -0,2302 | 0,0100 | 0,0245 | 0,0009 | **-0,2119** | -0,1957 |
| HFI_545_1 | -0,5709 | -0,5101 | 0,0100 | 0,0305 | 0,0023 | **-0,5304** | -0,4696 |
| HFI_545_2 | -0,1831 | -0,1318 | 0,0100 | 0,0305 | 0,0023 | **-0,1426** | -0,0913 |
| HFI_545_3 | -0,1610 | -0,1313 | 0,0100 | 0,0305 | 0,0023 | **-0,1205** | -0,0908 |
| HFI_545_4 | -0,3245 | -0,2606 | 0,0100 | 0,0305 | 0,0023 | **-0,2840** | -0,2201 |
| HFI_857_1 | 0,1588 | 0,2183 | 0,0100 | 0,0382 | 0,0056 | **0,2070** | 0,2665 |
| HFI_857_2 | 0,4789 | 0,4926 | 0,0100 | 0,0382 | 0,0056 | **0,5271** | 0,5408 |
| HFI_857_3 | 0,4450 | 0,4616 | 0,0100 | 0,0382 | 0,0056 | **0,4932** | 0,5098 |
| HFI_857_4 | 0,1530 | 0,1573 | 0,0100 | 0,0382 | 0,0056 | **0,2012** | 0,2055 |

Table 7.4-11 Determinist: Budget  (ns : not significant)

**Total Deterministic Budget**
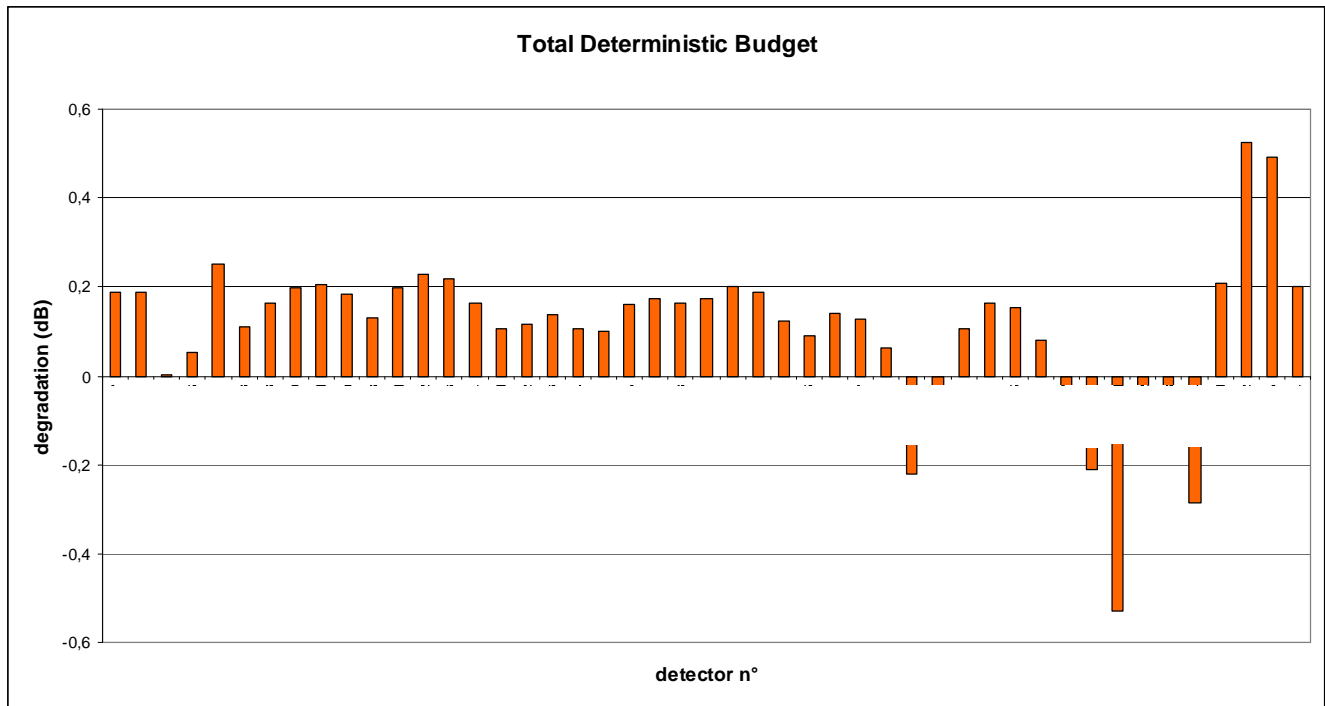


Figure 7.4-15 Determinist: Budget

ALCATEL ALENIA SPACE
An Alcatel/Finmeccanica company

REFERENCE : H-P-3-ASP-AN-323

DATE : 12/2/2007

ISSUE : 3

Page : 96/126

## 7.4.2.10 Conclusion

The deterministic budget have been established with updated data (only the main reflector surface has not been updated). The budget shows a maximum of gain degradation of 0.5 dB at 857 GHz and of less than 0.22 dB for the others horns. However, the deterministic configuration gives an improvement compared to theoretical model for HFI 545 horns and few 353 GHz horns.

## 7.4.3  Statistic contributors

### 7.4.3.1  Origin of inputs

These contributors could be divided into different levels:

> Telescope level
>
> Focal Plane Unit
>
> Telescope-FPU integration
>
> Contingency

The random case at operational is composed of numerous contributors. The data are of two main types: inputs furnished in WFE rms per horn, inputs described in term of BFE random displacements and distortions (translation, rotation, conicity, radius variations). The details of these data are presented in [RD 20]. In this §, only a recall of the inputs is presented followed by the corresponding gain degradation.

This § is divided into two parts: Manufacturing, accuracy budget per Horn and random displacements.

Each part is detailed in the following sections.

### 7.4.3.2  Manufacturing and accuracy budget per Horn

This section deals with:

> -BFE knowledge and structure videogrammetry
>
> -Others contributors: Horns manufacturing, Reflector settling and launch, Reflector coating. /Storage/Optical model

#### 7.4.3.2.1  BFE knowledge and structure videogrammetry

This contributor is the consequence of the measurements uncertainties of the real geometrical configuration of the FM reflectors and their positioning.

The inputs are extracted from optical analysis [RD23] and are recalled in the table below:

**ALCATEL ALENIA SPACE**
An Alcatel/Finmeccanica company

| RANDOM | CASE | BFE Knowledge and structure videogrammetry | | | | | |
| --- | --- | --- | --- | --- | --- | --- | --- |
| microns | microrad | | | | | | |
| REFLECTOR | | | | | | | |
|  | Tx | Ty | Tz | Rx | Ry | dR | dK |
| PR | 100 | 13 | 66 | 140 | 55 | 130 | 0,00010 |
| SR | 170 | 27 | 200 | 150 | 325 | 25 | 0,00009 |
| STRUCTURE | | | | | | | |
|  | Tx | Ty | Tz | Rx | Ry | dR | dK |
| PR | 135,9 | 27,1 | 26,9 | 62,5 | 102,9 | | |
| SR | 53,4 | 27,6 | 32,2 | 69,5 | 194,4 | | |
| FPU | 25 | 25 | 40 | | | | |

Table 7.4-12 Inputs for BFE Knowledge and structure videogrammetry

As the contributors are by nature random, for each deviation (each case of Table 7.4-12) must be computed independently and the degradation induced by each one added by RSS.

For illustration the Table 7.4-12 need $(7+7+5+5+3)\times 2\times 47=2538$ patterns. computation

The results are presented in the Table 7.4-13 by series a, b, c, d and e corresponding to each line of Table 7.4-12.

| detector n° | case a | case b | case c | case d | case e | BFE Know |
|---|---|---|---|---|---|---|
| | dB | dB | dB | dB | dB | dB |
| lfi_30_27 | 0,0045 | 0,0172 | 0,0045 | 0,0034 | 0,0008 | 0,0187 |
| lfi_30_28 | 0,0041 | 0,0173 | 0,0040 | 0,0036 | 0,0007 | 0,0186 |
| lfi_44_24 | 0,0136 | 0,0142 | 0,0094 | 0,0067 | 0,0010 | 0,0228 |
| lfi_44_25 | 0,0136 | 0,0141 | 0,0094 | 0,0068 | 0,0011 | 0,0228 |
| lfi_44_26 | 0,0049 | 0,0318 | 0,0038 | 0,0041 | 0,0008 | 0,0327 |
| lfi_70_18 | 0,0134 | 0,0126 | 0,0065 | 0,0051 | 0,0011 | 0,0202 |
| lfi_70_19 | 0,0144 | 0,0190 | 0,0058 | 0,0056 | 0,0011 | 0,0252 |
| lfi_70_20 | 0,0077 | 0,0287 | 0,0056 | 0,0056 | 0,0009 | 0,0308 |
| lfi_70_21 | 0,0073 | 0,0286 | 0,0058 | 0,0054 | 0,0009 | 0,0306 |
| lfi_70_22 | 0,0110 | 0,0188 | 0,0053 | 0,0058 | 0,0011 | 0,0232 |
| lfi_70_23 | 0,0113 | 0,0126 | 0,0065 | 0,0051 | 0,0011 | 0,0189 |
| hfi_100_1 | 0,0163 | 0,0158 | 0,0079 | 0,0064 | 0,0018 | 0,0249 |
| hfi_100_2 | 0,0108 | 0,0354 | 0,0069 | 0,0094 | 0,0025 | 0,0389 |
| hfi_100_3 | 0,0115 | 0,0354 | 0,0068 | 0,0094 | 0,0023 | 0,0391 |
| hfi_100_4 | 0,0226 | 0,0158 | 0,0095 | 0,0057 | 0,0018 | 0,0298 |
| hfi_143_1 | 0,0296 | 0,0268 | 0,0128 | 0,0111 | 0,0034 | 0,0435 |
| hfi_143_2 | 0,0112 | 0,0287 | 0,0086 | 0,0116 | 0,0035 | 0,0342 |
| hfi_143_3 | 0,0098 | 0,0292 | 0,0083 | 0,0068 | 0,0011 | 0,0326 |
| hfi_143_4 | 0,0296 | 0,0268 | 0,0128 | 0,0111 | 0,0034 | 0,0435 |
| hfi_143_5 | 0,0389 | 0,0419 | 0,0179 | 0,0123 | 0,0011 | 0,0612 |
| hfi_143_6 | 0,0202 | 0,0641 | 0,0158 | 0,0139 | 0,0009 | 0,0704 |
| hfi_143_7 | 0,0193 | 0,0626 | 0,0153 | 0,0125 | 0,0009 | 0,0684 |
| hfi_143_8 | 0,0302 | 0,0451 | 0,0149 | 0,0143 | 0,0027 | 0,0581 |
| hfi_217_1 | 0,0236 | 0,0203 | 0,0152 | 0,0097 | 0,0039 | 0,0362 |
| hfi_217_2 | 0,0197 | 0,0284 | 0,0189 | 0,0086 | 0,0019 | 0,0404 |
| hfi_217_3 | 0,0200 | 0,0285 | 0,0195 | 0,0080 | 0,0016 | 0,0407 |
| hfi_217_4 | 0,0281 | 0,0212 | 0,0162 | 0,0090 | 0,0034 | 0,0399 |
| hfi_217_5 | 0,0143 | 0,0209 | 0,0081 | 0,0066 | 0,0022 | 0,0275 |
| hfi_217_6 | 0,0085 | 0,0081 | 0,0130 | 0,0065 | 0,0030 | 0,0189 |
| hfi_217_7 | 0,0130 | 0,0138 | 0,0116 | 0,0062 | 0,0018 | 0,0231 |
| hfi_217_8 | 0,0192 | 0,0252 | 0,0081 | 0,0085 | 0,0025 | 0,0339 |
| hfi_353_1 | 0,0847 | 0,2232 | 0,0291 | 0,0347 | 0,0046 | 0,2430 |
| hfi_353_2 | 0,0461 | 0,1233 | 0,0230 | 0,0188 | 0,0033 | 0,1350 |
| hfi_353_3 | 0,0370 | 0,0558 | 0,0390 | 0,0176 | 0,0028 | 0,0795 |
| hfi_353_4 | 0,0450 | 0,0648 | 0,0494 | 0,0241 | 0,0027 | 0,0962 |
| hfi_353_5 | 0,0437 | 0,0645 | 0,0526 | 0,0254 | 0,0029 | 0,0974 |
| hfi_353_6 | 0,0294 | 0,0655 | 0,0397 | 0,0170 | 0,0031 | 0,0838 |
| hfi_353_7 | 0,0522 | 0,1340 | 0,0218 | 0,0220 | 0,0039 | 0,1472 |
| hfi_353_8 | 0,0831 | 0,2240 | 0,0327 | 0,0329 | 0,0048 | 0,2434 |
| hfi_545_1 | 0,1789 | 0,4296 | 0,0757 | 0,0679 | 0,0117 | 0,4765 |
| hfi_545_2 | 0,1246 | 0,2483 | 0,0691 | 0,0446 | 0,0119 | 0,2900 |
| hfi_545_3 | 0,1111 | 0,2818 | 0,0582 | 0,0474 | 0,0100 | 0,3122 |
| hfi_545_4 | 0,1639 | 0,4187 | 0,0635 | 0,0639 | 0,0099 | 0,4587 |
| hfi_857_1 | 0,2204 | 0,3651 | 0,2632 | 0,1212 | 0,0259 | 0,5162 |
| hfi_857_2 | 0,2484 | 0,4178 | 0,2967 | 0,1440 | 0,0232 | 0,5878 |
| hfi_857_3 | 0,2470 | 0,4094 | 0,2947 | 0,1388 | 0,0231 | 0,5790 |
| hfi_857_4 | 0,2094 | 0,3942 | 0,2485 | 0,1127 | 0,0276 | 0,5239 |

Table 7.4-13 Results for BFE knowledge and structure videogrammetry

## 7.4.3.2.2 Horns manufacturing and others contributors

| Frequency | 30 | 44 | 70 | 100 | 143 | 217 | 353 | 545 | 857 |
|---|---|---|---|---|---|---|---|---|---|
| Horn manufacture | 13 | 13 | 13 | 10 | 8 | 8 | 5 | 5 | 5 |
| Reflector settling launch | 1 | 1 | 1 | 1 | 1 | 1 | 1 | 1 | 1 |
| Reflector coating/storage | 2,5 | 2,5 | 2,5 | 2,5 | 2,5 | 2,5 | 2,5 | 2,5 | 2,5 |
| Optical model | 2 | 2 | 2 | 2 | 2 | 2 | 2 | 2 | 2 |
| | | | | | | | | | 0,6 |
| WFE (RSS) mm | 13,4 | 13,4 | 13,4 | 10,5 | 8,7 | 8,7 | 6,0 | 6,0 | 6,1 |
| DG (dB) (Ruze) | 0,0003 | 0,0007 | 0,0017 | 0,0021 | 0,0029 | 0,0068 | 0,0086 | 0,0205 | 0,0512 |

Table 7.4-14 Inputs in WFE for the others contributors and gain degradation

Table 7.4-14 gives the WFE per horns. [RD23]. The quantification in term of gain degradation is obtained through Ruze formula:

$$\Delta G_{dB} = \frac{10}{\ln(10)}\left(\frac{2p\ WFE}{l}\right)^2$$

### 7.4.3.2.3 Budget for Manufacturing and accuracy

The budget is computed by summing (RSS) of Table 7.4-13 and Table 7.4-14. The gain degradation associated with this contributor is depicted in Figure 7.4-16.

| detector n° | BFE Know | Other cont. | Total |
|---|---|---|---|
| | dB | dB | dB |
| lfi_30_27 | 0,0187 | 0,0030 | 0,0189 |
| lfi_30_28 | 0,0186 | 0,0030 | 0,0188 |
| lfi_44_24 | 0,0228 | 0,0007 | 0,0228 |
| lfi_44_25 | 0,0228 | 0,0007 | 0,0228 |
| lfi_44_26 | 0,0327 | 0,0007 | 0,0327 |
| lfi_70_18 | 0,0202 | 0,0017 | 0,0203 |
| lfi_70_19 | 0,0252 | 0,0017 | 0,0252 |
| lfi_70_20 | 0,0308 | 0,0017 | 0,0308 |
| lfi_70_21 | 0,0306 | 0,0017 | 0,0306 |
| lfi_70_22 | 0,0232 | 0,0017 | 0,0232 |
| lfi_70_23 | 0,0189 | 0,0017 | 0,0189 |
| hfi_100_1 | 0,0249 | 0,0021 | 0,0250 |
| hfi_100_2 | 0,0389 | 0,0021 | 0,0389 |
| hfi_100_3 | 0,0391 | 0,0021 | 0,0391 |
| hfi_100_4 | 0,0298 | 0,0021 | 0,0298 |
| hfi_143_1 | 0,0435 | 0,0029 | 0,0436 |
| hfi_143_2 | 0,0342 | 0,0029 | 0,0343 |
| hfi_143_3 | 0,0326 | 0,0029 | 0,0328 |
| hfi_143_4 | 0,0435 | 0,0029 | 0,0436 |
| hfi_143_5 | 0,0612 | 0,0029 | 0,0612 |
| hfi_143_6 | 0,0704 | 0,0029 | 0,0705 |
| hfi_143_7 | 0,0684 | 0,0029 | 0,0685 |
| hfi_143_8 | 0,0581 | 0,0029 | 0,0582 |
| hfi_217_1 | 0,0362 | 0,0068 | 0,0368 |
| hfi_217_2 | 0,0404 | 0,0068 | 0,0409 |
| hfi_217_3 | 0,0407 | 0,0068 | 0,0413 |
| hfi_217_4 | 0,0399 | 0,0068 | 0,0405 |
| hfi_217_5 | 0,0275 | 0,0068 | 0,0283 |
| hfi_217_6 | 0,0189 | 0,0068 | 0,0201 |
| hfi_217_7 | 0,0231 | 0,0068 | 0,0241 |
| hfi_217_8 | 0,0339 | 0,0068 | 0,0346 |
| hfi_353_1 | 0,2430 | 0,0086 | 0,2432 |
| hfi_353_2 | 0,1350 | 0,0086 | 0,1353 |
| hfi_353_3 | 0,0795 | 0,0086 | 0,0800 |
| hfi_353_4 | 0,0962 | 0,0086 | 0,0966 |
| hfi_353_5 | 0,0974 | 0,0086 | 0,0978 |
| hfi_353_6 | 0,0838 | 0,0086 | 0,0843 |
| hfi_353_7 | 0,1472 | 0,0086 | 0,1474 |
| hfi_353_8 | 0,2434 | 0,0086 | 0,2436 |
| hfi_545_1 | 0,4765 | 0,0205 | 0,4769 |
| hfi_545_2 | 0,2900 | 0,0205 | 0,2907 |
| hfi_545_3 | 0,3122 | 0,0205 | 0,3129 |
| hfi_545_4 | 0,4587 | 0,0205 | 0,4591 |
| hfi_857_1 | 0,5162 | 0,0512 | 0,5188 |
| hfi_857_2 | 0,5878 | 0,0512 | 0,5901 |
| hfi_857_3 | 0,5790 | 0,0512 | 0,5813 |
| hfi_857_4 | 0,5239 | 0,0512 | 0,5264 |

Table 7.4-15 Total budget for Manufacturing and accuracy

**Manufacturing and accuracy**
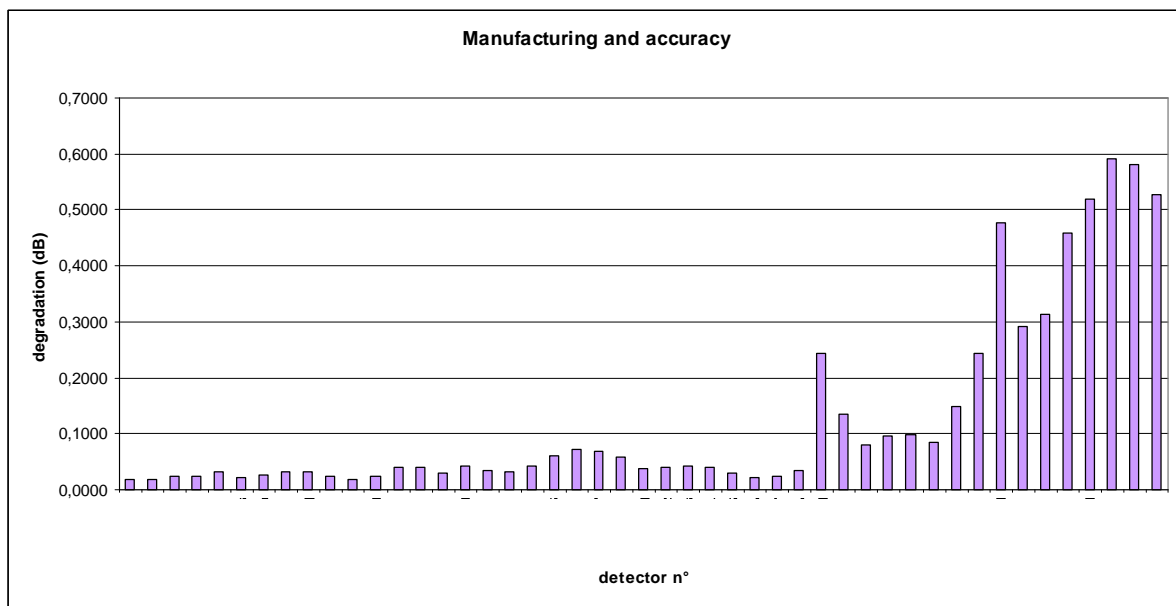


Figure 7.4-16 Budget for Manufacturing and accuracy

### 7.4.3.3 BFE random displacements and distortions

From [RD3 each contributor is expanded in the variations of seven parameters Rx, Ry, Tx, Ty, Tz, ΔK, ΔR in each coordinate system (OM1 , OM1C, OM2, OM2C and ORDP).

This chapter divided into two parts: FPU random displacement and PR and SR displacement case.

### 7.4.3.3.1 FPU random displacement

Inputs for random displacements: are given in Table 7.4-16

| RANDOM | CASE | FPU random budget | | | |
|---|---|---|---|---|---|
| microns | microrad | | | | |
| REFLECTOR | | | | | |
| | Tx | Ty | Tz | Rx | Ry |
| FPU | 120 | 107 | 287 | 0 | 0 |

Table 7.4-16 Inputs for FPU random case

The number of patterns to be calculated is $3 \times 2 \times 47 = 282$.

The results corresponding to this case are given in Table 7.4-17 and plotted in

Figure 7.4-17.

| detector n° | FPU |
|---|---|
| dB | random |
| lfi_30_27 | 0,0049 |
| lfi_30_28 | 0,0047 |
| lfi_44_24 | 0,0067 |
| lfi_44_25 | 0,0069 |
| lfi_44_26 | 0,0052 |
| lfi_70_18 | 0,0059 |
| lfi_70_19 | 0,0054 |
| lfi_70_20 | 0,0045 |
| lfi_70_21 | 0,0048 |
| lfi_70_22 | 0,0058 |
| lfi_70_23 | 0,006 |
| hfi_100_1 | 0,0069 |
| hfi_100_2 | 0,0042 |
| hfi_100_3 | 0,004 |
| hfi_100_4 | 0,0069 |
| hfi_143_1 | 0,0066 |
| hfi_143_2 | 0,0073 |
| hfi_143_3 | 0,004 |
| hfi_143_4 | 0,0066 |
| hfi_143_5 | 0,004 |
| hfi_143_6 | 0,0051 |
| hfi_143_7 | 0,0044 |
| hfi_143_8 | 0,0056 |
| hfi_217_1 | 0,0046 |
| hfi_217_2 | 0,002 |
| hfi_217_3 | 0,0013 |
| hfi_217_4 | 0,0038 |
| hfi_217_5 | 0,0032 |
| hfi_217_6 | 0,0024 |
| hfi_217_7 | 0,0022 |
| hfi_217_8 | 0,0026 |
| hfi_353_1 | 0,0223 |
| hfi_353_2 | 0,0206 |
| hfi_353_3 | 0,0122 |
| hfi_353_4 | 0,013 |
| hfi_353_5 | 0,0141 |
| hfi_353_6 | 0,0145 |
| hfi_353_7 | 0,018 |
| hfi_353_8 | 0,0235 |
| hfi_545_1 | 0,0728 |
| hfi_545_2 | 0,0643 |
| hfi_545_3 | 0,0669 |
| hfi_545_4 | 0,071 |
| hfi_857_1 | 0,1559 |
| hfi_857_2 | 0,1378 |
| hfi_857_3 | 0,1391 |
| hfi_857_4 | 0,16 |

Table 7.4-17 FPU random Budget
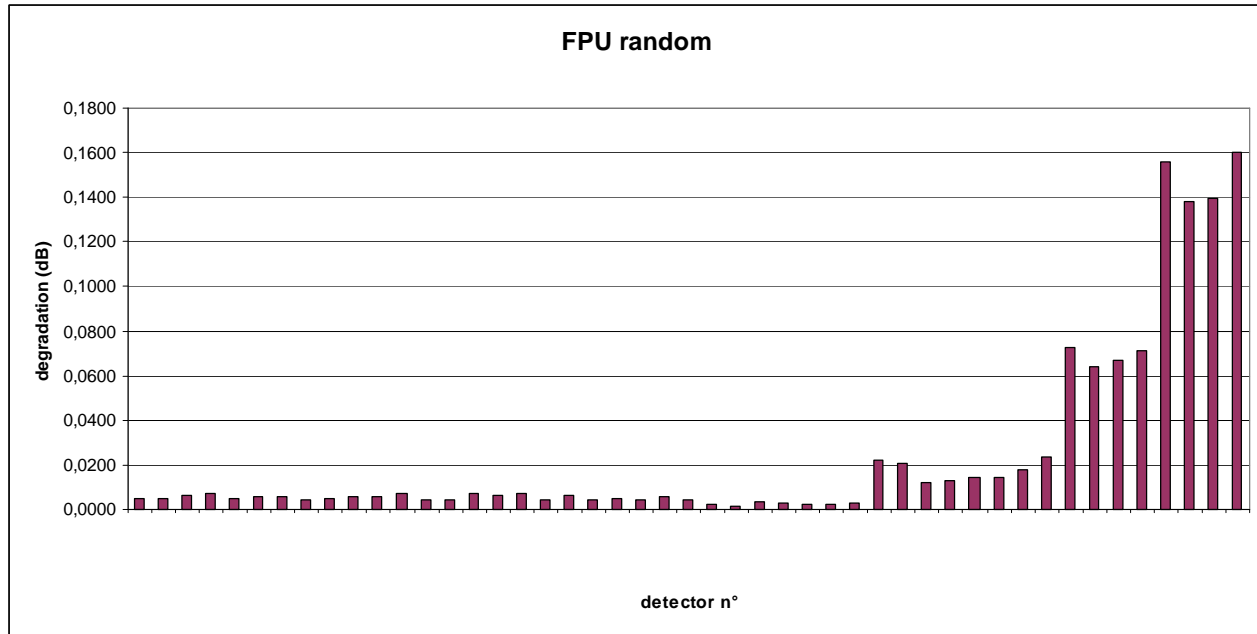
**FPU random**



Figure 7.4-17 FPU random budget

### 7.4.3.3.2  BFE deviation, PR and SR displacements

The contributors are listed in Table 2-14 and Table 2-15 with the details on data organisation. Each contributor impact is computed as defined in Table 2-16.

In order to facilitate the computation each line have been numbered by C1 to C68 (case 1 to 68). Each line has been calculated according to the description in Table 7.4-20. The results of these calculations are shown in the Table 7.4-21 to Table 7.4-27. The number of computation is almost = (24 x 4+16+26) x 2 x 47=12972 patterns.

| | | case n° | Tx µm | Ty µm | Tz µm | Rx µrad | Ry µrad | dR µm | dK | Correlated? | Refocus ? | Nature | Rep |
|---|---|---|---|---|---|---|---|---|---|---|---|---|---|
| PR | QM Videogram, | C1 | 48,0 | 0,0 | 168,0 | 0,0 | 69,1 | 0,0 | 0 | No | Yes | 2sig | OM1C |
| PR | QM T scaling | C2 | -4,8 | 0,0 | -2,7 | 0,0 | 0,1 | 0,0 | 0 | Yes(*) | Yes | 2sig | OM1C |
| PR | QM T know | C3 | -1,0 | 0,0 | -0,6 | 0,0 | 0,0 | 0,0 | 0 | Yes(*) | Yes | 2sig | OM1C |
| PR | CTE non-unif | Frame | C4 | 1,8 | 0,1 | -2,1 | 0,0 | -0,7 | 0,0 | 0 | Yes(*) | Yes | 2sig | OM1C |
| PR | CTE non-unif | Pr pan | C5 | -7,0 | 0,0 | -3,4 | 0,0 | -9,4 | 0,0 | 0 | Yes(*) | Yes | 2sig | OM1C |
| PR | CTE non-unif | SR pan | C6 | -0,1 | 0,0 | -0,2 | 0,0 | -0,1 | 0,0 | 0 | Yes(*) | Yes | 2sig | OM1C |
| PR | CTE non-unif | Fr st1 | C7 | -0,2 | 0,8 | -7,0 | -6,9 | 0,3 | 0,0 | 0 | Yes(*) | Yes | 2sig | OM1C |
| PR | CTE non-unif | Fr st2 | C8 | -0,2 | -0,8 | -6,9 | 9,0 | 0,3 | 0,0 | 0 | Yes(*) | Yes | 2sig | OM1C |
| PR | CTE non-unif | BBS | C9 | -0,2 | 0,0 | 7,7 | 0,0 | -8,2 | 0,0 | 0 | Yes(*) | Yes | 2sig | OM1C |
| PR | CTE non-unif | BTS | C10 | -0,2 | 0,0 | 6,9 | 0,0 | -7,4 | 0,0 | 0 | Yes(*) | Yes | 2sig | OM1C |
| PR | CTE non-unif | Sr st1 | C11 | 0,0 | 0,1 | 0,0 | -0,1 | 0,0 | 0,0 | 0 | Yes(*) | Yes | 2sig | OM1C |
| PR | CTE non-unif | SR st2 | C12 | 0,0 | -0,1 | 0,0 | 0,1 | 0,0 | 0,0 | 0 | Yes(*) | Yes | 2sig | OM1C |
| PR | CTE non-unif | Low st | C13 | -0,2 | 0,0 | 0,0 | 0,0 | -0,4 | 0,0 | 0 | Yes(*) | Yes | 2sig | OM1C |
| PR | CS IF load | | C14 | 3,3 | -0,5 | -1,1 | 0,2 | 8,6 | 0,0 | 0 | No | No | 2sig | OM1C |
| PR | Baffle IF load | | C15 | 1,8 | 0,0 | 9,6 | -0,1 | -0,7 | 0,0 | 0 | No | Yes | 2sig | OM1C |
| PR | FPU IF load | | C16 | 3,9 | 0,0 | -0,9 | 0,0 | 11,5 | 0,0 | 0 | No | No | 2sig | OM1C |
| PR | PR, SR, JFET | | C17 | -0,7 | 0,0 | 0,0 | 0,0 | -1,0 | 0,0 | 0 | No | Yes | 2sig | OM1C |
| PR | Gravity release | | C18 | 5,7 | 0,0 | -11,5 | 0,0 | 20,0 | 0,0 | 0 | No | No | 2sig | OM1C |
| PR | Moist release | Struc | C19 | -4,6 | 0,0 | 2,1 | 0,0 | -9,3 | 0,0 | 0 | No | No | 2sig | OM1C |
| PR | Moist release | refl | C20 | -12,0 | 0,0 | 1,4 | 0,0 | 12,3 | -13,2 | 0 | Yes | No | 2sig | OM1 |
| PR | Alignment | | C21 | 60,8 | 152,0 | 121,6 | 22,4 | 7,2 | 0,0 | 0 | No | No | 2sig | OM1C |
| PR | CS planarity | E | C22 | -0,6 | 0,0 | -37,2 | 0,0 | 92,6 | 0,0 | 0 | Yes(*) | Yes | 2sig | OM1C |
| PR | CS planarity | N-E | C23 | -31,7 | 53,6 | 1,6 | -21,7 | -48,2 | 0,0 | 0 | Yes(*) | No | 2sig | OM1C |
| PR | CS planarity | N-W | C24 | 4,2 | -8,5 | 47,4 | 50,3 | -4,1 | 0,0 | 0 | Yes(*) | No | 2sig | OM1C |
| PR | CS planarity | W | C25 | 0,4 | 0,0 | -0,8 | 0,0 | 1,4 | 0,0 | 0 | Yes(*) | No | 2sig | OM1C |
| PR | CS planarity | S-W | C26 | 4,2 | 8,5 | 47,4 | -50,3 | -4,1 | 0,0 | 0 | Yes(*) | No | 2sig | OM1C |
| PR | CS planarity | S-E | C27 | -31,7 | -53,6 | 1,6 | 21,7 | -48,2 | 0,0 | 0 | Yes(*) | No | 2sig | OM1C |
| PR | TTA | E | C28 | -1,1 | 0,0 | -8,1 | 0,0 | 18,7 | 0,0 | 0 | Yes(*) | No | 2sig | OM1C |
| PR | TTA | N-E | C29 | -6,3 | 10,8 | -0,2 | -4,0 | -7,8 | 0,0 | 0 | Yes(*) | No | 2sig | OM1C |
| PR | TTA | N-W | C30 | 0,3 | -0,4 | 7,8 | 7,5 | -1,7 | 0,0 | 0 | Yes(*) | No | 2sig | OM1C |
| PR | TTA | W | C31 | 0,1 | 0,0 | 0,2 | 0,0 | 0,2 | 0,0 | 0 | Yes(*) | No | 2sig | OM1C |
| PR | TTA | S-W | C32 | 0,3 | 0,4 | 7,8 | -7,5 | -1,7 | 0,0 | 0 | Yes(*) | No | 2sig | OM1C |
| PR | TTA | S-E | C33 | -6,3 | -10,8 | -0,2 | 4,0 | -7,8 | 0,0 | 0 | Yes(*) | No | 2sig | OM1C |
| PR | Structure launch | | C34 | 20,0 | 20,0 | 20,0 | 20,0 | 20,0 | 0,0 | 0 | No | No | 2sig | OM1C |
| PR | Structure creeping | | C35 | 20,0 | 20,0 | 20,0 | 20,0 | 20,0 | 0,0 | 0 | No | No | 2sig | OM1C |
| PR | Structure lifetime | | C36 | 20,0 | 20,0 | 20,0 | 20,0 | 20,0 | 0,0 | 0 | No | No | 2sig | OM1C |
| PR | dT in-orbit | Struc | C37 | -6,3 | 0,8 | -1,8 | 0,8 | 0,1 | 0,0 | 0 | Yes(*) | No | 2sig | OM1C |
| PR | dT in-orbit | refl | C38 | 7,0 | 0,0 | 1,6 | 0,0 | -0,2 | -9,0 | -0 | Yes(*) | No | 2sig | OM1 |
| PR | ISMA | Rad | C39 | 11,1 | 0,0 | -0,6 | 0,0 | -8,5 | 6,6 | -0 | Yes | No | 2sig | OM1 |
| PR | ISMA | Tang | C40 | 0,0 | -1,4 | 0,0 | 0,0 | 0,0 | 0,0 | 0 | Yes | No | 2sig | OM1 |
| PR | ISMA | Out-of-pl | C41 | 25,4 | 0,0 | -73,0 | 0,0 | 0,0 | 0,8 | -0 | Yes | No | 2sig | OM1 |
| PR | ISMA | Rotation | C42 | 0,0 | 1,7 | 0,0 | 0,0 | 0,0 | 0,0 | 0 | Yes | No | 2sig | OM1 |
| PR | ISM-B | Rad | C43 | -11,1 | 0,0 | -0,6 | 0,0 | 8,5 | 6,6 | -0 | Yes | No | 2sig | OM1 |
| PR | ISM-B | Tang | C44 | 0,0 | -1,4 | 0,0 | 0,0 | 0,0 | 0,0 | 0 | Yes | No | 2sig | OM1 |
| PR | ISM-B | Out-of-pl | C45 | 25,4 | 0,0 | -73,0 | 0,0 | 0,0 | 0,8 | -0 | Yes | No | 2sig | OM1 |
| PR | ISM-B | Rotation | C46 | 0,0 | 0,9 | 0,0 | 0,0 | 0,0 | 0,0 | 0 | Yes | No | 2sig | OM1 |
| PR | FEM acc | | C47 | 1,0 | 1,0 | 1,0 | 1,0 | 1,0 | 1,0 | 0 | No | No | 2sig | OM1 |

Table 7.4-18 Input parameters for the sensitivity analysis. Random case

| SR | | | Code | | | | | | | | | | | | |
|----|----------------|----------|------|-------|-------|-------|-------|--------|------|-----|--------|-------|------|------|
| SR | QM Videogram, | | C48 | 52,0 | 0,0 | 55,2 | 0,0 | 175,7 | 0,0 | 0 | No | Yes | 2sig | OM2C |
| SR | QM T scaling | | C2 | 6,9 | 0,0 | 4,7 | 0,0 | 31,6 | 0,0 | 0 | Yes(*) | Yes | 2sig | OM2C |
| SR | QM T know | | C3 | 1,5 | 0,0 | 1,0 | 0,0 | 6,7 | 0,0 | 0 | Yes(*) | Yes | 2sig | OM2C |
| SR | CTE non-unif | Frame | C4 | -5,1 | 0,0 | 3,4 | 0,0 | 23,6 | 0,0 | 0 | Yes(*) | Yes | 2sig | OM2C |
| SR | CTE non-unif | Pr pan | C5 | -0,5 | 0,0 | -0,8 | 0,0 | -0,7 | 0,0 | 0 | Yes(*) | Yes | 2sig | OM2C |
| SR | CTE non-unif | SR pan | C6 | 1,4 | 0,0 | -1,4 | 0,0 | -5,2 | 0,0 | 0 | Yes(*) | Yes | 2sig | OM2C |
| SR | CTE non-unif | Fr st1 | C7 | 0,0 | 0,0 | 0,0 | 0,0 | 0,0 | 0,0 | 0 | Yes(*) | Yes | 2sig | OM2C |
| SR | CTE non-unif | Fr st2 | C8 | 0,0 | 0,0 | 0,0 | 0,0 | 0,0 | 0,0 | 0 | Yes(*) | Yes | 2sig | OM2C |
| SR | CTE non-unif | BBS | C9 | 0,0 | 0,0 | -0,1 | 0,0 | -0,1 | 0,0 | 0 | Yes(*) | Yes | 2sig | OM2C |
| SR | CTE non-unif | BTS | C10 | 1,0 | 0,9 | -2,4 | -9,9 | -8,2 | 0,0 | 0 | Yes(*) | Yes | 2sig | OM2C |
| SR | CTE non-unif | Sr st1 | C11 | 1,0 | 0,9 | -2,4 | -9,9 | -8,2 | 0,0 | 0 | Yes(*) | Yes | 2sig | OM2C |
| SR | CTE non-unif | SR st2 | C12 | 1,0 | -0,9 | -2,4 | 10,0 | -8,2 | 0,0 | 0 | Yes(*) | Yes | 2sig | OM2C |
| SR | CTE non-unif | Low st | C13 | 0,0 | 0,0 | 0,1 | 0,0 | 0,1 | 0,0 | 0 | Yes(*) | Yes | 2sig | OM2C |
| SR | CS IF load | | C49 | 12,1 | 0,1 | 4,0 | 0,3 | -25,0 | 0,0 | 0 | No | No | 2sig | OM2C |
| SR | Baffle IF load | | C50 | -10,5 | 0,0 | -18,6 | 0,1 | 7,9 | 0,0 | 0 | No | No | 2sig | OM2C |
| SR | FPU IF load | | C51 | 0,5 | 0,0 | 1,4 | 0,0 | 0,6 | 0,0 | 0 | No | No | 2sig | OM2C |
| SR | PR, SR, JFET | | C52 | -0,5 | 0,0 | -0,5 | 0,0 | -0,4 | 0,0 | 0 | No | Yes | 2sig | OM2C |
| SR | Gravity release | | C53 | 4,0 | 0,0 | 0,6 | 0,0 | -8,5 | 0,0 | 0 | No | No | 2sig | OM2C |
| SR | Moist release | Struc | C54 | 1,5 | 0,0 | 0,5 | 0,0 | -2,7 | 0,0 | 0 | No | No | 2sig | OM2C |
| SR | Moist release | ref | C55 | 6,5 | 0,0 | -0,2 | 0,0 | -11,0 | 1,4 | 0 | Yes | No | | OM2 |
| SR | alignment | | C56 | 65,9 | 152,0 | 70,0 | 22,4 | 10,0 | 0,0 | 0 | No | Yes | 2sig | OM2C |
| SR | CS planarity | E | C22 | 1,4 | 0,0 | 3,4 | 0,0 | 4,3 | 0,0 | 0 | Yes(*) | No | 2sig | OM2C |
| SR | CS planarity | N-E | C23 | -2,0 | -0,6 | -2,0 | -0,4 | 0,5 | 0,0 | 0 | Yes(*) | No | 2sig | OM2C |
| SR | CS planarity | N-W | C24 | -10,7 | -0,8 | 14,9 | 29,6 | 61,0 | 0,0 | 0 | Yes(*) | No | 2sig | OM2C |
| SR | CS planarity | W | C25 | -46,9 | 0,0 | 36,1 | 0,0 | -150,0 | 0,0 | 0 | Yes(*) | No | 2sig | OM2C |
| SR | CS planarity | S-W | C26 | -10,7 | 0,8 | 14,9 | -29,6 | 61,0 | 0,0 | 0 | Yes(*) | No | 2sig | OM2C |
| SR | CS planarity | S-E | C27 | -2,0 | 0,6 | -2,0 | 0,4 | 0,5 | 0,0 | 0 | Yes(*) | No | 2sig | OM2C |
| SR | TTA | E | C28 | 0,2 | 0,0 | 0,5 | 0,0 | -0,4 | 0,0 | 0 | Yes(*) | No | 2sig | OM2C |
| SR | TTA | N-E | C29 | 0,0 | 0,1 | 0,6 | 0,8 | 1,2 | 0,0 | 0 | Yes(*) | No | 2sig | OM2C |
| SR | TTA | N-W | C30 | -1,9 | -0,6 | 2,5 | 4,1 | 9,4 | 0,0 | 0 | Yes(*) | No | 2sig | OM2C |
| SR | TTA | W | C31 | -7,1 | 0,0 | 4,6 | 0,0 | -21,0 | 0,0 | 0 | Yes(*) | No | 2sig | OM2C |
| SR | TTA | S-W | C32 | -1,9 | 0,6 | 2,5 | -4,1 | 9,4 | 0,0 | 0 | Yes(*) | No | 2sig | OM2C |
| SR | TTA | S-E | C33 | 0,0 | -0,1 | 0,6 | -0,8 | 1,2 | 0,0 | 0 | Yes(*) | No | 2sig | OM2C |
| SR | Structure launch | | C57 | 20,0 | 20,0 | 20,0 | 20,0 | 20,0 | 0,0 | 0 | No | No | 2sig | OM2C |
| SR | Structure creeping | | C58 | 20,0 | 20,0 | 20,0 | 20,0 | 20,0 | 0,0 | 0 | No | No | 2sig | OM2C |
| SR | Structure lifetime | | C59 | 20,0 | 20,0 | 20,0 | 20,0 | 20,0 | 0,0 | 0 | No | No | 2sig | OM2C |
| SR | dT in-orbit | Struc | C37 | 8,5 | -0,3 | 5,5 | 0,6 | 37,3 | 0,0 | 0 | Yes(*) | No | 2sig | OM2C |
| SR | dT in-orbit | refl | C38 | -3,3 | -0,1 | -0,7 | -0,2 | -0,6 | 4,0 | 0 | Yes(*) | No | 2sig | OM2 |
| SR | ISM-A | Rad | C60 | -11,5 | 0,0 | -1,5 | 0,0 | -15,5 | -2,0 | 0 | Yes | No | 2sig | OM2 |
| SR | ISM-A | Tang | C61 | 0,0 | -46,0 | 0,0 | 0,0 | 0,0 | 0,0 | 0 | Yes | No | 2sig | OM2 |
| SR | ISM-A | Out-of-pl | C62 | -34,0 | 0,0 | 60,0 | 0,0 | 0,0 | 0,3 | -0 | Yes | No | 2sig | OM2 |
| SR | ISM-A | Rotation | C63 | 0,0 | 6,0 | 0,0 | 0,0 | 0,0 | 0,0 | 0 | Yes | No | 2sig | OM2 |
| SR | ISM-B | Rad | C64 | 11,5 | 0,0 | -1,5 | 0,0 | 15,5 | -2,0 | 0 | Yes | No | 2sig | OM2 |
| SR | ISM-B | Tang | C65 | 0,0 | -46,0 | -0,1 | 0,0 | 0,0 | 0,0 | 0 | Yes | No | 2sig | OM2 |
| SR | ISM-B | Out-of-pl | C66 | -34,0 | 0,0 | 60,0 | 0,0 | 0,0 | 0,3 | -0 | Yes | No | 2sig | OM2 |
| SR | ISM-B | Rotation | C67 | 0,0 | 6,0 | 0,0 | 0,0 | 0,0 | 0,0 | 0 | Yes | No | 2sig | OM2 |
| SR | FEM acc | | C68 | 1,0 | 1,0 | 1,0 | 1,0 | 1,0 | 1,0 | 0 | No | No | 2sig | OM2 |

Table 7.4-19 Input parameters for sensitivity analysis: Random case

ALCATEL ALENIA SPACE
An Alcatel/Finmeccanica company

| | | | case | Tx | Ty | Tz | Rx | Ry | dR | dK | Correlated? | Refocus ? | Nature | Rep |
|---|---|---|---|---|---|---|---|---|---|---|---|---|---|---|
| | | | n° | µm | µm | µm | µrad | µrad | µm | | | | | |
| PR | QM Videogram, | | C1 | 48,0 | 0,0 | 168,0 | 0,0 | 69,1 | 0,0 | 0 | No | Yes | 2sig | OM1C |
| PR | QM T scaling | | C2 | -4,8 | 0,0 | -2,7 | 0,0 | 0,1 | 0,0 | 0 | Yes(*) | Yes | 2sig | OM1C |
| PR | QM T know | | C3 | -1,0 | 0,0 | -0,6 | 0,0 | 0,0 | 0,0 | 0 | Yes(*) | Yes | 2sig | OM1C |

**1      2      3      4      5   6   7 8   9   10   11**

Table 7.4-20 Descriptions of the columns

1 : SR (secondary reflector), PR (primary reflector) or FPU (focal plane unit)
2 : sub load case name
3 : case identification CX
4 : translation variation: Tx, Ty,Tz
5 : rotation variation: Rx , Ry
6 : radius variation dR
7 : conicity variation dK
8 : correlation type : No, Yes, Yes (* ) :

No : means that the gain degradation of all individual variation and his opposite variation (translation, rotation, radius or conicity) have been computed. The total gain degradation is obtained by a RSS summation of individual degradation due to each variation (or his opposite variation if it constitute the worst case).

Yes : means that the gain degradation of the set of variations (translations, rotation, radius and conicity) and his opposite set) for the PR or the SR have been computed. The worst case between the set of variation and the opposite has been taken as gain degradation for this case.

Yes(*) : means that the gain degradation of the set of variations (translations, rotations, radius and conicity) and his opposite set) the SR and PR have been computed. The worst case between the set of variation and the opposite has been taken as gain degradation for this case.

 9 : Refocus compensation. Random decentring cases are with (Yes) or without refocus (No). As the RF routine is without refocus, the magnitude of the refocus cases has been decreased to take into account the sensitivity difference.

10 : Error type
11 : Coordinate system ( OM1, OM2, OM1C, OM2C, ORDP)

| detector n° | case1 | case2 | case3 | case4 | case5 | case6 | case7 | case8 | case9 | case10 |
|---|---|---|---|---|---|---|---|---|---|---|
| | dB | dB | dB | dB | dB | dB | dB | dB | dB | dB |
| lfi_70_18 | 0.0036 | 0.0006 | 0.0002 | 0.0004 | 0.0006 | 0.0003 | 0.0003 | 0.0003 | 0.0001 | 0.0003 |
| lfi_70_19 | 0.0036 | 0.0008 | 0.0002 | 0.0014 | 0.0010 | 0.0003 | 0.0007 | 0.0006 | 0.0004 | 0.0014 |
| lfi_70_20 | 0.0071 | 0.0013 | 0.0002 | 0.0025 | 0.0021 | 0.0006 | 0.0007 | 0.0003 | 0.0008 | 0.0016 |
| lfi_70_21 | 0.0071 | 0.0013 | 0.0002 | 0.0025 | 0.0021 | 0.0006 | 0.0002 | 0.0008 | 0.0008 | 0.0012 |
| lfi_70_22 | 0.0036 | 0.0008 | 0.0002 | 0.0014 | 0.0010 | 0.0003 | 0.0004 | 0.0009 | 0.0004 | 0.0005 |
| lfi_70_23 | 0.0036 | 0.0006 | 0.0002 | 0.0004 | 0.0006 | 0.0003 | 0.0002 | 0.0004 | 0.0001 | 0.0005 |
| lfi_44_24 | 0.0052 | 0.0005 | 0.0001 | 0.0013 | 0.0010 | 0.0003 | 0.0003 | 0.0004 | 0.0002 | 0.0004 |
| lfi_44_25 | 0.0039 | 0.0004 | 0.0001 | 0.0002 | 0.0006 | 0.0000 | 0.0007 | 0.0006 | 0.0004 | 0.0005 |
| lfi_44_26 | 0.0039 | 0.0004 | 0.0001 | 0.0003 | 0.0006 | 0.0000 | 0.0004 | 0.0009 | 0.0004 | 0.0012 |
| lfi_30_27 | 0.0030 | 0.0006 | 0.0001 | 0.0009 | 0.0006 | 0.0002 | 0.0001 | 0.0002 | 0.0003 | 0.0004 |
| lfi_30_28 | 0.0030 | 0.0006 | 0.0001 | 0.0009 | 0.0006 | 0.0002 | 0.0002 | 0.0001 | 0.0003 | 0.0006 |
| hfi_100_1 | 0.0030 | 0.0022 | 0.0004 | 0.0011 | 0.0015 | 0.0008 | 0.0012 | 0.0020 | 0.0017 | 0.0007 |
| hfi_100_2 | 0.0083 | 0.0031 | 0.0005 | 0.0032 | 0.0035 | 0.0012 | 0.0017 | 0.0012 | 0.0019 | 0.0050 |
| hfi_100_3 | 0.0083 | 0.0031 | 0.0005 | 0.0032 | 0.0035 | 0.0012 | 0.0007 | 0.0021 | 0.0019 | 0.0027 |
| hfi_100_4 | 0.0030 | 0.0022 | 0.0004 | 0.0011 | 0.0015 | 0.0008 | 0.0015 | 0.0017 | 0.0017 | 0.0038 |
| hfi_143_1 | 0.0035 | 0.0015 | 0.0005 | 0.0009 | 0.0006 | 0.0010 | 0.0021 | 0.0025 | 0.0015 | 0.0033 |
| hfi_143_2 | 0.0066 | 0.0028 | 0.0008 | 0.0038 | 0.0032 | 0.0014 | 0.0009 | 0.0009 | 0.0018 | 0.0026 |
| hfi_143_3 | 0.0056 | 0.0003 | 0.0003 | 0.0020 | 0.0007 | 0.0006 | 0.0004 | 0.0006 | 0.0013 | 0.0003 |
| hfi_143_4 | 0.0035 | 0.0015 | 0.0005 | 0.0009 | 0.0006 | 0.0010 | 0.0021 | 0.0025 | 0.0015 | 0.0033 |
| hfi_143_5 | 0.0090 | 0.0009 | 0.0001 | 0.0025 | 0.0014 | 0.0002 | 0.0004 | 0.0004 | 0.0006 | 0.0013 |
| hfi_143_6 | 0.0153 | 0.0010 | 0.0002 | 0.0037 | 0.0025 | 0.0002 | 0.0009 | 0.0008 | 0.0007 | 0.0016 |
| hfi_143_7 | 0.0146 | 0.0005 | 0.0001 | 0.0032 | 0.0018 | 0.0002 | 0.0005 | 0.0012 | 0.0006 | 0.0006 |
| hfi_143_8 | 0.0092 | 0.0025 | 0.0005 | 0.0025 | 0.0028 | 0.0012 | 0.0005 | 0.0003 | 0.0018 | 0.0027 |
| hfi_217_1 | 0.0114 | 0.0027 | 0.0009 | 0.0023 | 0.0026 | 0.0016 | 0.0020 | 0.0021 | 0.0024 | 0.0048 |
| hfi_217_2 | 0.0099 | 0.0012 | 0.0006 | 0.0030 | 0.0021 | 0.0012 | 0.0007 | 0.0024 | 0.0006 | 0.0021 |
| hfi_217_3 | 0.0102 | 0.0008 | 0.0005 | 0.0028 | 0.0019 | 0.0011 | 0.0018 | 0.0015 | 0.0004 | 0.0003 |
| hfi_217_4 | 0.0120 | 0.0023 | 0.0009 | 0.0016 | 0.0022 | 0.0014 | 0.0015 | 0.0020 | 0.0020 | 0.0031 |
| hfi_217_5 | 0.0200 | 0.0008 | 0.0006 | 0.0018 | 0.0024 | 0.0012 | 0.0007 | 0.0004 | 0.0007 | 0.0015 |
| hfi_217_6 | 0.0120 | 0.0018 | 0.0005 | 0.0014 | 0.0012 | 0.0012 | 0.0008 | 0.0008 | 0.0023 | 0.0006 |
| hfi_217_7 | 0.0102 | 0.0006 | 0.0006 | 0.0018 | 0.0008 | 0.0013 | 0.0005 | 0.0015 | 0.0007 | 0.0017 |
| hfi_217_8 | 0.0197 | 0.0006 | 0.0006 | 0.0007 | 0.0014 | 0.0015 | 0.0016 | 0.0017 | 0.0020 | 0.0009 |
| hfi_353_1 | 0.0838 | 0.0022 | 0.0014 | 0.0090 | 0.0083 | 0.0027 | 0.0036 | 0.0027 | 0.0021 | 0.0040 |
| hfi_353_2 | 0.0559 | 0.0023 | 0.0008 | 0.0034 | 0.0045 | 0.0019 | 0.0036 | 0.0029 | 0.0017 | 0.0032 |
| hfi_353_3 | 0.0415 | 0.0014 | 0.0008 | 0.0010 | 0.0013 | 0.0015 | 0.0022 | 0.0014 | 0.0012 | 0.0012 |
| hfi_353_4 | 0.0357 | 0.0009 | 0.0007 | 0.0023 | 0.0005 | 0.0019 | 0.0020 | 0.0013 | 0.0023 | 0.0018 |
| hfi_353_5 | 0.0328 | 0.0018 | 0.0008 | 0.0015 | 0.0010 | 0.0013 | 0.0028 | 0.0027 | 0.0028 | 0.0037 |
| hfi_353_6 | 0.0430 | 0.0011 | 0.0008 | 0.0014 | 0.0012 | 0.0013 | 0.0034 | 0.0029 | 0.0006 | 0.0025 |
| hfi_353_7 | 0.0612 | 0.0010 | 0.0012 | 0.0050 | 0.0043 | 0.0019 | 0.0032 | 0.0032 | 0.0011 | 0.0007 |
| hfi_353_8 | 0.0842 | 0.0033 | 0.0004 | 0.0074 | 0.0090 | 0.0017 | 0.0021 | 0.0032 | 0.0020 | 0.0040 |
| hfi_545_1 | 0.1421 | 0.0046 | 0.0014 | 0.0144 | 0.0152 | 0.0044 | 0.0091 | 0.0019 | 0.0030 | 0.0107 |
| hfi_545_2 | 0.1164 | 0.0021 | 0.0007 | 0.0055 | 0.0073 | 0.0024 | 0.0078 | 0.0006 | 0.0015 | 0.0041 |
| hfi_545_3 | 0.1234 | 0.0020 | 0.0008 | 0.0072 | 0.0076 | 0.0015 | 0.0013 | 0.0073 | 0.0007 | 0.0026 |
| hfi_545_4 | 0.1405 | 0.0050 | 0.0019 | 0.0139 | 0.0154 | 0.0046 | 0.0015 | 0.0098 | 0.0032 | 0.0021 |
| hfi_857_1 | 0.1937 | 0.0014 | 0.0007 | 0.0011 | 0.0004 | 0.0005 | 0.0100 | 0.0031 | 0.0068 | 0.0032 |
| hfi_857_2 | 0.1643 | 0.0023 | 0.0017 | 0.0088 | 0.0064 | 0.0033 | 0.0067 | 0.0039 | 0.0086 | 0.0097 |
| hfi_857_3 | 0.1706 | 0.0020 | 0.0006 | 0.0083 | 0.0048 | 0.0031 | 0.0058 | 0.0095 | 0.0079 | 0.0120 |
| hfi_857_4 | 0.2025 | 0.0013 | 0.0010 | 0.0005 | 0.0035 | 0.0006 | 0.0042 | 0.0135 | 0.0058 | 0.0098 |

Table 7.4-21 random case (1 to 10)

| detector n° | case11 dB | case12 dB | case13 dB | case14 dB | case15 dB | case16 dB | case17 dB | case18 dB | case19 dB | case20 dB |
|---|---|---|---|---|---|---|---|---|---|---|
| lfi_70_18 | 0.0006 | 0.0001 | 0.0000 | 0.0001 | 0.0001 | 0.0003 | 0.0000 | 0.0009 | 0.0001 | 0.0004 |
| lfi_70_19 | 0.0010 | 0.0004 | 0.0000 | 0.0006 | 0.0002 | 0.0008 | 0.0001 | 0.0013 | 0.0006 | 0.0004 |
| lfi_70_20 | 0.0011 | 0.0004 | 0.0001 | 0.0013 | 0.0005 | 0.0017 | 0.0001 | 0.0021 | 0.0014 | 0.0000 |
| lfi_70_21 | 0.0006 | 0.0009 | 0.0001 | 0.0013 | 0.0005 | 0.0017 | 0.0001 | 0.0021 | 0.0014 | 0.0000 |
| lfi_70_22 | 0.0002 | 0.0009 | 0.0000 | 0.0006 | 0.0002 | 0.0008 | 0.0001 | 0.0013 | 0.0006 | 0.0004 |
| lfi_70_23 | 0.0000 | 0.0005 | 0.0000 | 0.0001 | 0.0001 | 0.0003 | 0.0000 | 0.0009 | 0.0001 | 0.0004 |
| lfi_44_24 | 0.0004 | 0.0003 | 0.0000 | 0.0005 | 0.0003 | 0.0007 | 0.0001 | 0.0014 | 0.0005 | 0.0005 |
| lfi_44_25 | 0.0007 | 0.0008 | 0.0000 | 0.0003 | 0.0002 | 0.0004 | 0.0000 | 0.0008 | 0.0003 | 0.0005 |
| lfi_44_26 | 0.0008 | 0.0007 | 0.0000 | 0.0003 | 0.0002 | 0.0004 | 0.0000 | 0.0008 | 0.0003 | 0.0005 |
| lfi_30_27 | 0.0002 | 0.0003 | 0.0000 | 0.0004 | 0.0002 | 0.0005 | 0.0001 | 0.0008 | 0.0004 | 0.0003 |
| lfi_30_28 | 0.0004 | 0.0001 | 0.0000 | 0.0004 | 0.0002 | 0.0005 | 0.0001 | 0.0008 | 0.0004 | 0.0003 |
| hfi_100_1 | 0.0009 | 0.0024 | 0.0001 | 0.0022 | 0.0004 | 0.0020 | 0.0002 | 0.0015 | 0.0024 | 0.0018 |
| hfi_100_2 | 0.0030 | 0.0005 | 0.0001 | 0.0028 | 0.0008 | 0.0036 | 0.0003 | 0.0029 | 0.0031 | 0.0013 |
| hfi_100_3 | 0.0006 | 0.0025 | 0.0001 | 0.0028 | 0.0008 | 0.0036 | 0.0003 | 0.0029 | 0.0031 | 0.0013 |
| hfi_100_4 | 0.0027 | 0.0011 | 0.0001 | 0.0022 | 0.0004 | 0.0020 | 0.0002 | 0.0015 | 0.0024 | 0.0018 |
| hfi_143_1 | 0.0036 | 0.0016 | 0.0001 | 0.0016 | 0.0004 | 0.0008 | 0.0002 | 0.0009 | 0.0014 | 0.0006 |
| hfi_143_2 | 0.0015 | 0.0008 | 0.0002 | 0.0024 | 0.0009 | 0.0029 | 0.0004 | 0.0036 | 0.0026 | 0.0020 |
| hfi_143_3 | 0.0012 | 0.0009 | 0.0001 | 0.0009 | 0.0003 | 0.0003 | 0.0001 | 0.0019 | 0.0007 | 0.0007 |
| hfi_143_4 | 0.0036 | 0.0016 | 0.0001 | 0.0016 | 0.0004 | 0.0008 | 0.0002 | 0.0009 | 0.0014 | 0.0006 |
| hfi_143_5 | 0.0007 | 0.0008 | 0.0000 | 0.0009 | 0.0001 | 0.0008 | 0.0000 | 0.0028 | 0.0010 | 0.0015 |
| hfi_143_6 | 0.0010 | 0.0012 | 0.0000 | 0.0005 | 0.0003 | 0.0015 | 0.0001 | 0.0039 | 0.0008 | 0.0003 |
| hfi_143_7 | 0.0011 | 0.0010 | 0.0000 | 0.0006 | 0.0004 | 0.0010 | 0.0000 | 0.0034 | 0.0007 | 0.0006 |
| hfi_143_8 | 0.0017 | 0.0011 | 0.0001 | 0.0026 | 0.0008 | 0.0027 | 0.0003 | 0.0023 | 0.0029 | 0.0005 |
| hfi_217_1 | 0.0039 | 0.0026 | 0.0002 | 0.0024 | 0.0008 | 0.0027 | 0.0004 | 0.0021 | 0.0026 | 0.0015 |
| hfi_217_2 | 0.0010 | 0.0027 | 0.0001 | 0.0007 | 0.0010 | 0.0015 | 0.0003 | 0.0028 | 0.0010 | 0.0003 |
| hfi_217_3 | 0.0029 | 0.0012 | 0.0001 | 0.0004 | 0.0009 | 0.0012 | 0.0003 | 0.0027 | 0.0006 | 0.0003 |
| hfi_217_4 | 0.0020 | 0.0031 | 0.0002 | 0.0019 | 0.0005 | 0.0023 | 0.0004 | 0.0018 | 0.0020 | 0.0010 |
| hfi_217_5 | 0.0008 | 0.0012 | 0.0001 | 0.0008 | 0.0003 | 0.0018 | 0.0002 | 0.0032 | 0.0011 | 0.0004 |
| hfi_217_6 | 0.0009 | 0.0014 | 0.0001 | 0.0019 | 0.0002 | 0.0009 | 0.0002 | 0.0010 | 0.0017 | 0.0017 |
| hfi_217_7 | 0.0008 | 0.0014 | 0.0001 | 0.0009 | 0.0011 | 0.0006 | 0.0003 | 0.0018 | 0.0009 | 0.0002 |
| hfi_217_8 | 0.0018 | 0.0015 | 0.0002 | 0.0020 | 0.0014 | 0.0015 | 0.0004 | 0.0025 | 0.0019 | 0.0008 |
| hfi_353_1 | 0.0035 | 0.0016 | 0.0005 | 0.0052 | 0.0049 | 0.0061 | 0.0010 | 0.0133 | 0.0057 | 0.0021 |
| hfi_353_2 | 0.0037 | 0.0025 | 0.0001 | 0.0039 | 0.0030 | 0.0042 | 0.0002 | 0.0079 | 0.0041 | 0.0023 |
| hfi_353_3 | 0.0010 | 0.0020 | 0.0001 | 0.0014 | 0.0015 | 0.0020 | 0.0003 | 0.0024 | 0.0019 | 0.0034 |
| hfi_353_4 | 0.0023 | 0.0027 | 0.0001 | 0.0014 | 0.0013 | 0.0011 | 0.0003 | 0.0027 | 0.0019 | 0.0032 |
| hfi_353_5 | 0.0028 | 0.0025 | 0.0002 | 0.0017 | 0.0024 | 0.0012 | 0.0005 | 0.0033 | 0.0018 | 0.0015 |
| hfi_353_6 | 0.0013 | 0.0016 | 0.0002 | 0.0008 | 0.0029 | 0.0010 | 0.0005 | 0.0044 | 0.0010 | 0.0021 |
| hfi_353_7 | 0.0019 | 0.0013 | 0.0004 | 0.0033 | 0.0040 | 0.0031 | 0.0008 | 0.0084 | 0.0035 | 0.0020 |
| hfi_353_8 | 0.0014 | 0.0013 | 0.0002 | 0.0055 | 0.0033 | 0.0073 | 0.0003 | 0.0120 | 0.0060 | 0.0037 |
| hfi_545_1 | 0.0099 | 0.0042 | 0.0003 | 0.0084 | 0.0074 | 0.0113 | 0.0009 | 0.0209 | 0.0089 | 0.0038 |
| hfi_545_2 | 0.0044 | 0.0030 | 0.0003 | 0.0038 | 0.0060 | 0.0053 | 0.0005 | 0.0114 | 0.0042 | 0.0064 |
| hfi_545_3 | 0.0009 | 0.0032 | 0.0002 | 0.0047 | 0.0055 | 0.0056 | 0.0002 | 0.0121 | 0.0049 | 0.0058 |
| hfi_545_4 | 0.0012 | 0.0069 | 0.0007 | 0.0084 | 0.0079 | 0.0118 | 0.0014 | 0.0213 | 0.0091 | 0.0036 |
| hfi_857_1 | 0.0028 | 0.0043 | 0.0003 | 0.0029 | 0.0097 | 0.0031 | 0.0006 | 0.0125 | 0.0038 | 0.0131 |
| hfi_857_2 | 0.0024 | 0.0048 | 0.0005 | 0.0051 | 0.0088 | 0.0051 | 0.0012 | 0.0131 | 0.0063 | 0.0126 |
| hfi_857_3 | 0.0048 | 0.0018 | 0.0003 | 0.0030 | 0.0084 | 0.0037 | 0.0006 | 0.0112 | 0.0044 | 0.0134 |
| hfi_857_4 | 0.0045 | 0.0040 | 0.0006 | 0.0035 | 0.0109 | 0.0037 | 0.0009 | 0.0143 | 0.0045 | 0.0142 |

Table 7.4-22 random case (11 to 20)

| detector n° | case21 | case22 | case23 | case24 | case25 | case26 | case27 | case28 | case29 | case30 |
|---|---|---|---|---|---|---|---|---|---|---|
| | dB | dB | dB | dB | dB | dB | dB | dB | dB | dB |
| lfi_70_18 | 0.0120 | 0.0041 | 0.0051 | 0.0029 | 0.0008 | 0.0054 | 0.0003 | 0.0007 | 0.0007 | 0.0007 |
| lfi_70_19 | 0.0118 | 0.0015 | 0.0006 | 0.0062 | 0.0031 | 0.0019 | 0.0042 | 0.0010 | 0.0001 | 0.0015 |
| lfi_70_20 | 0.0081 | 0.0041 | 0.0035 | 0.0057 | 0.0049 | 0.0022 | 0.0058 | 0.0020 | 0.0013 | 0.0015 |
| lfi_70_21 | 0.0081 | 0.0041 | 0.0058 | 0.0016 | 0.0049 | 0.0062 | 0.0035 | 0.0020 | 0.0019 | 0.0009 |
| lfi_70_22 | 0.0118 | 0.0015 | 0.0042 | 0.0023 | 0.0031 | 0.0060 | 0.0006 | 0.0010 | 0.0013 | 0.0003 |
| lfi_70_23 | 0.0120 | 0.0041 | 0.0003 | 0.0052 | 0.0008 | 0.0025 | 0.0051 | 0.0007 | 0.0005 | 0.0004 |
| lfi_44_24 | 0.0057 | 0.0035 | 0.0043 | 0.0040 | 0.0063 | 0.0047 | 0.0043 | 0.0008 | 0.0006 | 0.0007 |
| lfi_44_25 | 0.0166 | 0.0037 | 0.0067 | 0.0081 | 0.0034 | 0.0064 | 0.0004 | 0.0008 | 0.0012 | 0.0012 |
| lfi_44_26 | 0.0166 | 0.0037 | 0.0004 | 0.0061 | 0.0034 | 0.0076 | 0.0067 | 0.0008 | 0.0003 | 0.0009 |
| lfi_30_27 | 0.0057 | 0.0007 | 0.0021 | 0.0019 | 0.0033 | 0.0048 | 0.0011 | 0.0005 | 0.0007 | 0.0003 |
| lfi_30_28 | 0.0057 | 0.0007 | 0.0011 | 0.0048 | 0.0033 | 0.0018 | 0.0021 | 0.0005 | 0.0003 | 0.0005 |
| hfi_100_1 | 0.0160 | 0.0012 | 0.0060 | 0.0104 | 0.0052 | 0.0043 | 0.0034 | 0.0017 | 0.0034 | 0.0017 |
| hfi_100_2 | 0.0092 | 0.0041 | 0.0052 | 0.0073 | 0.0053 | 0.0020 | 0.0096 | 0.0023 | 0.0029 | 0.0044 |
| hfi_100_3 | 0.0092 | 0.0041 | 0.0096 | 0.0011 | 0.0053 | 0.0081 | 0.0052 | 0.0023 | 0.0040 | 0.0009 |
| hfi_100_4 | 0.0160 | 0.0012 | 0.0034 | 0.0039 | 0.0052 | 0.0095 | 0.0060 | 0.0017 | 0.0016 | 0.0037 |
| hfi_143_1 | 0.0225 | 0.0001 | 0.0076 | 0.0085 | 0.0023 | 0.0069 | 0.0053 | 0.0004 | 0.0006 | 0.0043 |
| hfi_143_2 | 0.0107 | 0.0068 | 0.0068 | 0.0016 | 0.0064 | 0.0083 | 0.0042 | 0.0031 | 0.0029 | 0.0016 |
| hfi_143_3 | 0.0112 | 0.0043 | 0.0044 | 0.0090 | 0.0054 | 0.0031 | 0.0068 | 0.0011 | 0.0006 | 0.0018 |
| hfi_143_4 | 0.0225 | 0.0001 | 0.0076 | 0.0085 | 0.0023 | 0.0069 | 0.0053 | 0.0004 | 0.0006 | 0.0043 |
| hfi_143_5 | 0.0258 | 0.0079 | 0.0126 | 0.0031 | 0.0077 | 0.0159 | 0.0045 | 0.0015 | 0.0015 | 0.0008 |
| hfi_143_6 | 0.0152 | 0.0114 | 0.0116 | 0.0069 | 0.0105 | 0.0130 | 0.0109 | 0.0025 | 0.0012 | 0.0020 |
| hfi_143_7 | 0.0150 | 0.0109 | 0.0113 | 0.0120 | 0.0108 | 0.0085 | 0.0120 | 0.0019 | 0.0011 | 0.0015 |
| hfi_143_8 | 0.0256 | 0.0090 | 0.0029 | 0.0157 | 0.0068 | 0.0016 | 0.0110 | 0.0020 | 0.0025 | 0.0027 |
| hfi_217_1 | 0.0232 | 0.0014 | 0.0074 | 0.0072 | 0.0038 | 0.0092 | 0.0071 | 0.0020 | 0.0038 | 0.0043 |
| hfi_217_2 | 0.0116 | 0.0075 | 0.0041 | 0.0094 | 0.0033 | 0.0028 | 0.0081 | 0.0024 | 0.0008 | 0.0019 |
| hfi_217_3 | 0.0118 | 0.0082 | 0.0088 | 0.0022 | 0.0034 | 0.0091 | 0.0046 | 0.0022 | 0.0014 | 0.0033 |
| hfi_217_4 | 0.0227 | 0.0009 | 0.0059 | 0.0095 | 0.0038 | 0.0066 | 0.0068 | 0.0018 | 0.0032 | 0.0030 |
| hfi_217_5 | 0.0167 | 0.0081 | 0.0090 | 0.0026 | 0.0058 | 0.0091 | 0.0054 | 0.0022 | 0.0011 | 0.0013 |
| hfi_217_6 | 0.0094 | 0.0019 | 0.0007 | 0.0020 | 0.0018 | 0.0014 | 0.0018 | 0.0020 | 0.0021 | 0.0013 |
| hfi_217_7 | 0.0105 | 0.0030 | 0.0021 | 0.0025 | 0.0017 | 0.0023 | 0.0012 | 0.0012 | 0.0009 | 0.0018 |
| hfi_217_8 | 0.0182 | 0.0069 | 0.0047 | 0.0103 | 0.0065 | 0.0031 | 0.0078 | 0.0007 | 0.0020 | 0.0030 |
| hfi_353_1 | 0.0577 | 0.0370 | 0.0332 | 0.0418 | 0.0405 | 0.0313 | 0.0390 | 0.0072 | 0.0060 | 0.0073 |
| hfi_353_2 | 0.0396 | 0.0146 | 0.0140 | 0.0207 | 0.0241 | 0.0172 | 0.0172 | 0.0027 | 0.0032 | 0.0057 |
| hfi_353_3 | 0.0281 | 0.0021 | 0.0016 | 0.0093 | 0.0169 | 0.0097 | 0.0028 | 0.0010 | 0.0012 | 0.0012 |
| hfi_353_4 | 0.0243 | 0.0094 | 0.0076 | 0.0047 | 0.0134 | 0.0050 | 0.0071 | 0.0022 | 0.0014 | 0.0014 |
| hfi_353_5 | 0.0239 | 0.0083 | 0.0044 | 0.0039 | 0.0115 | 0.0042 | 0.0052 | 0.0014 | 0.0027 | 0.0028 |
| hfi_353_6 | 0.0300 | 0.0031 | 0.0074 | 0.0113 | 0.0191 | 0.0130 | 0.0057 | 0.0010 | 0.0005 | 0.0014 |
| hfi_353_7 | 0.0419 | 0.0183 | 0.0209 | 0.0193 | 0.0291 | 0.0262 | 0.0176 | 0.0039 | 0.0029 | 0.0030 |
| hfi_353_8 | 0.0597 | 0.0360 | 0.0382 | 0.0277 | 0.0405 | 0.0438 | 0.0319 | 0.0058 | 0.0072 | 0.0035 |
| hfi_545_1 | 0.1396 | 0.0565 | 0.0356 | 0.0976 | 0.0727 | 0.0277 | 0.0781 | 0.0107 | 0.0062 | 0.0168 |
| hfi_545_2 | 0.1102 | 0.0185 | 0.0069 | 0.0660 | 0.0582 | 0.0131 | 0.0395 | 0.0031 | 0.0015 | 0.0110 |
| hfi_545_3 | 0.1165 | 0.0253 | 0.0446 | 0.0146 | 0.0632 | 0.0730 | 0.0130 | 0.0053 | 0.0098 | 0.0026 |
| hfi_545_4 | 0.1407 | 0.0559 | 0.0771 | 0.0196 | 0.0718 | 0.1024 | 0.0350 | 0.0108 | 0.0155 | 0.0032 |
| hfi_857_1 | 0.1624 | 0.0288 | 0.0309 | 0.0749 | 0.0946 | 0.0140 | 0.0101 | 0.0054 | 0.0060 | 0.0118 |
| hfi_857_2 | 0.1222 | 0.0575 | 0.0464 | 0.0374 | 0.0743 | 0.0115 | 0.0360 | 0.0119 | 0.0085 | 0.0049 |
| hfi_857_3 | 0.1302 | 0.0554 | 0.0313 | 0.0189 | 0.0780 | 0.0396 | 0.0466 | 0.0115 | 0.0044 | 0.0022 |
| hfi_857_4 | 0.1763 | 0.0187 | 0.0226 | 0.0174 | 0.1019 | 0.0854 | 0.0250 | 0.0045 | 0.0073 | 0.0035 |

Table 7.4-23 random case (21 to 30)

ALCATEL ALENIA SPACE
An Alcatel/Finmeccanica company

| detector n° | case31 | case32 | case33 | case34 | case35 | case36 | case37 | case38 | case39 | case40 |
|---|---|---|---|---|---|---|---|---|---|---|
| | dB | dB | dB | dB | dB | dB | dB | dB | dB | dB |
| lfi_70_18 | 0.0007 | 0.0004 | 0.0005 | 0.0020 | 0.0020 | 0.0020 | 0.0007 | 0.0004 | 0.0004 | 0.0001 |
| lfi_70_19 | 0.0007 | 0.0003 | 0.0013 | 0.0031 | 0.0031 | 0.0031 | 0.0011 | 0.0001 | 0.0001 | 0.0001 |
| lfi_70_20 | 0.0011 | 0.0009 | 0.0019 | 0.0032 | 0.0032 | 0.0032 | 0.0017 | 0.0003 | 0.0003 | 0.0001 |
| lfi_70_21 | 0.0011 | 0.0015 | 0.0013 | 0.0032 | 0.0032 | 0.0032 | 0.0014 | 0.0003 | 0.0003 | 0.0001 |
| lfi_70_22 | 0.0007 | 0.0015 | 0.0001 | 0.0031 | 0.0031 | 0.0031 | 0.0007 | 0.0001 | 0.0001 | 0.0001 |
| lfi_70_23 | 0.0007 | 0.0007 | 0.0007 | 0.0020 | 0.0020 | 0.0020 | 0.0006 | 0.0004 | 0.0004 | 0.0001 |
| lfi_44_24 | 0.0006 | 0.0007 | 0.0006 | 0.0018 | 0.0018 | 0.0018 | 0.0006 | 0.0001 | 0.0001 | 0.0000 |
| lfi_44_25 | 0.0005 | 0.0009 | 0.0003 | 0.0031 | 0.0031 | 0.0031 | 0.0008 | 0.0004 | 0.0004 | 0.0001 |
| lfi_44_26 | 0.0005 | 0.0012 | 0.0012 | 0.0031 | 0.0031 | 0.0031 | 0.0003 | 0.0004 | 0.0004 | 0.0001 |
| lfi_30_27 | 0.0006 | 0.0005 | 0.0003 | 0.0012 | 0.0012 | 0.0012 | 0.0006 | 0.0002 | 0.0002 | 0.0000 |
| lfi_30_28 | 0.0006 | 0.0003 | 0.0007 | 0.0012 | 0.0012 | 0.0012 | 0.0007 | 0.0002 | 0.0002 | 0.0000 |
| hfi_100_1 | 0.0010 | 0.0037 | 0.0016 | 0.0053 | 0.0053 | 0.0053 | 0.0013 | 0.0010 | 0.0010 | 0.0002 |
| hfi_100_2 | 0.0021 | 0.0009 | 0.0040 | 0.0054 | 0.0054 | 0.0054 | 0.0040 | 0.0014 | 0.0014 | 0.0002 |
| hfi_100_3 | 0.0021 | 0.0044 | 0.0029 | 0.0054 | 0.0054 | 0.0054 | 0.0034 | 0.0014 | 0.0014 | 0.0002 |
| hfi_100_4 | 0.0010 | 0.0017 | 0.0034 | 0.0053 | 0.0053 | 0.0053 | 0.0022 | 0.0010 | 0.0010 | 0.0002 |
| hfi_143_1 | 0.0019 | 0.0021 | 0.0027 | 0.0058 | 0.0058 | 0.0058 | 0.0018 | 0.0013 | 0.0013 | 0.0003 |
| hfi_143_2 | 0.0022 | 0.0014 | 0.0024 | 0.0053 | 0.0053 | 0.0053 | 0.0030 | 0.0009 | 0.0009 | 0.0000 |
| hfi_143_3 | 0.0011 | 0.0018 | 0.0002 | 0.0036 | 0.0036 | 0.0036 | 0.0004 | 0.0009 | 0.0009 | 0.0000 |
| hfi_143_4 | 0.0019 | 0.0021 | 0.0027 | 0.0058 | 0.0058 | 0.0058 | 0.0018 | 0.0013 | 0.0013 | 0.0003 |
| hfi_143_5 | 0.0006 | 0.0008 | 0.0016 | 0.0050 | 0.0050 | 0.0050 | 0.0008 | 0.0005 | 0.0005 | 0.0001 |
| hfi_143_6 | 0.0004 | 0.0012 | 0.0012 | 0.0045 | 0.0045 | 0.0045 | 0.0016 | 0.0008 | 0.0008 | 0.0000 |
| hfi_143_7 | 0.0006 | 0.0021 | 0.0011 | 0.0041 | 0.0041 | 0.0041 | 0.0007 | 0.0006 | 0.0006 | 0.0000 |
| hfi_143_8 | 0.0022 | 0.0012 | 0.0040 | 0.0062 | 0.0062 | 0.0062 | 0.0023 | 0.0011 | 0.0011 | 0.0001 |
| hfi_217_1 | 0.0018 | 0.0041 | 0.0038 | 0.0059 | 0.0059 | 0.0059 | 0.0034 | 0.0022 | 0.0022 | 0.0004 |
| hfi_217_2 | 0.0009 | 0.0029 | 0.0017 | 0.0049 | 0.0049 | 0.0049 | 0.0018 | 0.0018 | 0.0018 | 0.0001 |
| hfi_217_3 | 0.0011 | 0.0022 | 0.0004 | 0.0048 | 0.0048 | 0.0048 | 0.0009 | 0.0016 | 0.0016 | 0.0001 |
| hfi_217_4 | 0.0014 | 0.0036 | 0.0031 | 0.0048 | 0.0048 | 0.0048 | 0.0022 | 0.0014 | 0.0014 | 0.0004 |
| hfi_217_5 | 0.0005 | 0.0016 | 0.0013 | 0.0043 | 0.0043 | 0.0043 | 0.0010 | 0.0006 | 0.0006 | 0.0001 |
| hfi_217_6 | 0.0019 | 0.0013 | 0.0013 | 0.0037 | 0.0037 | 0.0037 | 0.0009 | 0.0014 | 0.0014 | 0.0002 |
| hfi_217_7 | 0.0012 | 0.0017 | 0.0004 | 0.0035 | 0.0035 | 0.0035 | 0.0013 | 0.0014 | 0.0014 | 0.0001 |
| hfi_217_8 | 0.0025 | 0.0022 | 0.0017 | 0.0056 | 0.0056 | 0.0056 | 0.0004 | 0.0011 | 0.0011 | 0.0001 |
| hfi_353_1 | 0.0055 | 0.0045 | 0.0059 | 0.0164 | 0.0164 | 0.0164 | 0.0025 | 0.0019 | 0.0019 | 0.0001 |
| hfi_353_2 | 0.0045 | 0.0052 | 0.0053 | 0.0104 | 0.0104 | 0.0104 | 0.0029 | 0.0031 | 0.0031 | 0.0003 |
| hfi_353_3 | 0.0018 | 0.0022 | 0.0024 | 0.0041 | 0.0041 | 0.0041 | 0.0014 | 0.0012 | 0.0012 | 0.0002 |
| hfi_353_4 | 0.0018 | 0.0022 | 0.0016 | 0.0048 | 0.0048 | 0.0048 | 0.0008 | 0.0006 | 0.0006 | 0.0002 |
| hfi_353_5 | 0.0029 | 0.0033 | 0.0016 | 0.0061 | 0.0061 | 0.0061 | 0.0005 | 0.0032 | 0.0032 | 0.0003 |
| hfi_353_6 | 0.0023 | 0.0031 | 0.0007 | 0.0062 | 0.0062 | 0.0062 | 0.0004 | 0.0019 | 0.0019 | 0.0001 |
| hfi_353_7 | 0.0042 | 0.0049 | 0.0035 | 0.0106 | 0.0106 | 0.0106 | 0.0014 | 0.0024 | 0.0024 | 0.0001 |
| hfi_353_8 | 0.0052 | 0.0066 | 0.0066 | 0.0159 | 0.0159 | 0.0159 | 0.0044 | 0.0016 | 0.0016 | 0.0000 |
| hfi_545_1 | 0.0103 | 0.0033 | 0.0155 | 0.0325 | 0.0325 | 0.0325 | 0.0073 | 0.0035 | 0.0035 | 0.0011 |
| hfi_545_2 | 0.0079 | 0.0013 | 0.0079 | 0.0213 | 0.0213 | 0.0213 | 0.0039 | 0.0029 | 0.0029 | 0.0003 |
| hfi_545_3 | 0.0086 | 0.0122 | 0.0011 | 0.0216 | 0.0216 | 0.0216 | 0.0015 | 0.0038 | 0.0038 | 0.0010 |
| hfi_545_4 | 0.0100 | 0.0167 | 0.0053 | 0.0326 | 0.0326 | 0.0326 | 0.0047 | 0.0037 | 0.0037 | 0.0010 |
| hfi_857_1 | 0.0105 | 0.0015 | 0.0053 | 0.0275 | 0.0275 | 0.0275 | 0.0045 | 0.0082 | 0.0082 | 0.0014 |
| hfi_857_2 | 0.0089 | 0.0025 | 0.0055 | 0.0229 | 0.0229 | 0.0229 | 0.0015 | 0.0092 | 0.0092 | 0.0008 |
| hfi_857_3 | 0.0095 | 0.0059 | 0.0087 | 0.0221 | 0.0221 | 0.0221 | 0.0011 | 0.0089 | 0.0089 | 0.0009 |
| hfi_857_4 | 0.0131 | 0.0154 | 0.0059 | 0.0293 | 0.0293 | 0.0293 | 0.0037 | 0.0092 | 0.0092 | 0.0008 |

Table 7.4-24 random case (31 to 40)

| detector n° | case41 | case42 | case43 | case44 | case45 | case46 | case47 | case48 | case49 | case50 |
|---|---|---|---|---|---|---|---|---|---|---|
| | dB | dB | dB | dB | dB | dB | dB | dB | dB | dB |
| lfi_70_18 | 0.0015 | 0.0001 | 0.0005 | 0.0001 | 0.0015 | 0.0001 | 0.0001 | 0.0022 | 0.0005 | 0.0005 |
| lfi_70_19 | 0.0023 | 0.0002 | 0.0001 | 0.0001 | 0.0023 | 0.0001 | 0.0001 | 0.0057 | 0.0015 | 0.0009 |
| lfi_70_20 | 0.0039 | 0.0001 | 0.0002 | 0.0001 | 0.0039 | 0.0001 | 0.0001 | 0.0091 | 0.0027 | 0.0015 |
| lfi_70_21 | 0.0039 | 0.0001 | 0.0002 | 0.0001 | 0.0039 | 0.0001 | 0.0001 | 0.0091 | 0.0027 | 0.0015 |
| lfi_70_22 | 0.0023 | 0.0002 | 0.0001 | 0.0001 | 0.0023 | 0.0001 | 0.0001 | 0.0057 | 0.0015 | 0.0009 |
| lfi_70_23 | 0.0015 | 0.0001 | 0.0005 | 0.0001 | 0.0015 | 0.0001 | 0.0001 | 0.0022 | 0.0005 | 0.0005 |
| lfi_44_24 | 0.0037 | 0.0000 | 0.0002 | 0.0000 | 0.0037 | 0.0000 | 0.0001 | 0.0088 | 0.0014 | 0.0009 |
| lfi_44_25 | 0.0008 | 0.0002 | 0.0004 | 0.0001 | 0.0008 | 0.0001 | 0.0001 | 0.0032 | 0.0005 | 0.0008 |
| lfi_44_26 | 0.0008 | 0.0002 | 0.0004 | 0.0001 | 0.0008 | 0.0001 | 0.0001 | 0.0032 | 0.0005 | 0.0008 |
| lfi_30_27 | 0.0017 | 0.0000 | 0.0002 | 0.0000 | 0.0017 | 0.0000 | 0.0000 | 0.0041 | 0.0010 | 0.0007 |
| lfi_30_28 | 0.0017 | 0.0000 | 0.0002 | 0.0000 | 0.0017 | 0.0000 | 0.0000 | 0.0041 | 0.0010 | 0.0007 |
| hfi_100_1 | 0.0018 | 0.0003 | 0.0010 | 0.0002 | 0.0018 | 0.0002 | 0.0003 | 0.0073 | 0.0022 | 0.0019 |
| hfi_100_2 | 0.0047 | 0.0002 | 0.0012 | 0.0002 | 0.0047 | 0.0001 | 0.0003 | 0.0096 | 0.0048 | 0.0030 |
| hfi_100_3 | 0.0047 | 0.0002 | 0.0012 | 0.0002 | 0.0047 | 0.0001 | 0.0003 | 0.0096 | 0.0048 | 0.0030 |
| hfi_100_4 | 0.0018 | 0.0003 | 0.0010 | 0.0002 | 0.0018 | 0.0002 | 0.0003 | 0.0073 | 0.0022 | 0.0019 |
| hfi_143_1 | 0.0025 | 0.0004 | 0.0011 | 0.0003 | 0.0025 | 0.0002 | 0.0003 | 0.0042 | 0.0021 | 0.0024 |
| hfi_143_2 | 0.0039 | 0.0000 | 0.0008 | 0.0000 | 0.0039 | 0.0000 | 0.0003 | 0.0110 | 0.0045 | 0.0030 |
| hfi_143_3 | 0.0047 | 0.0001 | 0.0010 | 0.0000 | 0.0047 | 0.0000 | 0.0001 | 0.0107 | 0.0014 | 0.0011 |
| hfi_143_4 | 0.0025 | 0.0004 | 0.0011 | 0.0003 | 0.0025 | 0.0002 | 0.0003 | 0.0042 | 0.0021 | 0.0024 |
| hfi_143_5 | 0.0064 | 0.0001 | 0.0006 | 0.0001 | 0.0064 | 0.0001 | 0.0001 | 0.0138 | 0.0020 | 0.0008 |
| hfi_143_6 | 0.0094 | 0.0001 | 0.0009 | 0.0000 | 0.0094 | 0.0000 | 0.0001 | 0.0204 | 0.0032 | 0.0012 |
| hfi_143_7 | 0.0098 | 0.0001 | 0.0008 | 0.0000 | 0.0098 | 0.0000 | 0.0001 | 0.0201 | 0.0026 | 0.0013 |
| hfi_143_8 | 0.0046 | 0.0001 | 0.0008 | 0.0001 | 0.0046 | 0.0001 | 0.0002 | 0.0149 | 0.0041 | 0.0031 |
| hfi_217_1 | 0.0035 | 0.0005 | 0.0020 | 0.0004 | 0.0035 | 0.0003 | 0.0006 | 0.0053 | 0.0034 | 0.0030 |
| hfi_217_2 | 0.0007 | 0.0001 | 0.0018 | 0.0001 | 0.0007 | 0.0001 | 0.0003 | 0.0106 | 0.0025 | 0.0016 |
| hfi_217_3 | 0.0009 | 0.0002 | 0.0017 | 0.0001 | 0.0009 | 0.0001 | 0.0002 | 0.0108 | 0.0021 | 0.0015 |
| hfi_217_4 | 0.0036 | 0.0004 | 0.0012 | 0.0004 | 0.0036 | 0.0003 | 0.0006 | 0.0049 | 0.0028 | 0.0027 |
| hfi_217_5 | 0.0074 | 0.0001 | 0.0009 | 0.0001 | 0.0074 | 0.0001 | 0.0003 | 0.0089 | 0.0019 | 0.0017 |
| hfi_217_6 | 0.0024 | 0.0002 | 0.0012 | 0.0002 | 0.0024 | 0.0001 | 0.0003 | 0.0062 | 0.0026 | 0.0031 |
| hfi_217_7 | 0.0032 | 0.0002 | 0.0014 | 0.0001 | 0.0032 | 0.0001 | 0.0003 | 0.0051 | 0.0013 | 0.0017 |
| hfi_217_8 | 0.0085 | 0.0002 | 0.0010 | 0.0001 | 0.0085 | 0.0001 | 0.0004 | 0.0101 | 0.0019 | 0.0029 |
| hfi_353_1 | 0.0377 | 0.0001 | 0.0018 | 0.0001 | 0.0377 | 0.0000 | 0.0008 | 0.0661 | 0.0099 | 0.0094 |
| hfi_353_2 | 0.0231 | 0.0004 | 0.0027 | 0.0003 | 0.0231 | 0.0002 | 0.0006 | 0.0344 | 0.0055 | 0.0068 |
| hfi_353_3 | 0.0150 | 0.0002 | 0.0008 | 0.0002 | 0.0150 | 0.0001 | 0.0004 | 0.0174 | 0.0018 | 0.0045 |
| hfi_353_4 | 0.0101 | 0.0002 | 0.0003 | 0.0002 | 0.0101 | 0.0001 | 0.0004 | 0.0138 | 0.0012 | 0.0045 |
| hfi_353_5 | 0.0088 | 0.0003 | 0.0032 | 0.0003 | 0.0088 | 0.0002 | 0.0006 | 0.0144 | 0.0023 | 0.0050 |
| hfi_353_6 | 0.0156 | 0.0001 | 0.0018 | 0.0001 | 0.0156 | 0.0001 | 0.0004 | 0.0210 | 0.0020 | 0.0052 |
| hfi_353_7 | 0.0257 | 0.0001 | 0.0020 | 0.0001 | 0.0257 | 0.0001 | 0.0006 | 0.0405 | 0.0057 | 0.0072 |
| hfi_353_8 | 0.0391 | 0.0001 | 0.0019 | 0.0000 | 0.0391 | 0.0000 | 0.0005 | 0.0665 | 0.0103 | 0.0091 |
| hfi_545_1 | 0.0657 | 0.0013 | 0.0034 | 0.0011 | 0.0657 | 0.0007 | 0.0014 | 0.1127 | 0.0182 | 0.0167 |
| hfi_545_2 | 0.0472 | 0.0004 | 0.0020 | 0.0003 | 0.0472 | 0.0002 | 0.0008 | 0.0703 | 0.0102 | 0.0145 |
| hfi_545_3 | 0.0520 | 0.0012 | 0.0031 | 0.0010 | 0.0520 | 0.0007 | 0.0013 | 0.0790 | 0.0105 | 0.0142 |
| hfi_545_4 | 0.0648 | 0.0012 | 0.0033 | 0.0010 | 0.0648 | 0.0007 | 0.0015 | 0.1127 | 0.0178 | 0.0164 |
| hfi_857_1 | 0.0650 | 0.0017 | 0.0080 | 0.0014 | 0.0650 | 0.0010 | 0.0023 | 0.0931 | 0.0086 | 0.0246 |
| hfi_857_2 | 0.0424 | 0.0010 | 0.0085 | 0.0008 | 0.0424 | 0.0006 | 0.0020 | 0.0737 | 0.0077 | 0.0227 |
| hfi_857_3 | 0.0469 | 0.0011 | 0.0085 | 0.0009 | 0.0469 | 0.0006 | 0.0017 | 0.0780 | 0.0066 | 0.0241 |
| hfi_857_4 | 0.0707 | 0.0012 | 0.0080 | 0.0008 | 0.0707 | 0.0004 | 0.0016 | 0.1024 | 0.0111 | 0.0273 |

Table 7.4-25 random case (41 to 50)

| detector n° | case51 | case52 | case53 | case54 | case55 | case56 | case57 | case58 | case59 | case60 |
|---|---|---|---|---|---|---|---|---|---|---|
| | dB | dB | dB | dB | dB | dB | dB | dB | dB | dB |
| lfi_70_18 | 0.0000 | 0.0000 | 0.0004 | 0.0001 | 0.0002 | 0.0113 | 0.0014 | 0.0014 | 0.0014 | 0.0002 |
| lfi_70_19 | 0.0001 | 0.0000 | 0.0005 | 0.0002 | 0.0005 | 0.0113 | 0.0030 | 0.0030 | 0.0030 | 0.0002 |
| lfi_70_20 | 0.0001 | 0.0001 | 0.0008 | 0.0003 | 0.0011 | 0.0076 | 0.0034 | 0.0034 | 0.0034 | 0.0004 |
| lfi_70_21 | 0.0001 | 0.0001 | 0.0008 | 0.0003 | 0.0011 | 0.0076 | 0.0034 | 0.0034 | 0.0034 | 0.0004 |
| lfi_70_22 | 0.0001 | 0.0000 | 0.0005 | 0.0002 | 0.0005 | 0.0113 | 0.0030 | 0.0030 | 0.0030 | 0.0002 |
| lfi_70_23 | 0.0000 | 0.0000 | 0.0004 | 0.0001 | 0.0002 | 0.0113 | 0.0014 | 0.0014 | 0.0014 | 0.0002 |
| lfi_44_24 | 0.0001 | 0.0000 | 0.0004 | 0.0001 | 0.0004 | 0.0066 | 0.0017 | 0.0017 | 0.0017 | 0.0002 |
| lfi_44_25 | 0.0001 | 0.0000 | 0.0001 | 0.0000 | 0.0003 | 0.0187 | 0.0029 | 0.0029 | 0.0029 | 0.0003 |
| lfi_44_26 | 0.0001 | 0.0000 | 0.0001 | 0.0000 | 0.0003 | 0.0187 | 0.0029 | 0.0029 | 0.0029 | 0.0003 |
| lfi_30_27 | 0.0000 | 0.0000 | 0.0004 | 0.0001 | 0.0004 | 0.0048 | 0.0013 | 0.0013 | 0.0013 | 0.0001 |
| lfi_30_28 | 0.0000 | 0.0000 | 0.0004 | 0.0001 | 0.0004 | 0.0048 | 0.0013 | 0.0013 | 0.0013 | 0.0001 |
| hfi_100_1 | 0.0001 | 0.0001 | 0.0010 | 0.0003 | 0.0018 | 0.0183 | 0.0054 | 0.0054 | 0.0054 | 0.0002 |
| hfi_100_2 | 0.0002 | 0.0001 | 0.0017 | 0.0005 | 0.0025 | 0.0090 | 0.0061 | 0.0061 | 0.0061 | 0.0006 |
| hfi_100_3 | 0.0002 | 0.0001 | 0.0017 | 0.0005 | 0.0025 | 0.0090 | 0.0061 | 0.0061 | 0.0061 | 0.0006 |
| hfi_100_4 | 0.0001 | 0.0001 | 0.0010 | 0.0003 | 0.0018 | 0.0183 | 0.0054 | 0.0054 | 0.0054 | 0.0002 |
| hfi_143_1 | 0.0001 | 0.0001 | 0.0014 | 0.0004 | 0.0020 | 0.0246 | 0.0046 | 0.0046 | 0.0046 | 0.0003 |
| hfi_143_2 | 0.0002 | 0.0002 | 0.0020 | 0.0008 | 0.0022 | 0.0120 | 0.0056 | 0.0056 | 0.0056 | 0.0007 |
| hfi_143_3 | 0.0000 | 0.0000 | 0.0008 | 0.0002 | 0.0012 | 0.0097 | 0.0031 | 0.0031 | 0.0031 | 0.0002 |
| hfi_143_4 | 0.0001 | 0.0001 | 0.0014 | 0.0004 | 0.0020 | 0.0246 | 0.0046 | 0.0046 | 0.0046 | 0.0003 |
| hfi_143_5 | 0.0000 | 0.0000 | 0.0003 | 0.0001 | 0.0007 | 0.0237 | 0.0043 | 0.0043 | 0.0043 | 0.0003 |
| hfi_143_6 | 0.0001 | 0.0000 | 0.0003 | 0.0001 | 0.0003 | 0.0127 | 0.0045 | 0.0045 | 0.0045 | 0.0004 |
| hfi_143_7 | 0.0001 | 0.0000 | 0.0004 | 0.0001 | 0.0009 | 0.0121 | 0.0039 | 0.0039 | 0.0039 | 0.0004 |
| hfi_143_8 | 0.0002 | 0.0001 | 0.0018 | 0.0005 | 0.0027 | 0.0254 | 0.0059 | 0.0059 | 0.0059 | 0.0006 |
| hfi_217_1 | 0.0002 | 0.0002 | 0.0020 | 0.0008 | 0.0028 | 0.0229 | 0.0054 | 0.0054 | 0.0054 | 0.0006 |
| hfi_217_2 | 0.0001 | 0.0001 | 0.0013 | 0.0005 | 0.0006 | 0.0130 | 0.0043 | 0.0043 | 0.0043 | 0.0003 |
| hfi_217_3 | 0.0001 | 0.0001 | 0.0015 | 0.0004 | 0.0002 | 0.0132 | 0.0040 | 0.0040 | 0.0040 | 0.0003 |
| hfi_217_4 | 0.0002 | 0.0002 | 0.0017 | 0.0008 | 0.0025 | 0.0226 | 0.0043 | 0.0043 | 0.0043 | 0.0005 |
| hfi_217_5 | 0.0001 | 0.0001 | 0.0015 | 0.0004 | 0.0011 | 0.0136 | 0.0038 | 0.0038 | 0.0038 | 0.0003 |
| hfi_217_6 | 0.0001 | 0.0001 | 0.0016 | 0.0004 | 0.0027 | 0.0086 | 0.0031 | 0.0031 | 0.0031 | 0.0003 |
| hfi_217_7 | 0.0001 | 0.0001 | 0.0018 | 0.0005 | 0.0003 | 0.0097 | 0.0033 | 0.0033 | 0.0033 | 0.0003 |
| hfi_217_8 | 0.0002 | 0.0001 | 0.0021 | 0.0006 | 0.0013 | 0.0154 | 0.0043 | 0.0043 | 0.0043 | 0.0007 |
| hfi_353_1 | 0.0007 | 0.0005 | 0.0044 | 0.0018 | 0.0022 | 0.0462 | 0.0136 | 0.0136 | 0.0136 | 0.0028 |
| hfi_353_2 | 0.0004 | 0.0002 | 0.0030 | 0.0006 | 0.0026 | 0.0266 | 0.0080 | 0.0080 | 0.0080 | 0.0002 |
| hfi_353_3 | 0.0003 | 0.0001 | 0.0012 | 0.0005 | 0.0016 | 0.0195 | 0.0053 | 0.0053 | 0.0053 | 0.0005 |
| hfi_353_4 | 0.0003 | 0.0002 | 0.0022 | 0.0006 | 0.0025 | 0.0198 | 0.0047 | 0.0047 | 0.0047 | 0.0007 |
| hfi_353_5 | 0.0004 | 0.0002 | 0.0018 | 0.0008 | 0.0038 | 0.0184 | 0.0050 | 0.0050 | 0.0050 | 0.0010 |
| hfi_353_6 | 0.0004 | 0.0002 | 0.0020 | 0.0009 | 0.0019 | 0.0217 | 0.0055 | 0.0055 | 0.0055 | 0.0008 |
| hfi_353_7 | 0.0006 | 0.0003 | 0.0030 | 0.0014 | 0.0017 | 0.0309 | 0.0087 | 0.0087 | 0.0087 | 0.0018 |
| hfi_353_8 | 0.0005 | 0.0002 | 0.0029 | 0.0006 | 0.0025 | 0.0459 | 0.0142 | 0.0142 | 0.0142 | 0.0018 |
| hfi_545_1 | 0.0010 | 0.0004 | 0.0071 | 0.0021 | 0.0028 | 0.1314 | 0.0303 | 0.0303 | 0.0303 | 0.0029 |
| hfi_545_2 | 0.0010 | 0.0004 | 0.0047 | 0.0011 | 0.0030 | 0.0992 | 0.0215 | 0.0215 | 0.0215 | 0.0016 |
| hfi_545_3 | 0.0010 | 0.0004 | 0.0033 | 0.0007 | 0.0019 | 0.1030 | 0.0215 | 0.0215 | 0.0215 | 0.0015 |
| hfi_545_4 | 0.0011 | 0.0006 | 0.0074 | 0.0028 | 0.0029 | 0.1335 | 0.0294 | 0.0294 | 0.0294 | 0.0027 |
| hfi_857_1 | 0.0018 | 0.0007 | 0.0029 | 0.0011 | 0.0116 | 0.1367 | 0.0302 | 0.0302 | 0.0302 | 0.0042 |
| hfi_857_2 | 0.0018 | 0.0008 | 0.0031 | 0.0019 | 0.0131 | 0.1012 | 0.0253 | 0.0253 | 0.0253 | 0.0049 |
| hfi_857_3 | 0.0017 | 0.0006 | 0.0016 | 0.0015 | 0.0120 | 0.1080 | 0.0269 | 0.0269 | 0.0269 | 0.0057 |
| hfi_857_4 | 0.0022 | 0.0009 | 0.0029 | 0.0020 | 0.0104 | 0.1485 | 0.0337 | 0.0337 | 0.0337 | 0.0048 |

Table 7.4-26 random case (51 to 60)

| detector N° | case61 | case62 | case63 | case64 | case65 | case66 | case67 | case68 |
|---|---|---|---|---|---|---|---|---|
| | dB | dB | dB | dB | dB | dB | dB | dB |
| lfi_70_18 | 0,0039 | 0,0015 | 0,0003 | 0,0003 | 0,0039 | 0,0015 | 0,0003 | 0,0001 |
| lfi_70_19 | 0,0039 | 0,0027 | 0,0006 | 0,0002 | 0,0039 | 0,0027 | 0,0006 | 0,0001 |
| lfi_70_20 | 0,0022 | 0,0040 | 0,0004 | 0,0003 | 0,0022 | 0,0040 | 0,0004 | 0,0002 |
| lfi_70_21 | 0,0022 | 0,0040 | 0,0004 | 0,0003 | 0,0022 | 0,0040 | 0,0004 | 0,0002 |
| lfi_70_22 | 0,0039 | 0,0027 | 0,0006 | 0,0002 | 0,0039 | 0,0027 | 0,0006 | 0,0001 |
| lfi_70_23 | 0,0039 | 0,0015 | 0,0003 | 0,0003 | 0,0039 | 0,0015 | 0,0003 | 0,0001 |
| lfi_44_24 | 0,0001 | 0,0031 | 0,0001 | 0,0002 | 0,0001 | 0,0031 | 0,0001 | 0,0001 |
| lfi_44_25 | 0,0055 | 0,0029 | 0,0007 | 0,0004 | 0,0055 | 0,0029 | 0,0007 | 0,0001 |
| lfi_44_26 | 0,0055 | 0,0029 | 0,0007 | 0,0004 | 0,0055 | 0,0029 | 0,0007 | 0,0001 |
| lfi_30_27 | 0,0018 | 0,0023 | 0,0001 | 0,0002 | 0,0018 | 0,0023 | 0,0001 | 0,0001 |
| lfi_30_28 | 0,0018 | 0,0023 | 0,0001 | 0,0002 | 0,0018 | 0,0023 | 0,0001 | 0,0001 |
| hfi_100_1 | 0,0039 | 0,0016 | 0,0013 | 0,0001 | 0,0039 | 0,0016 | 0,0013 | 0,0003 |
| hfi_100_2 | 0,0007 | 0,0064 | 0,0010 | 0,0005 | 0,0008 | 0,0064 | 0,0010 | 0,0003 |
| hfi_100_3 | 0,0007 | 0,0064 | 0,0010 | 0,0005 | 0,0007 | 0,0064 | 0,0010 | 0,0003 |
| hfi_100_4 | 0,0039 | 0,0016 | 0,0013 | 0,0001 | 0,0040 | 0,0016 | 0,0013 | 0,0003 |
| hfi_143_1 | 0,0067 | 0,0018 | 0,0018 | 0,0005 | 0,0067 | 0,0018 | 0,0018 | 0,0004 |
| hfi_143_2 | 0,0024 | 0,0039 | 0,0002 | 0,0007 | 0,0024 | 0,0039 | 0,0002 | 0,0004 |
| hfi_143_3 | 0,0020 | 0,0025 | 0,0002 | 0,0003 | 0,0020 | 0,0025 | 0,0002 | 0,0001 |
| hfi_143_4 | 0,0067 | 0,0018 | 0,0018 | 0,0005 | 0,0067 | 0,0018 | 0,0018 | 0,0004 |
| hfi_143_5 | 0,0069 | 0,0035 | 0,0002 | 0,0003 | 0,0069 | 0,0035 | 0,0002 | 0,0001 |
| hfi_143_6 | 0,0017 | 0,0056 | 0,0005 | 0,0003 | 0,0017 | 0,0056 | 0,0005 | 0,0001 |
| hfi_143_7 | 0,0017 | 0,0059 | 0,0005 | 0,0003 | 0,0017 | 0,0059 | 0,0005 | 0,0001 |
| hfi_143_8 | 0,0074 | 0,0045 | 0,0002 | 0,0004 | 0,0074 | 0,0045 | 0,0002 | 0,0003 |
| hfi_217_1 | 0,0067 | 0,0045 | 0,0018 | 0,0005 | 0,0067 | 0,0045 | 0,0018 | 0,0006 |
| hfi_217_2 | 0,0038 | 0,0021 | 0,0011 | 0,0008 | 0,0038 | 0,0021 | 0,0011 | 0,0003 |
| hfi_217_3 | 0,0038 | 0,0025 | 0,0011 | 0,0007 | 0,0038 | 0,0025 | 0,0011 | 0,0002 |
| hfi_217_4 | 0,0061 | 0,0038 | 0,0019 | 0,0004 | 0,0060 | 0,0038 | 0,0019 | 0,0006 |
| hfi_217_5 | 0,0037 | 0,0054 | 0,0007 | 0,0004 | 0,0037 | 0,0054 | 0,0007 | 0,0003 |
| hfi_217_6 | 0,0028 | 0,0036 | 0,0007 | 0,0001 | 0,0028 | 0,0036 | 0,0007 | 0,0003 |
| hfi_217_7 | 0,0033 | 0,0031 | 0,0007 | 0,0006 | 0,0033 | 0,0031 | 0,0007 | 0,0003 |
| hfi_217_8 | 0,0050 | 0,0067 | 0,0007 | 0,0006 | 0,0050 | 0,0067 | 0,0007 | 0,0004 |
| hfi_353_1 | 0,0049 | 0,0329 | 0,0005 | 0,0022 | 0,0050 | 0,0329 | 0,0005 | 0,0011 |
| hfi_353_2 | 0,0033 | 0,0230 | 0,0013 | 0,0003 | 0,0033 | 0,0230 | 0,0013 | 0,0006 |
| hfi_353_3 | 0,0011 | 0,0195 | 0,0016 | 0,0007 | 0,0011 | 0,0195 | 0,0016 | 0,0004 |
| hfi_353_4 | 0,0008 | 0,0167 | 0,0015 | 0,0009 | 0,0008 | 0,0167 | 0,0015 | 0,0004 |
| hfi_353_5 | 0,0009 | 0,0150 | 0,0011 | 0,0011 | 0,0009 | 0,0150 | 0,0011 | 0,0007 |
| hfi_353_6 | 0,0016 | 0,0196 | 0,0015 | 0,0019 | 0,0015 | 0,0196 | 0,0015 | 0,0005 |
| hfi_353_7 | 0,0021 | 0,0259 | 0,0011 | 0,0022 | 0,0021 | 0,0259 | 0,0011 | 0,0008 |
| hfi_353_8 | 0,0068 | 0,0339 | 0,0004 | 0,0009 | 0,0068 | 0,0339 | 0,0004 | 0,0005 |
| hfi_545_1 | 0,0332 | 0,0587 | 0,0055 | 0,0022 | 0,0333 | 0,0587 | 0,0055 | 0,0015 |
| hfi_545_2 | 0,0232 | 0,0553 | 0,0041 | 0,0038 | 0,0232 | 0,0553 | 0,0041 | 0,0010 |
| hfi_545_3 | 0,0247 | 0,0570 | 0,0033 | 0,0030 | 0,0247 | 0,0570 | 0,0033 | 0,0013 |
| hfi_545_4 | 0,0337 | 0,0585 | 0,0044 | 0,0018 | 0,0336 | 0,0585 | 0,0044 | 0,0018 |
| hfi_857_1 | 0,0259 | 0,0983 | 0,0043 | 0,0071 | 0,0259 | 0,0983 | 0,0043 | 0,0023 |
| hfi_857_2 | 0,0101 | 0,0843 | 0,0005 | 0,0060 | 0,0102 | 0,0843 | 0,0005 | 0,0025 |
| hfi_857_3 | 0,0117 | 0,0891 | 0,0008 | 0,0083 | 0,0116 | 0,0891 | 0,0008 | 0,0020 |
| hfi_857_4 | 0,0290 | 0,1029 | 0,0047 | 0,0072 | 0,0288 | 0,1029 | 0,0047 | 0,0024 |

Table 7.4-27 random case (61 to 68)

ALCATEL ALENIA SPACE
An Alcatel/Finmeccanica company
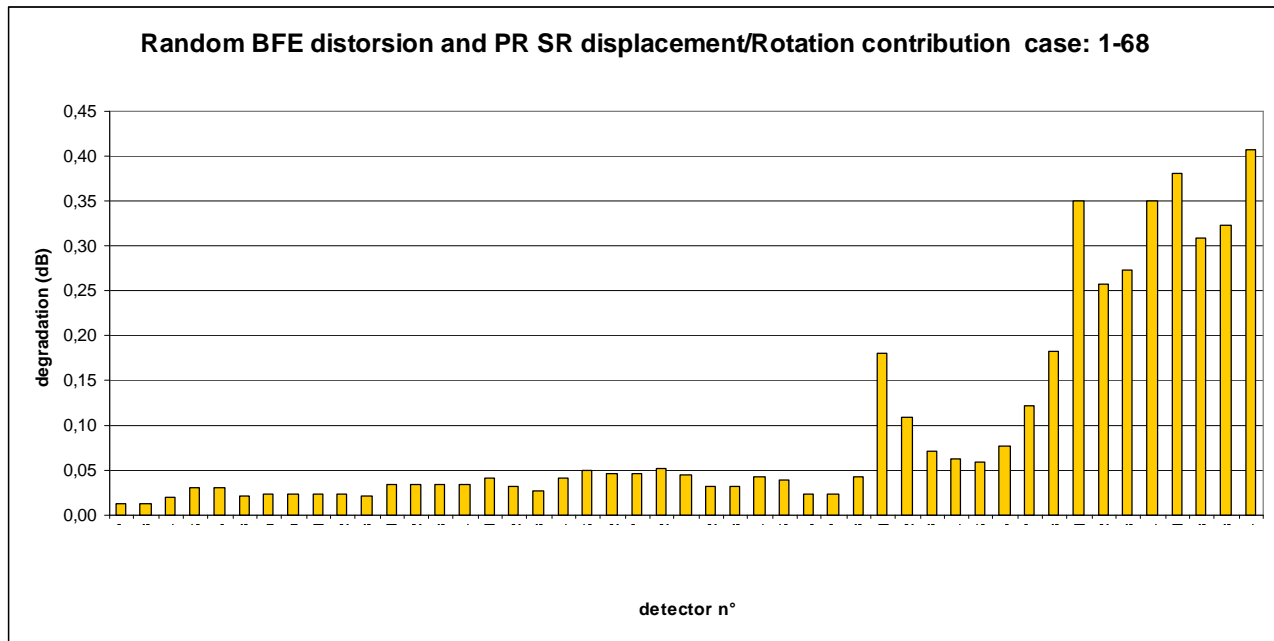


Figure 7.4-18 Budget for Random BFE distortion and PR SR displacements/rotations

### 7.4.3.4 Total random case

The complete budget for the random contributors is presented in the Table below. The last column corresponds to the RSS of and Table 7.4-28.

ALCATEL ALENIA SPACE
An Alcatel/Finmeccanica company

| detector n° | BFE know. accuracy other cont. | FPU random | Random BFE distorsion and displacements contribution case: 1-68 | TOTAL RANDOM BUDGET |
|---|---|---|---|---|
| | dB | dB | dB | dB |
| LFI_30_27 | 0,0189 | 0,0049 | 0,0128 | 0,0234 |
| LFI_30_28 | 0,0188 | 0,0047 | 0,0128 | 0,0233 |
| LFI_44_24 | 0,0228 | 0,0067 | 0,0196 | 0,0309 |
| LFI_44_25 | 0,0228 | 0,0069 | 0,0312 | 0,0393 |
| LFI_44_26 | 0,0327 | 0,0052 | 0,0310 | 0,0454 |
| LFI_70_18 | 0,0203 | 0,0059 | 0,0209 | 0,0297 |
| LFI_70_19 | 0,0252 | 0,0054 | 0,0228 | 0,0344 |
| LFI_70_20 | 0,0308 | 0,0045 | 0,0240 | 0,0393 |
| LFI_70_21 | 0,0306 | 0,0048 | 0,0240 | 0,0392 |
| LFI_70_22 | 0,0232 | 0,0058 | 0,0227 | 0,0330 |
| LFI_70_23 | 0,0189 | 0,0060 | 0,0208 | 0,0287 |
| HFI_100_1 | 0,0250 | 0,0069 | 0,0342 | 0,0430 |
| HFI_100_2 | 0,0389 | 0,0042 | 0,0333 | 0,0514 |
| HFI_100_3 | 0,0391 | 0,0040 | 0,0331 | 0,0514 |
| HFI_100_4 | 0,0298 | 0,0069 | 0,0342 | 0,0459 |
| HFI_143_1 | 0,0436 | 0,0066 | 0,0417 | 0,0607 |
| HFI_143_2 | 0,0343 | 0,0073 | 0,0327 | 0,0480 |
| HFI_143_3 | 0,0328 | 0,0040 | 0,0271 | 0,0427 |
| HFI_143_4 | 0,0436 | 0,0066 | 0,0417 | 0,0607 |
| HFI_143_5 | 0,0612 | 0,0040 | 0,0493 | 0,0787 |
| HFI_143_6 | 0,0705 | 0,0051 | 0,0469 | 0,0848 |
| HFI_143_7 | 0,0685 | 0,0044 | 0,0462 | 0,0827 |
| HFI_143_8 | 0,0582 | 0,0056 | 0,0517 | 0,0781 |
| HFI_217_1 | 0,0368 | 0,0046 | 0,0455 | 0,0587 |
| HFI_217_2 | 0,0409 | 0,0020 | 0,0320 | 0,0520 |
| HFI_217_3 | 0,0413 | 0,0013 | 0,0323 | 0,0524 |
| HFI_217_4 | 0,0405 | 0,0038 | 0,0428 | 0,0591 |
| HFI_217_5 | 0,0283 | 0,0032 | 0,0400 | 0,0491 |
| HFI_217_6 | 0,0201 | 0,0024 | 0,0238 | 0,0312 |
| HFI_217_7 | 0,0241 | 0,0022 | 0,0233 | 0,0336 |
| HFI_217_8 | 0,0346 | 0,0026 | 0,0433 | 0,0555 |
| HFI_353_1 | 0,2432 | 0,0223 | 0,1806 | 0,3038 |
| HFI_353_2 | 0,1353 | 0,0206 | 0,1083 | 0,1745 |
| HFI_353_3 | 0,0800 | 0,0122 | 0,0717 | 0,1081 |
| HFI_353_4 | 0,0966 | 0,0130 | 0,0625 | 0,1157 |
| HFI_353_5 | 0,0978 | 0,0141 | 0,0589 | 0,1151 |
| HFI_353_6 | 0,0843 | 0,0145 | 0,0777 | 0,1155 |
| HFI_353_7 | 0,1474 | 0,0180 | 0,1214 | 0,1918 |
| HFI_353_8 | 0,2436 | 0,0235 | 0,1817 | 0,3048 |
| HFI_545_1 | 0,4769 | 0,0728 | 0,3502 | 0,5962 |
| HFI_545_2 | 0,2907 | 0,0643 | 0,2567 | 0,3931 |
| HFI_545_3 | 0,3129 | 0,0669 | 0,2741 | 0,4213 |
| HFI_545_4 | 0,4591 | 0,0710 | 0,3503 | 0,5818 |
| HFI_857_1 | 0,5188 | 0,1559 | 0,3798 | 0,6616 |
| HFI_857_2 | 0,5901 | 0,1378 | 0,3088 | 0,6801 |
| HFI_857_3 | 0,5813 | 0,1391 | 0,3235 | 0,6796 |
| HFI_857_4 | 0,5264 | 0,1600 | 0,4072 | 0,6844 |

Table 7.4-28 Total Random budget

**Total Random Budget**
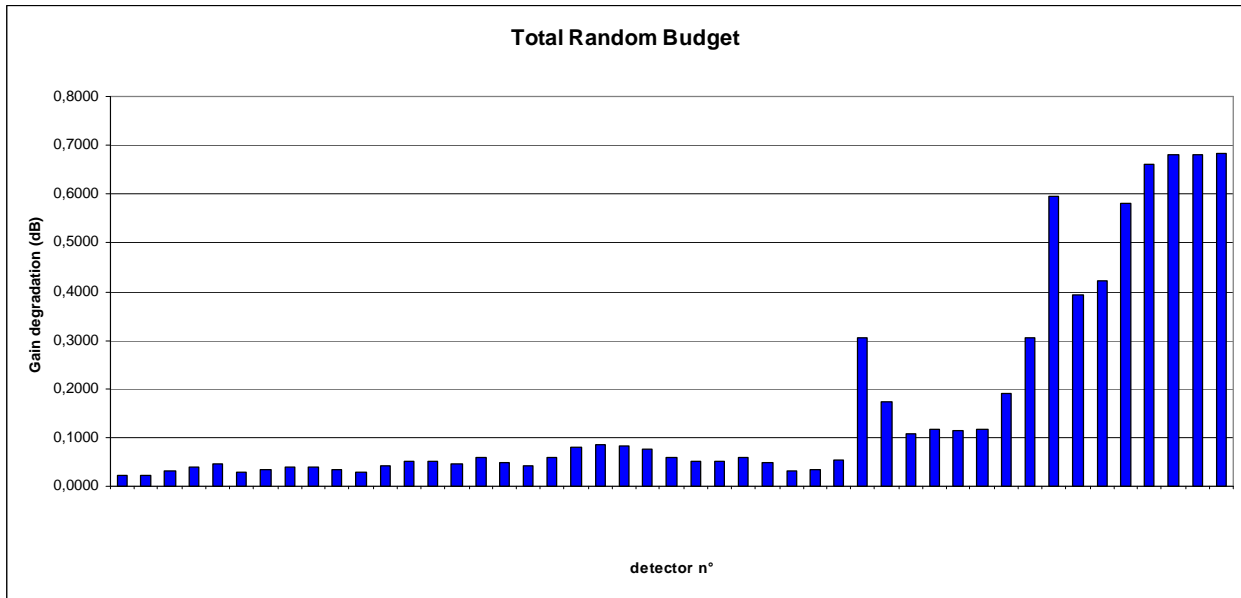
Figure 7.4-19 Total Random Budget

A major contributor appears in the random budget compared to previous CDR budget. The post : "BFE knowlegde and accuracy" is an important contributor. Paradoxically, inherent to a better knowledge of the deterministic case (by videogrammetry measurements) induced a significant uncertainties.

ALCATEL ALENIA SPACE
An Alcatel/Finmeccanica company

REFERENCE : H-P-3-ASP-AN-323

DATE : 12/2/2007

ISSUE : 3

Page : 121/126

## 7.4.4 Complete Budget

The RF main lobe performance budget of Planck Telescope is shown in the following Table 7.4-29 and the following Figure 7.4-20. The column "Total Budget" is obtained by summing Table 7.4-11and Table 7.4-24.

| detector n° | Total Deterministe | Total Random | Total Budget | Specifications |
|---|---|---|---|---|
| | dB | dB | dB | dB |
| LFI_30_27 | 0,1889 | 0,0234 | 0,2123 | 0,5 |
| LFI_30_28 | 0,1886 | 0,0233 | 0,2119 | 0,5 |
| LFI_44_24 | 0,0032 | 0,0309 | 0,0341 | 0,5 |
| LFI_44_25 | 0,0521 | 0,0393 | 0,0914 | 0,5 |
| LFI_44_26 | 0,2508 | 0,0454 | 0,2961 | 0,5 |
| LFI_70_18 | 0,1109 | 0,0297 | 0,1405 | 0,5 |
| LFI_70_19 | 0,1647 | 0,0344 | 0,1991 | 0,5 |
| LFI_70_20 | 0,1972 | 0,0393 | 0,2365 | 0,5 |
| LFI_70_21 | 0,2057 | 0,0392 | 0,2450 | 0,5 |
| LFI_70_22 | 0,1851 | 0,0330 | 0,2181 | 0,5 |
| LFI_70_23 | 0,1305 | 0,0287 | 0,1592 | 0,5 |
| HFI_100_1 | 0,1971 | 0,0430 | 0,2401 | 0,5 |
| HFI_100_2 | 0,2292 | 0,0514 | 0,2806 | 0,5 |
| HFI_100_3 | 0,2171 | 0,0514 | 0,2685 | 0,5 |
| HFI_100_4 | 0,1647 | 0,0459 | 0,2106 | 0,5 |
| HFI_143_1 | 0,1057 | 0,0607 | 0,1664 | 0,5 |
| HFI_143_2 | 0,1162 | 0,0480 | 0,1642 | 0,5 |
| HFI_143_3 | 0,1358 | 0,0427 | 0,1785 | 0,5 |
| HFI_143_4 | 0,1057 | 0,0607 | 0,1664 | 0,5 |
| HFI_143_5 | 0,0989 | 0,0787 | 0,1776 | 0,5 |
| HFI_143_6 | 0,1594 | 0,0848 | 0,2442 | 0,5 |
| HFI_143_7 | 0,1752 | 0,0827 | 0,2579 | 0,5 |
| HFI_143_8 | 0,1629 | 0,0781 | 0,2410 | 0,5 |
| HFI_217_1 | 0,1724 | 0,0587 | 0,2312 | 1 |
| HFI_217_2 | 0,1995 | 0,0520 | 0,2515 | 1 |
| HFI_217_3 | 0,1864 | 0,0524 | 0,2388 | 1 |
| HFI_217_4 | 0,1226 | 0,0591 | 0,1816 | 1 |
| HFI_217_5 | 0,0909 | 0,0491 | 0,1400 | 1 |
| HFI_217_6 | 0,1396 | 0,0312 | 0,1708 | 1 |
| HFI_217_7 | 0,1267 | 0,0336 | 0,1603 | 1 |
| HFI_217_8 | 0,0615 | 0,0555 | 0,1170 | 1 |
| HFI_353_1 | -0,2231 | 0,3038 | 0,0807 | 1 |
| HFI_353_2 | -0,0255 | 0,1745 | 0,1490 | 1 |
| HFI_353_3 | 0,1058 | 0,1081 | 0,2138 | 1 |
| HFI_353_4 | 0,1653 | 0,1157 | 0,2810 | 1 |
| HFI_353_5 | 0,1555 | 0,1151 | 0,2705 | 1 |
| HFI_353_6 | 0,0781 | 0,1155 | 0,1937 | 1 |
| HFI_353_7 | -0,0530 | 0,1918 | 0,1387 | 1 |
| HFI_353_8 | -0,2119 | 0,3048 | 0,0929 | 1 |
| HFI_545_1 | -0,5304 | 0,5962 | 0,0658 | 1,4 |
| HFI_545_2 | -0,1426 | 0,3931 | 0,2505 | 1,4 |
| HFI_545_3 | -0,1205 | 0,4213 | 0,3008 | 1,4 |
| HFI_545_4 | -0,2840 | 0,5818 | 0,2978 | 1,4 |
| HFI_857_1 | 0,2070 | 0,6616 | 0,8686 | 2,5 |
| HFI_857_2 | 0,5271 | 0,6801 | 1,2072 | 2,5 |
| HFI_857_3 | 0,4932 | 0,6796 | 1,1729 | 2,5 |
| HFI_857_4 | 0,2012 | 0,6844 | 0,8856 | 2,5 |

Table 7.4-29 Complete Budget
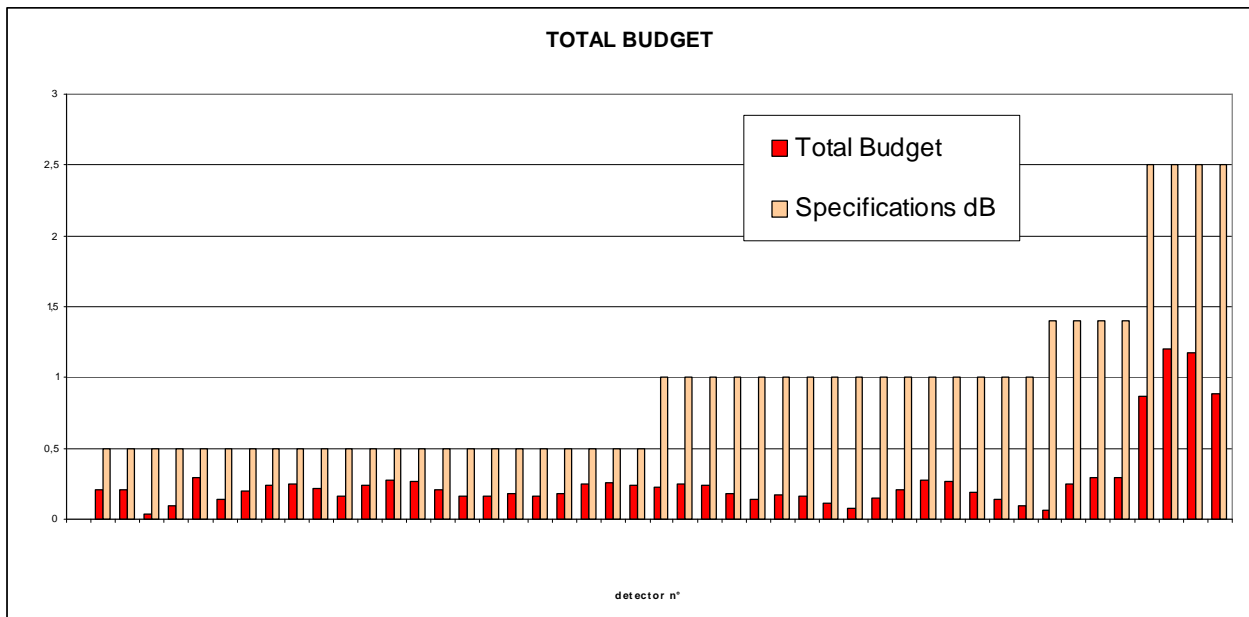
Figure 7.4-20 Total RF Budget of Planck Telescope

## 7.4.5 Ellipticity of LFI horns

The table below gives the value of beam ellipticity :

|  | theory | deterministe |  |
|---|---|---|---|
|  | R=a/b | R=a/b | DR/R |
|  |  |  | % |
| lfi_20_27 | 1,35224 | 1,32328 | 2,14157 |
| lfi_30_28 | 1,35218 | 1,31356 | 2,85643 |
| lfi_44_24 | 1,34416 | 1,29661 | 3,53786 |
| lfi_44_25 | 1,25483 | 1,25009 | 0,37745 |
| lfi_44_26 | 1,25459 | 1,25774 | 0,25115 |
| lfi_70_18 | 1,27488 | 1,25857 | 1,27912 |
| lfi_70_19 | 1,28046 | 1,25771 | 1,77663 |
| lfi_70_20 | 1,28697 | 1,25427 | 2,54033 |
| lfi_70_21 | 1,28699 | 1,25829 | 2,22987 |
| lfi_70_22 | 1,28047 | 1,25564 | 1,93898 |
| lfi_70_23 | 1,27401 | 1,26050 | 1,06075 |

Figure 7.4-21 : Ellipticity variation
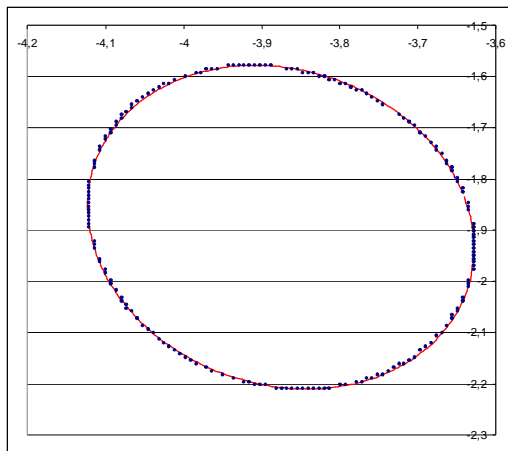


Figure 7.4-22 : Example : LFI_30_28 horn (deterministic case and best fit)

In figure 7.4-22, the best fit ellipse and the 3 dB contour are plotted.
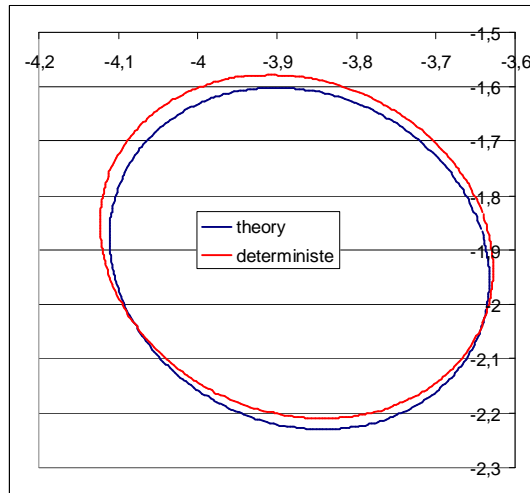
Figure -7.4-23 Comparison between the two best fit ellipses  LFI_30_28

## 7.5 Conclusion

In this chapter, the RF main lobe performance of Planck Telescope budget is presented. The deterministic model and the inputs for random budget have been updated since CDR. The modifications are in the sense of knowledge enhancements of the telescope at operational:

For deterministic case:
- BFE measurement data (videogrammetry)
- Sub-reflector data HF(interferometry)
- Optimisation-Realignment
- Alignment data of Flight model

For random case:
- Manufacturing and accuracy ( videogrammetry measurement uncertainties)
- FPU random displacement

Although the degradation of the budget since the CDR budget, compared to the specifications, the margin remains comfortable.

# 8. CONCLUSION

For the requirement toward the Earth Sun and Moon, the results of the computation performed in the frame of the RF expertise (ideal reflector surfaces, no dust, sharp edges) show a significant margin (see section 6.4)

For the self spacecraft emission a significant margin is obtained. The most critical surface is the reflector then the other elements in the optical cavity. the results are synthesized in section 4.

On final the main lobe performance degradation is well below the allowed degradation. Anyhow the only deviation with a requirement is the beam ellipticity of the LFI horns (see section 7.4.4.) (see RFW H-P-221000-ASP-RD-0024).

## END OF DOCUMENT